Photonic crystal fibre: The ultra-flattened dispersion regime

Reeves, William Henry

Award date:
2003

Awarding institution:
University of Bath

PHOTONIC CRYSTAL FIBRE: THE ULTRA-FLATTENED DISPERSION REGIME

Submitted by William Henry Reeves
for the degree of
Doctor of Philosophy
of the University of Bath
2003

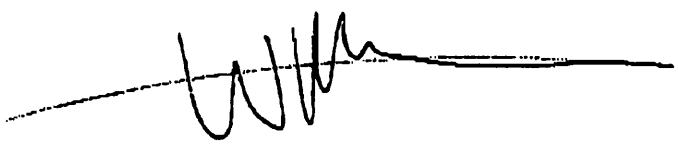

ProQuest LLC
789 East Eisenhower Parkway
P.O. Box 1346
Ann Arbor, MI 48106-1346

Abstract

This thesis describes the fabrication, characterisation, and ultra-short pulse propagation in a new family of photonic crystal fibres with ultra-flattened dispersion profiles (UFD-PCF).

The UFD-PCF had flattened dispersion regions centered near 1550 nm and had values between +16 and -7 ps/nm/km. Typical values of dispersion slope were less than ± 0.02 ps/nm^2.km in the wavelength range 1.36-1.7 μm. The smallest value of dispersion for a flattened region was 0.5 ps/nm.km, with a slope less than $\pm$ 0.007 ps/nm^2.km, in the range between 1.44 and 1.7 μm. Losses in these fibres were of the order of 25 dB/km at 1.55 μm.

Ultra-short pulse propagation and spectral broadening was investigated experimentally by launching 100 fs pulses, at a wavelength of 1550 nm, into the UFD-PCF. From the resultant data, maps of the spectral and spatial behaviour as a function of power were compiled. A range of nonlinear optical processes, and their dependance on the magnitude and shape of the dispersion, can be clearly seen.

For high input powers, broadband supercontinuum generation is observed. For a fibre with a nominal value of dispersion of 0.5 ps/nm.km this continuum extends from 1.1 to 1.9 μm with a variation of only 10 dB. This continuum is expected to be single mode for all generated wavelengths due to the fibre's structure.

Ultra-short pulse propagation and spectral broadening was also investigated in extruded SF6 glass fibre with zero dispersion wavelengths near 1.55 μm. The continuum generated was the broadest reported, spanning at least 0.35 to 2.2 μm.

We conclude that the concept of dispersion-flattened PCF can be implemented in practice, and that it could lead to many applications in fields such as metrology and telecommunications.

Acknowledgements

I apologise in advance for this acknowledgements section, but there are so many people I feel I should thank I best get started!

I'd firstly like to thank my supervisor Jonathan Knight for all the help, support, suggestions, ideas and advice over the last three (almost four!) years that has enabled me to complete this thesis.

The optogroup massive (and it really is); Thanks for making my PhD enjoyable, in particular:

Arturo, thanks for putting up with me in the labs and also inviting me to lunch, teaching me the spanish national anthem, introducing me to the spanish omelette and being "horrible to me" (ka-ching!) - I'm very sorry for book thing by the way! ... keep in touch!

William Wadsworth for loads of stuff including answering my stupid questions, giving me advice, help in the lab, technological discussions and help with rigging surveys - all much appreciated!

Many thanks to Greg for being such a great "cough cough cough", George we'll get that PC built!, Geraud "pyromaniac" Bowmans ... what *do* you want? Fetah (ok so you won the bet!) and Alan George. Thanks to Fabio and Dmitry for their marvellous code used to model ultra short pulse propagation in optical fibre. Thanks also to Fabio for helping me with the nonlinear stuff! Massive thanks to John "Theory boy/man" Pottage and Ravi for proof reading this thesis - sorry it took so long guys!

There are many other people at the University of Bath outside of the optogroup that I have to thank: Eva, for knowing what to do in *every* situation and being one of the most helpful and organised people on the planet! Miklos, Mike, Victor, and Barry for help and advice when demonstrating in the undergraduate labs. Thanks also to Wendy, Adrian, Bob and "David's (ex) Birds".

The Blaze Photonics Possé: Alan and Lance for fabrication assistance, fun and support, Francios and Matt for fitting me in to their busy schedule to run some

characterisation experiments. Special thanks to John Roberts for the multipole modelling of the flat dispersion fibre and the really pretty plots!

Special thanks goes to the guys from Los Alamos for inviting me over there to do some work: Fioerenzo Omenetto and Tony Taylor. An extra special thanks also to Anatoly for letting me completely take over his lab for an entire month! Enjoyed time in LA - the weather, the work, the introduction to the chilly cheese burger and the jam sessions!

My friends: Jim Gregory and David Lawton for agreeing to sharing a house with me, endless philosophical discussions, introducing me to some of the films that I should have seen and all the memories of times past... "urr, I'm sorry, what I said was..."

Massive thanks to Brian Mangan for many many things including: Advice on all aspects of PCF fabrication and how to write a thesis! Thanks for looking after me and letting me stay with you when I was homeless and broke!

Mum and Dad, thanks for all the support you've given me in not only the last three years, but the entire 23 years of my education!... Yep, I think now it's time to get a *real* job!

Finally I'd like to thank Philip Russell for allowing me the privilege of working in such a fantastic research group!

Contents

List of Figures

Chapter 1

Synopsis

In 1854 a Irish physicist by the name of John Tyndall popularised the concept of light guiding in a demonstration that involved bending light around a corner by confining it within a curved jet of water. He had demonstrated what is now known as total internal reflection (TIR), the basis for light guidance in conventional fibre optics. The first practical application of TIR arrived in the 1930s and involved an un-coated plastic fibre to guide light to an area of inspection for medical purposes.

With the invention of the LASER in the 1960s the field of fibre optics exploded and also fuelled the birth of nonlinear fibre optics due to the high light energy densities and the long interaction lengths now made possible. During the 1970s the refinement of both ultra low loss glass fibres and the laser enabled fibre optic transmission over large distances to be implemented. These distances were increased further with the invention of fibre amplifiers and fibre lasers. Today, fibres with losses of less than 0.2 dB/km and (Dense) Wavelength Division Multiplexers (DWDM) enable transmission rates of many terabits per second over thousands of kilometers in a single optical fibre.

The 'digital revolution' has already started to give the consumer a taste of a feature rich and interactive environment. Digital services, such as broadband internet, are becoming increasingly popular and the demand for bandwidth is therefore increasing. For example, the mainstream introduction of wireless networking products are expected to necessitate an increase in the bandwidth of the communications infrastructure by a factor of ten in approximately two years[1].

As the majority of communications is carried at some stage by fibre optics, research must continue in order to satisfy the future demands. One promising new field of optical fibre research began in the 90s with the proposal and subsequent demonstration of photonic crystal fibre.[2, 3] .

Photonic Crystal Fibre (PCF), also known as 'Holey Fibre' and 'Microstructured Optical Fibre (MOF)', is the first major departure from standard, step index, fibre design. PCFs are all-silica optical fibres with an array of air holes running down their entire length.

Even though PCF technology is still in its infancy many exciting results and applications have already been published and discovered. For example, PCF can possess the property of being 'endlessly single mode'[4] and have large mode areas[5]. They can be used to generate broadband supercontinuum[6], made into lasers[7] and made highly birefringent[8]. Photonic band-gap guidance has also been demonstrated in PCF where light is guided in an 'air' core[9] seemingly defying physics. PCF research strives to improve on existing fibres and fibre devices and also investigate new properties and applications unique to PCF.

This thesis focuses on novel PCFs with modified dispersion profiles, specifically those that are flat over a wide wavelength window. It has been suggested that fibres of this type could be used to generate flat supercontinuum in the infrared[10] and be used in optical parametric amplifiers[11]. PCF with ultra-flattened dispersion profiles may also find a role in wavelength-division multiplexing (WDM) data transmission where it may be possible to increase bandwidth by increasing the number of data carrying channels.

Thesis outline

Chapters 2, 3 and 4 are intended to be introductory chapters. Chapter 5 and 6 detail original work undertaken for this thesis.

Chapter 2 begins with a discussion on the main principles of conventional optical fibre as an introduction to PCF. PCF is then introduced and compared to conventional fibre and examples of fibres with properties unique to PCF are presented. Measuring chromatic dispersion is of great relevance to this thesis.

This chapter therefore closes with a detailed explanation of the method used to characterise the PCF at the University of Bath.

Chapter 3 outlines the fabrication procedure used to create the fibres detailed in this thesis. Chapter 4 reviews some of the non-linear effects in optical fibre and is presented as an aid to understanding the nonlinear effects observed in chapter 6

Chapter 5 details work undertaken to produce a PCF with a ultra-flattened dispersion profile over a wide wavelength window. Chapter 6 details an experimental investigation into ultra-short pulse propagation in ultra-flattened dispersion PCF. Chapter 7 includes a brief investigation of supercontinuum generation in PCF made from a high index glass named SF6 using ultra-short pulses.

Chapter 8 contains the summary and Future work

The appendix includes abbreviations used in this thesis, published papers and conference papers.

Chapter 2

Introduction

2.1 Overview

There are many reasons why optical fibres have become the communications medium of choice. They allow low loss transmission, have large bandwidth, have unparalleled signal security and are thin, light and flexible. They are fabricated from glass so they are electrically non conductive and are relatively cheap to manufacture. They can also be used as sensors and are especially useful in hazardous environments where electric discharge is a potential danger.

This chapter briefly reviews the field of fibre optics and photonic crystal fibres. The first section outlines the guidance mechanism, fundamental parameters and characteristics, and the fabrication method for conventional fibre. The second introduces photonic crystal fibre (PCF), the design parameters and guidance mechanisms. PCF have many potential advantages over conventional fibre and some of these are highlighted by reviewing previous work in the field. The last section outlines a measurement technique used to measure dispersion.

2.2 Conventional optical fibre

2.2.1 Light guidance in optical fibre

Conventional optical fibres guide light by the phenomenon of total internal reflection (TIR). A ray of light will be totally reflected at a boundary between two dielectric media when incident from the medium with higher refractive index at an angle of incidence greater than a critical value θ_c determined by Snell's Law:

$$\theta_c = \sin^{-1} \frac{n_2}{n_1} \tag{2.1}$$

where n_1 and n_2 are the refractive indices where $n_1 > n_1$.

An optical fibre is a cylindrically symmetric waveguide formed by inserting a medium of high refractive index into a medium of lower refractive index. This forms the basis of all conventional optical fibre design and is shown in figure 2.1. An outer polymer coating may be applied to protect the glass from scratches and thus improve the fibre's durability.

Fibre modes and the normalized frequency

When electromagnetic radiation is confined to a waveguide it can only propagate in certain modes. The number and intensity profile of these modes is governed by the physical parameters of the waveguide and can be found by solving Maxwell's equations[12]. However, the solution methods are non trivial and will not be derived here.

All the fibres presented in this thesis only allow one mode to propagate (the fundamental), all the others are said to be 'cut-off'. The discussion here will therefore be restricted to 'single mode' fibres.

When calculating mode cut-offs for conventional fibres it is convenient to use the 'normalised frequency' or V parameter:

$$V = \frac{2\pi r}{\lambda} \sqrt{n_{core}^2 - n_{clad}^2} = \frac{2\pi}{\lambda}\, a(NA) \tag{2.2}$$

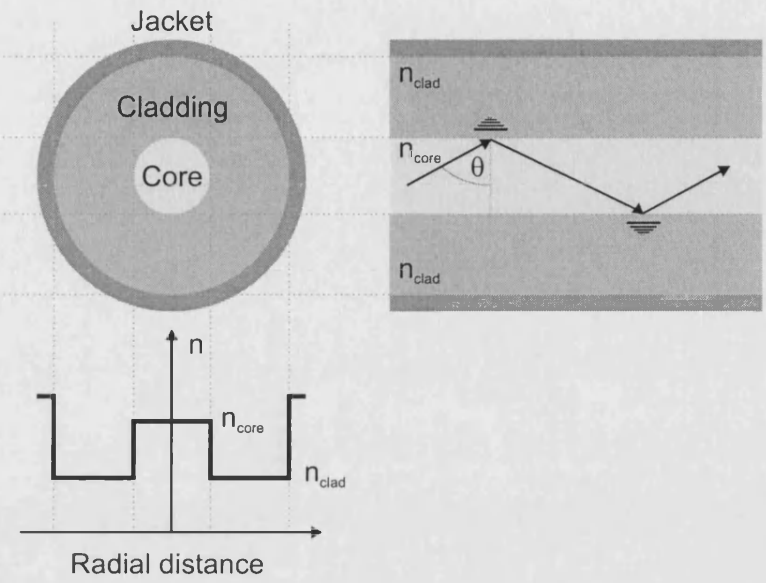

Figure 2.1: Schematic of the index profile and guidance mechanism of a conventional step index optical fibre. The fibre will guide light provided that θ is greater than the critical angle as defined by Snell's law. The fibre jacket is usually made from a polymer and has a higher refractive index than the cladding.

where NA is the numerical aperture which is discussed in section 2.2.2 and λ is the free-space wavelength of the light. A conventional step-index fibre will be single mode for V < 2.405, which is a value given by the first zero of the J_0 Bessel function (one solution to the cylindrically symmetric waveguide).[13]

Equation 2.2 clearly shows that the V is inversely proportional to wavelength. Conventional fibres can therefore be single mode for a limited wavelength range but for wavelengths shorter than a critical value (λ_c) the fibre will become multimode:

$$\lambda_c = \frac{2\pi r}{2.405}\sqrt{n_{core}^2 - n_{clad}^2} \tag{2.3}$$

The dependence of V on the core and index step therefore puts restrictions on the fibre design if the fibre has to be single mode at a specific wavelength.

2.2.2 Optical fibre characteristics

This section summarises a number of characteristics that determine how light propagates in optical fibres. Firstly, in order to launch light efficiently into a

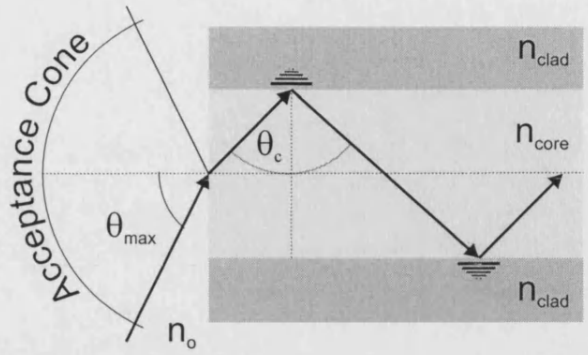

Figure 2.2: The maximum acceptance angle θ_{max} for launching light into an optical fibre with a large core. θ_c is the critical angle governed by Snell's law.

fibre it is useful to know the numerical aperture.

Numerical aperture

> *Numerical aperture is an expression of the extent of the fibre's ability to accept, in its bound modes, non-normal incident rays.*
>
> *American National Standard T1.523- 2001*

In multi-mode fibres a definition of NA can be found by using a geometric optics approach and Snell's Law - figure 2.2. Only light rays with a sufficiently small incident angle upon the fibre end face($\theta < \theta_{max}$), with respect to the axis normal to propagation, will have angles of incidence inside the fibre greater than the critical angle θ_c.

From this geometry and by using the trigonometric identity $sin^2 + cos^2 = 1$ it is possible to derive the following relation:

$$n_0 sin\ \theta_{max} = \sqrt{(n_{core}^2 - n_{clad}^2)} \tag{2.4}$$

Normally light is launched into fibres from air so NA is defined as:

$$NA = sin\ \theta_{max} = \sqrt{(n_{core}^2 - n_{clad}^2)} = n_{core}\sqrt{2\Delta} \tag{2.5}$$

where

$$\Delta = \frac{n_{core}^2 - n_{clad}^2}{n_{core}^2} \approx \frac{n_1 - n_{clad}}{n_{core}} \quad \text{for } \Delta \ll 1 \tag{2.6}$$

Effective area

The energy guided in the core of a fibre is not of uniform intensity and it also spreads into the cladding to an extent related to the wavelength and the index contrast. The calculation of intensity by dividing the transmitted power by the physical area of the core is therefore inaccurate. Instead the effective core area A_{eff} can be defined as[14]:

$$A_{eff} = \frac{\left(\iint |F(x,y)|^2 dxdy\right)^2}{\iint |F(x,y)|^4 dxdy} \tag{2.7}$$

Where $F(x,y)$ is the amplitude and $F(x,y)^2$ is the intensity of the modal distribution of the fundamental mode in a plane perpendicular to the light propagation. A_{eff} is dependant on both the fibre parameters and the wavelength of the light.

Effective area is especially important in nonlinear fibre optics as the nonlinear refractive index (detailed in chapter 4) varies with intensity. This means that fibres designed for nonlinear applications have small cores and small A_{eff} which results in a high light intensity.

In this thesis the effective area was not measured but calculated from modelling results.

Group velocity dispersion

Group velocity dispersion (GVD) plays a fundamentally important role in fibre optics and is covered by many text books for example: [15, 14]. It governs the spreading of light pulses (which is relevant particularly in telecommunications) and dictates how light of differing frequencies interact and generate new frequencies (for example, in supercontinuum generation). This thesis is dedicated to dispersion profile engineering in optical fibres, a topic that is discussed in detail in later chapters.

Light is transmitted through bulk media via interactions with bound electrons. Chromatic dispersion is related to the characteristic resonance frequencies at which the medium absorbs the light. These resonances determine how the refractive index n, and the propagation (phase) velocity, varies with frequency:

$$\text{phase velocity} = \frac{c}{n(\omega)} \tag{2.8}$$

where c is the speed of light in a vacuum.

When light of more than one frequency propagates in a medium, the resultant interference causes a intensity modulation in the wave. Figure 2.3 shows a simple case where a uniform plane wave is composed of two equal amplitude fields at two frequencies ω_1 and ω_2 where $\omega_1 < \omega_2$. The resultant field comprises of a carrier wave at a frequency $\omega_0 = \omega_1 + \Delta\omega = \omega_2 - \Delta\omega$ that is modulated by a sinusoidal envelope at the "beat" frequency $\Delta\omega$.

The carrier has a phase velocity of $\nu_p = \omega 0/\beta_0$ whilst the envelope (or group) will move at the group velocity $\nu_g = \Delta\omega/\Delta\beta$. If $\beta(\omega)$ and ω are related to each other by a multiplying factor that does not vary with frequency the group velocity will be equal to the phase velocity.

As $\Delta\omega$ becomes small $\Delta\omega/\Delta\beta$ approaches $d\omega/d\beta$, the slope of the ω verses β curve for a given medium (figure 2.4 . $d\omega/d\beta$ is the frequency dependent group velocity function $\nu_g(\omega)$ of the medium and is interpreted as the velocity of a "group" of waves whose frequencies are distributed over an infinitesimally small bandwidth centered at ω.

For signals of small bandwidth the ω verses β curve will appear to be a straight line - ν_g will be sharply defined. However, if a broad frequency range is present, for example when propagating ultra short pulses in fibres, the ω verses β curve may not be a straight line. As a result different components of the spectrum will propagate at different group velocities leading to signal distortion - including pulse broadening. This effect is called group velocity dispersion.

The broadening of ultra short pulses in fibres can be substantial due to the large range of associated frequencies. In order to examine the dispersion of short pulses the mode propagation constant β can be expanded about the central frequency

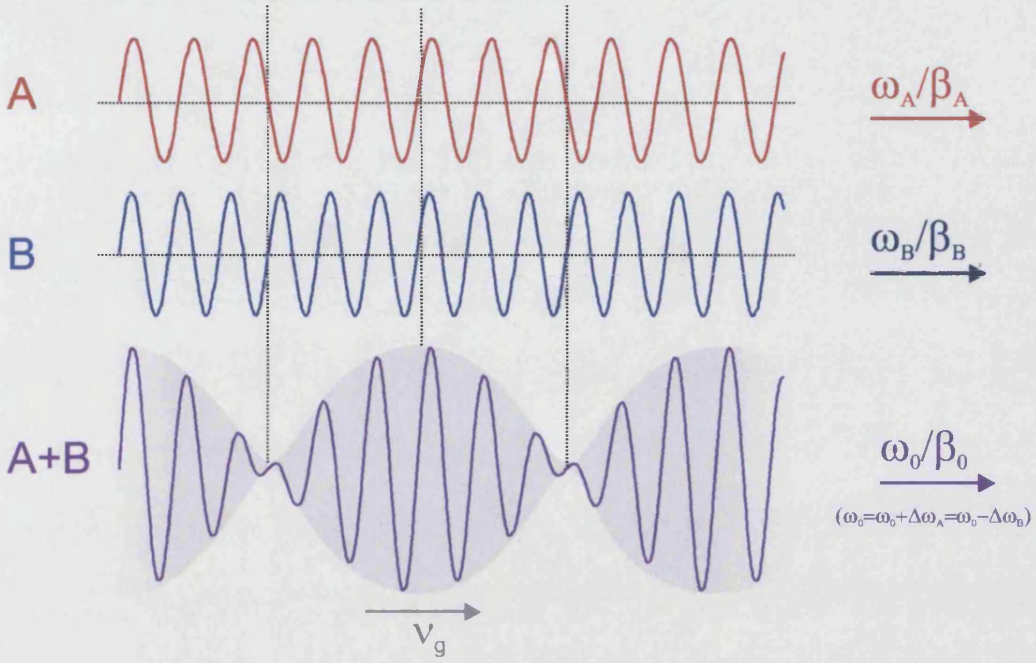

Figure 2.3: The effect of adding two monochromatic waves together with different frequencies.

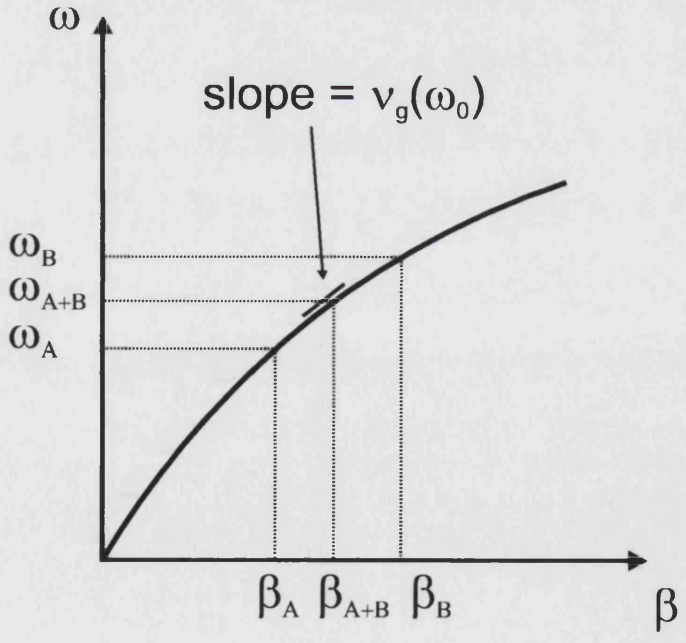

Figure 2.4: $\omega - \beta$ plot for a typical material, showing the variation of group velocity with frequency.

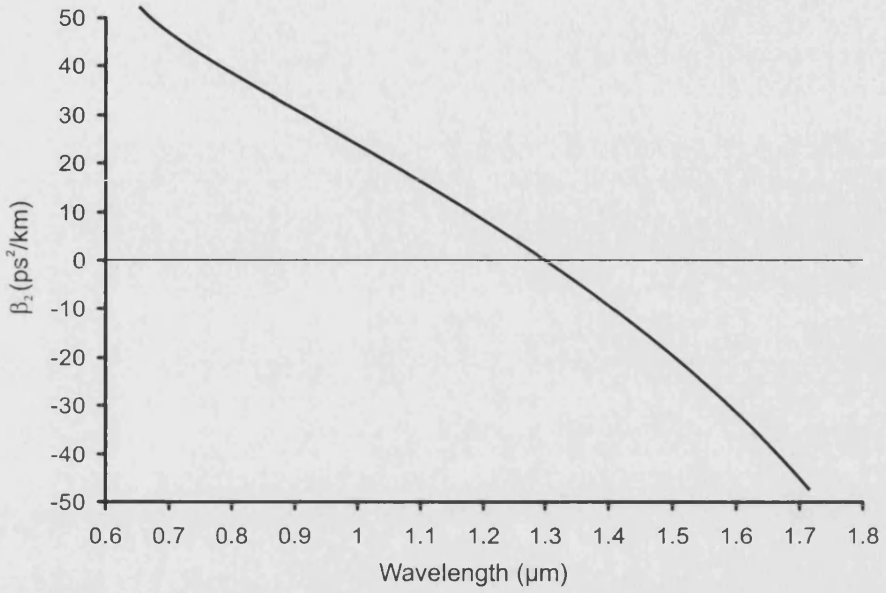

Figure 2.5: Variation of β_2 with wavelength for fused silica. $\beta_2 = 0$ at a wavelength near 1.27μm

using a taylor series.

$$\beta(\omega) = n(\omega)\frac{\omega}{c} = \beta_0 + \beta_1(\omega - \omega_0) + \frac{1}{2}\beta_2(\omega - \omega_0)^2 + \ldots, \tag{2.9}$$

where

$$\beta_m = \left(\frac{d^m\beta}{d\omega^m}\right)_{\omega=\omega_0} \qquad (m = 0, 1, 2, 3, \ldots) \tag{2.10}$$

furthermore,

$$\beta_1 = \frac{1}{v_g} = \frac{n_g}{c} = \frac{1}{c}\left(n + \omega\frac{dn}{d\omega}\right), \tag{2.11}$$

$$\beta_2 = \frac{1}{c}\left(2\frac{dn}{d\omega} + \omega\frac{d^2n}{d\omega^2}\right), \tag{2.12}$$

β_1 is inversely proportional to (v_g), the velocity of the pulse, is proportional to the group index n_g, and is known as the 'group delay'. β_2 is known as the GVD parameter and figure 2.5 shows β_2 against wavelength for silica.

GVD can be positive, called normal (where blue components travel slower), or negative, called anomalous (where red components travel slower). Normal dispersion is so-called as this it the type of dispersion that *normally* exists in most materials for visible wavelengths. The wavelength at which β_2 is zero is known

as the zero dispersion wavelength (ZDW). However, this can be misleading as the overall dispersion may not be zero due to higher order dispersion terms. The most significant of these, β_3, is related to the slope of β_2 and is called the third order dispersion (TOD). TOD is only significant when using pulses with wavelengths close to the ZDW where it distorts ultrashort pulses. This is discussed in more detail in section 4.4.3.

In fibre optics the dispersion parameter D is often used instead of the GVD parameter. It is related to β_2 by the following relation:

$$D = \frac{d\beta_1}{d\lambda} = -\frac{2\pi c}{\lambda^2}\beta_2 \approx \frac{\lambda}{c}\frac{d^2n}{d\lambda^2} \tag{2.13}$$

D is typically associated with the practical units of ps/nm.km, for pulse lengths of the order of picoseconds, wavelengths of the order of nanometers and fibre lengths of the order of kilometers.

Dispersion in single mode[1] fibre has contributions from three sources: the dispersion caused by the bulk material, the dispersion induced by the confinement of light to the fibre core (called waveguide or geometric dispersion), and a profile dispersion parameter (which is proportional to $d\Delta/d\lambda$ where Δ is the core-cladding index difference). The profile dispersion parameter is typically less than 0.5 ps/nm.km and is often neglected, giving a total dispersion of

$$D_{total} \approx D_{material} + D_{waveguide} \tag{2.14}$$

As the material dispersion cannot be controlled extensively without introducing large concentrations of index-changing dopants, the easiest way of engineering the dispersion is through the waveguide dispersion. In conventional fibre this is achieved by choosing appropriate core radii and the index difference. Alternatively, fibres with more than one index contrast can be fabricated. Figure 2.6 shows one such example, a 'W' fibre.

[1]For multi-mode fibres there is an additional inter-modal dispersion, however, all fibres presented in this thesis are single mode and so this is not discussed here.

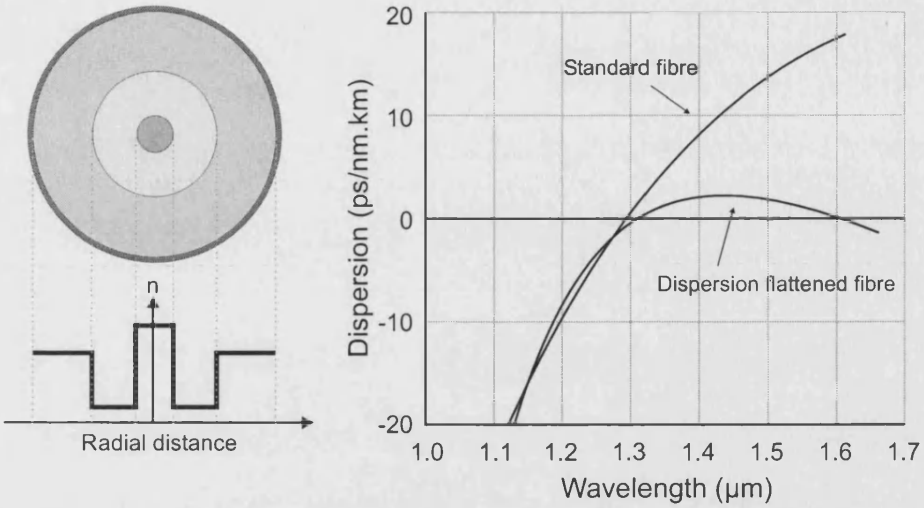

Figure 2.6: A schematic of a dispersion flattened 'W-fibre' (left) and example dispersion profiles of standard and dispersion flattened fibres (right).

Attenuation

There are three main loss mechanisms in optical fibres: absorption, scattering and bend loss.

Material absorption dissipates optical power as heat and is related to the material composition. In silica fibres the main cause of this loss is the interaction of photons with the atomic vibrational spectrum of SiO_2, specifically the vibrations of the Si-O bond. Even though the resonant wavelength is at 9.2 μm, infrared losses start to dominate above 1.5 μm. Absorption also occurs in the ultraviolet due to the electronic transitions in silica.

Impurities within the glass also cause absorbtion, mainly due to the hydroxyl group OH^- of water with a resonance between 2.7 and 4.2 μm (depending upon the O-H bond position in the glass network). Harmonic overtones of this vibration at 1.38, 0.95 and 0.72 μm cause significant losses in the visible and IR spectrum. It is for this reason that the standard telecommunications wavelength windows were chosen near 1.3 and 1.55 μm. This is where the losses are relatively unaffected by the OH absorbtion provided the water content of the glass is reduced below one part in 10^7. The material absorption is also at a minimum near these wavelengths. Figure 2.7 shows a schematic that includes these losses.

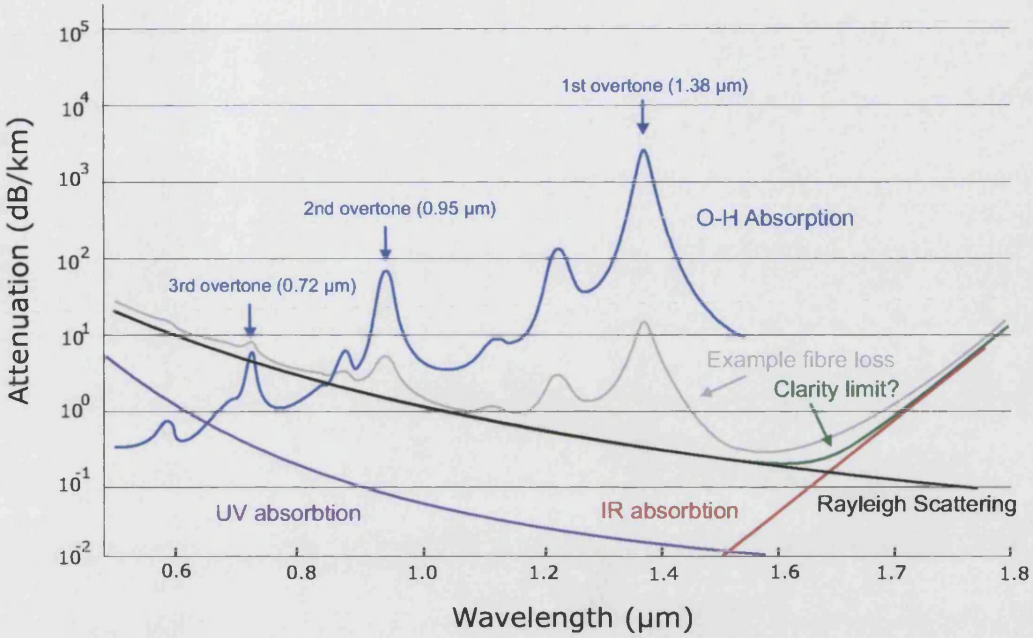

Figure 2.7: A schematic diagram showing various sources of loss in optical fibre.

As figure 2.7 illustrates, scattering also plays a large role in the transmission of light in optical fibre. Rayleigh scattering is proportional to λ^{-4} and is the dominant intrinsic loss mechanism at short wavelengths. It arises from inhomogeneities occurring on a small length scale compared to the wavelength of the light.

Figure 2.7 also shows what is believed to be the clarity limit, the ultimate goal for conventional fibres at which the glass is maximally transparent, and is calculated from the summation of the Rayleigh scattering and SiO_2 vibrational spectra[16, 17].

Other sources of scattering loss arise from inhomogeneities comparable to the guided wavelength. Examples include irregularities in the fibre structure, fibre diameter fluctuations, strains, bubbles and impurities (dirt). Scattering losses via frequency conversion can occur by way of photon interaction with either acoustic phonons (Brillouin scattering) or optical phonons (Raman scattering) and these are discussed in chapter 4.

Optical fibres suffer radiation losses at bends or curves in their propagation axes. This is due to the radially evanescent waves at the bend exceeding the velocity

of the light in the cladding. As the value of β is then larger than the maximum value permitted to travel in the cladding this light is lost through radiation.

Bend loss in fibres depends on two factors: the physical structure of the waveguide and the wavelength of the propagating light. The longer the wavelength, the greater the extent of the bend loss experienced for a given radius of curvature. In fibres, penetration into the cladding can be reduced in two ways: by propagating shorter wavelengths of light and by increasing the index contrast between the core and cladding.

Bend loss can also occur for short wavelengths. When the path difference between the inside and outside of the fundamental mode becomes large the resultant phase change converts the mode to the second order. In single mode fibre, higher order modes are not supported so this light is lost to the cladding.

2.2.3 Fabrication

There are many different ways to fabricate conventional optical fibre. This section focuses on a vapour-phase fabrication technique where glass is created from high purity component gasses using the commonly employed modified chemical vapor deposition (MCVD) process. Further information on other techniques can be found from many sources including [18].

Regardless of the origin of the glass, fibre fabrication usually has two stages. In the first a preform with the desired refractive index contrast and relative core-cladding dimensions is made. Figure 2.8a shows a schematic of this for the MCVD process. Initially layers of SiO_2 are built up on the inside of a fused silica tube by mixing $SiCl_4$ and O_2 at temperatures around 1800 °C. These layers will eventually form the cladding of the fibre and, if desired, can be doped with boron or fluorine during this stage to depress the refractive index. After sufficient cladding material has been deposited, the glass composition is changed to that for the core. This is usually achieved by adding the index-raising dopants GeO_2 or P_2O_5 to the vapor mixture in the desired quantity to give reactions similar to

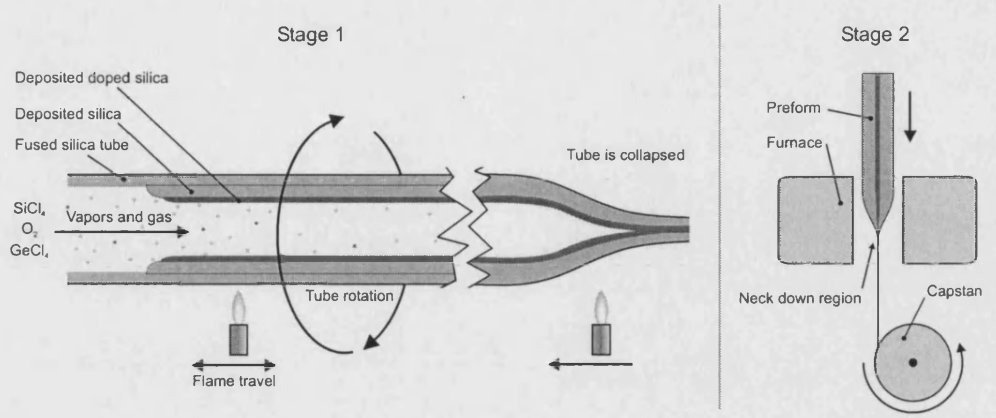

Figure 2.8: Schematic of the procedure for fabricating conventional optical fibre. (Stage1) Fabrication of the preform by modified chemical vapor deposition (MCVD). (Stage2) The preform is slowly fed into the furnace and fibre is pulled by a motorized drum called the capstan.

the following:

$$\underset{(Vapour)}{SiCl_4} + \underset{(gas)}{O_2} \xrightarrow{heat} \underset{(Solid)}{SiO_2} + \underset{(gas)}{2Cl_2} \tag{2.15}$$

$$\underset{(Vapour)}{GeCl_4} + \underset{(gas)}{O_2} \xrightarrow{heat} \underset{(Solid)}{GeO_2} + \underset{(gas)}{2Cl_2} \tag{2.16}$$

Laser fibres may be fabricated by introducing appropriate dopants, such as Erbium, to the core region.

As soon as all the required layers have been deposited the flame temperature is raised to collapse the tube into a preform rod.

In the second and final stage (figure 2.8 stage 2) the preform is 'drawn' to fibre by feeding the preform into the top of a furnace while pulling from the bottom at a faster rate. Due to the amorphous nature of the glass, the only effect this has is the simple reduction in scale of the structure. The size reduction takes place in a small area near the furnace element called the 'neck down' region. To improve the durability of the fibre an external polymer coating is usually applied during this stage to protect the fibre from scratches. By using this method hundreds or even thousands of kilometers of fibre, typically 125 μm in diameter, can be drawn from a single preform.

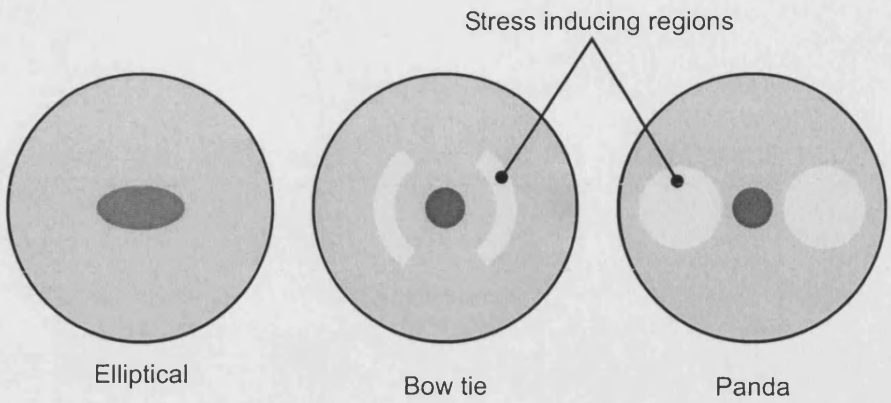

Figure 2.9: Examples of highly birefringent conventional optical fibres. They are also examples of micro-structuring in optical fibre.

While the procedure described here is for a cylindrically symmetric fibres, conventional fibres can also be made birefringent by either shaping the core (form birefringence, as in elliptical-core fibre) or by introducing stress forming defects that make the fibre birefringent. Figure 2.9 shows examples of 'elliptical', 'panda' and 'bow tie' birefringent fibres.

2.3 Photonic crystal fibre (PCF)

Today, optical fibres are used extensively in telecommunications due to their excellent guidance properties and low attenuation, low cost, and high bandwidth. However, as there are only two fundamental fibre parameters, core diameter and index difference, there are limitations on the variations in structure that can be fabricated.

Fibre optics changed radically in the 1990s with the first demonstration[2, 3] of a new family of optical fibres that can have an endless variety of structures.

Photonic Crystal Fibre (PCF), also known as 'Holey Fibre' and 'Microstructured Optical Fibre' (MOF), is unlike conventional fibre in that it is usually manufactured from only one material, the most popular being pure silica.

PCF have a cladding that is perforated with a periodic 2-dimensional array of air holes that run down the entire length of the fibre. The core is a 'defect' that breaks the periodicity of this array. Light is confined to the core by the surrounding air holes and not by any material index differences within the glass. Important design parameters for PCF are therefore hole diameter d and hole-to-hole pitch Λ.

PCF fabrication is similar to that of conventional fibre in the sense that a preform is made which is drawn to fibre. In order to incorporate air holes of the desired size and formation most PCF preforms are fabricated using a stacking technique. In its simplest form, a PCF preform is built by stacking capillaries into a hexagonal lattice around a central solid rod. The preform is then drawn to fibre in a similar way to conventional fibre. This is an over-simplification of the so called 'Stack and Draw' fabrication technique and more detailed information can be found in chapter 3.

Today, PCFs are starting to be made from other glasses such as SF6[19] or even other transparent materials like polymers. Polymer PCF has potential for use in local area computer networks, as a cheap alternative to glass fibre, and for terahertz propagation[20].

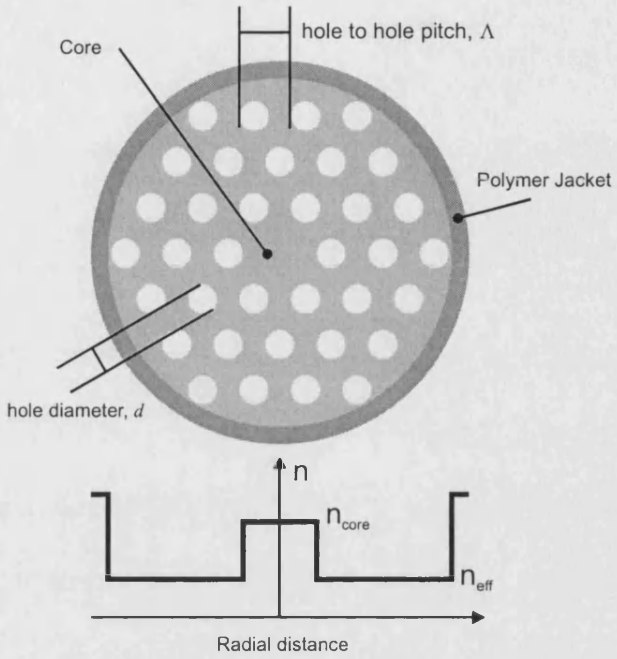

Figure 2.10: The basic structure of an index guiding PCF, the white regions are holes (air), the light gray region is glass.

2.3.1 Light guidance in PCF

Unlike conventional fibre, PCF can guide light by two mechanisms. If the 'defect' in the holey array is of 'high index' (for example a missing air hole) the fibre can guide by what can be considered as total internal reflection[21]. Should the 'defect' be of 'low index' (such as an enlarged hole) light may still be guided, by being confined by a photonic band gap in the cladding[9].

Index guiding PCF: high index defects

The case where light will be confined to a high index defect by TIR, much like a conventional fibre, is shown schematically in figure 2.10. The omission of an air hole results in a high index core situated within an air-silica microstructure with a lower average or 'effective' refractive index.

Mathematically, in direct analogy to conventional fibre, for index-guiding PCF to guide by total internal reflection there must be eigenmodes that lie within the

following range of propagation constants β:

$$\beta_{FSM} < \beta < kn_{core} \tag{2.17}$$

where $k = 2\pi/\lambda$, n_{core} is normally the index of silica and β_{FSM} is the propagation constant of the fundamental space-filling mode (FSM). The FSM is the fundamental mode of an infinitely tiled version of the cladding without defects. In analogy with conventional fibre theory the effective refractive index can therefore be defined as:

$$n_{eff} = \frac{\beta_{FSM}}{k} \tag{2.18}$$

Of course, PCF design does not have to be constrained merely to using pure silica. Fibres with 'hole-assisted' guidance have also been demonstrated[22] where a doped glass with higher refractive index may be introduced to the defect region. In this way light is guided in the conventional manner, however, the holes can still affect the guidance properties of the fibre. Similarly, PCF lasers have been fabricated with a Ytterbium doped core[7].

Band gap guiding PCF: low index defects

Instead of removing a hole, if an existing hole is greatly enlarged to create a low index defect, light guidance is still possible. This was first shown in 1999 when Cregan *et al*[9] demonstrated fibres with hollow, air filled, cores. Light of certain frequencies and angles of incidence can be confined to the defect via constructive multiple beam interference within the fibre's periodic structure. These frequencies lie within the photonic band gap (PBG) of the fibre and therefore cannot escape from the core.

Figure 2.11 shows an example of one of these fibres[2]. These 'air guiding' PCF could be used in many applications, including Raman effect studies of gasses (by introducing the gas to the fibre core[23]) and cold atom guidance[24]. Band gap fibres are ultimately projected to have lower losses than glass-cored fibres since the light is confined to air in which material absorption is negligible.

[2]Fibre fabricated by, and images courtesy of, Dr. B.J. Mangan

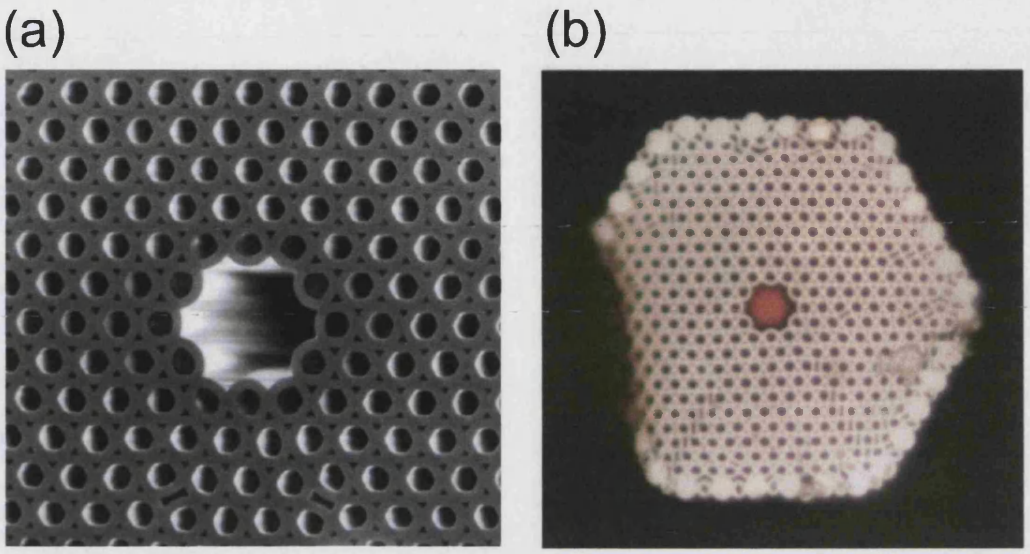

Figure 2.11: An example of band gap guiding PCF. (a) a scanning electron micrograph. (b) a photograph of the near-field of the PCF shown in (a) when illuminated with white light.

Confinement loss in PCF

Ideally, PCF only experience losses attributed to the materials in their structure. However, whether guidance is achieved by TIR or a band gap, PCF do not comprise of an infinite lattice of air holes. Attenuation due to the finite nature of the waveguide structure must also be considered. In general the larger the number of periods/rings of holes in the cladding, the lower the loss.

Modelling PCF using the multipole method[25] and the finite element method[26] has shown how confinement loss varies with the number of periods and the value of d/Λ. For a large d/Λ only a few periods are required (e.g. for d/Λ greater than 0.4, 4-6 periods are usually adequate) while for small d/Λ ratios many more are needed. There also seems to be an approximately linear relationship between the confinement loss (in dB) and the number of periods for a fixed d/Λ, see [26] figures 3a and b.

2.3.2 Advantages of PCF

This section highlights some of the differences between PCF and conventional fibre by examining some of the novel and potentially useful properties unique to PCF.

Endlessly single mode

Section 2.2.1 introduced the normalised frequency parameter, V, and the requirement that it must have a value less than 2.405 for single-mode operation. PCF has a similar expression for the effective V parameter[4].

$$V_{eff} = \frac{2\pi r}{\lambda}\sqrt{n_{core}^2 - n_{eff}^2} \tag{2.19}$$

where Λ is often arbitrarily chosen as the approximate core radius.

As equation 2.19 shows, V is still explicitly inversely proportional to wavelength but the effective index of the cladding also changes rapidly with wavelength. Long wavelengths tend to fill the entire cladding structure and therefore experience a cladding index close to the average of the cladding. Conversely, shorter wavelengths become more confined to the silica regions and avoid the holes. This results in an increase of the effective cladding index with decreasing wavelength which reduces the dependence of V on wavelength - V becomes almost constant for short wavelengths[21].

If the d/Λ ratio is small enough (less than or equal to 0.4[27]), the fibre will remain in the single mode regime for all measurable wavelengths. If the d/Λ ratio is larger than this, the gaps between the holes become small enough to isolate the core from the cladding and the fibre will become multi-mode.

As the only requirement for entering the endlessly single mode regime is on the d/Λ ratio, unlike conventional fibre, there is no constraint on core diameter. Additionally, the fabrication of conventional LMA fibre is non-trivial as it is difficult to obtain completely uniform doping throughout large core fibres. Any irregularities would distort the shape of the mode thus degrading beam quality and possibly have the effect of providing a mechanism of coupling light into lossy

higher order mode. PCF is therefore at another advantage as no dopants are required. The lack of dopants is also be beneficial when propagating light in the UV as less light will be absorbed.

The only real limit on the size of the core for the LMA PCF is the loss due to bending.

The critical bend radius, for which bend loss becomes large, can be expressed in the following form[13]:

$$R_c = \frac{8\pi^2 n_{core}^2 r^2}{\lambda^2 W^3} \tag{2.20}$$

This equation is not quantitatively accurate but does nevertheless give the correct parametric dependence of R_c, the critical bend radius, with core radius (r), core refractive index (n_{core}) and the parameter W which is a function of V.

For long wavelengths PCF have similar bend loss properties to conventional fibre as V and V_{eff} (equations 2.2 and 2.19), make W proportional to to $1/\lambda$. Consequently R_c is proportional to λ. For short wavelengths V_{eff} tends towards a constant. So while in conventional fibre R_c remains proportional to λ, in PCF R_c is proportional to λ^{-2}. This means that PCF has a short wavelength bend loss edge in addition to the long wavelength bend loss edge.

Figure 2.12 shows a typical result of a bend loss measurement made on PCF. This graph shows bend loss measurements made on 10 μm (SEM insert) and 15 μm diameter core LMA ESM PCF. For this experiment the fibre was looped only once and emersed in index matching oil. The cut-off wavelength was determined at the point at which 10 dB of attenuation had been reached. For example, if the 15 μm core fibre were bent into a single loop of bend radius 25 mm, light with a wavelength less than 750 nm would be attenuated by more than 10 dB. It should be noted that the long wavelength bend loss edge was at a value greater than 1750 nm and could not be measured with the equipment available.

Large core single mode PCF are ideal for transmitting large optical powers and have also been doped to form large mode area lasers[28].

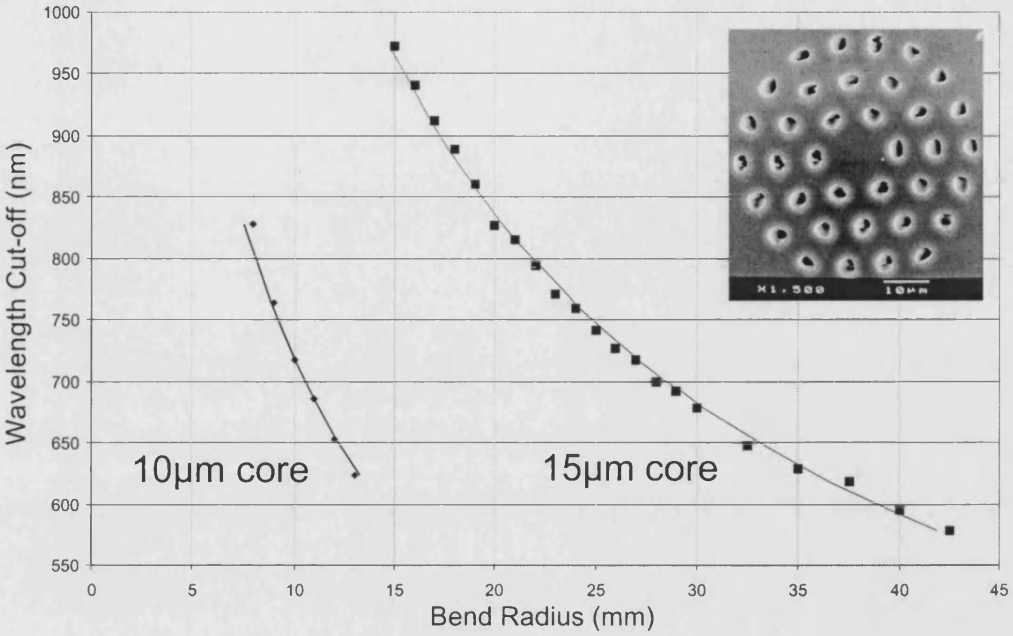

Figure 2.12: Measured short wavelength cutoff with bend radius for large mode area PCF with 10μm core left and 15μm core right. Fits proportional to λ^{-2} have been applied. Inset shows SEM image of the 10μm core fibre

Novel structures

The flexibility of the stack and draw fabrication process, detailed in chapter 3, allows a seemingly endless variety of structures to be fabricated. Figure 2.13 shows a few examples of PCF fabricated at the University of Bath. Photograph (a) shows a multi-core fibre[3] More information on this type of fibre can be found in[29]. Image (b) shows a highly birefringent fibre[4][8] with form birefringence formed by holes in one axis having a different size to that of the rest of the cladding. Fibres of this type have very short beat-lengths that can be as small as 0.4mm[8]. Picture (c) shows an example of a 'pacman' PCF that was fabricated for use as a gas sensor.

[3]Fibre fabricated by, and SEM image courtesy of, Dr. B.J. Mangan
[4]Fibre fabricated by, and SEM image curtesy of, Dr. A. Ortigosa-Blanch

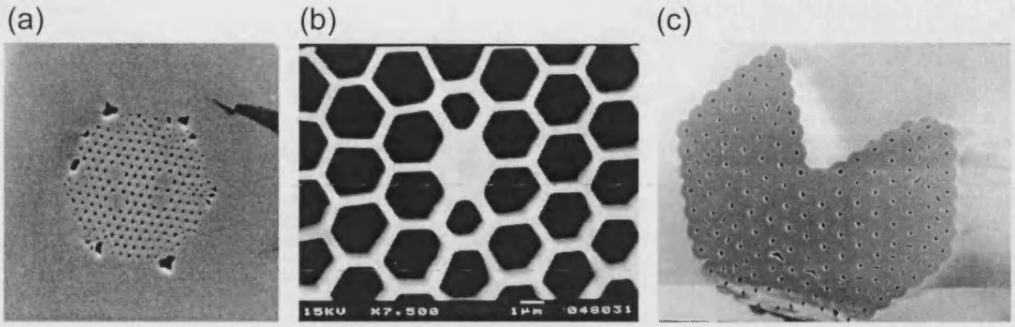

Figure 2.13: Novel microstructured fibres. (a) A PCF with four cores. (b) Highly birefringent PCF. (c) 'Pacman' PCF for possible gas sensing applications.

GVD managed PCF

Section 2.2.2 introduced dispersion in optical fibres and its relation to refractive index. The larger dependance of effective refractive index with wavelength and the d/Λ ratio in PCF means that the waveguide dispersion has a greater influence over the total dispersion than in conventional fibre.

The extreme cases of PCF, where the d/Λ ratio is either very large or very small, yield novel dispersion profiles.

The large d/Λ case corresponds to a fibre that can be approximated to a small silica strand surrounded by air - so called "Cobweb" PCF. It was predicted that such a structure (with a core diameter of ≈ 1 μm) would have anomalous dispersion at wavelengths much shorter than that attainable in conventional fibre - down to around 500nm. It has therefore been possible to use Ti:Sapphire lasers to pump Cobweb fibres with femtosecond-long pulses, at wavelengths in the anomalous dispersion regime near the ZDW, to generate ultra-broadband supercontinua.[6] Figure 2.14(a) shows an example of one such fibre[5], and (b) shows a photograph of the supercontinuum spectrum generated using the fibre and light from a Ti:Sapphire laser.

In the other extreme, PCF with a small d/Λ ratio can shift the ZDW to longer wavelengths. PCF of this type can also exhibit ultra-flattened dispersion profiles, the main topic of this thesis.

[5]Fibre fabricated by, and picture courtesy of, Dr. W.J. Wadsworth

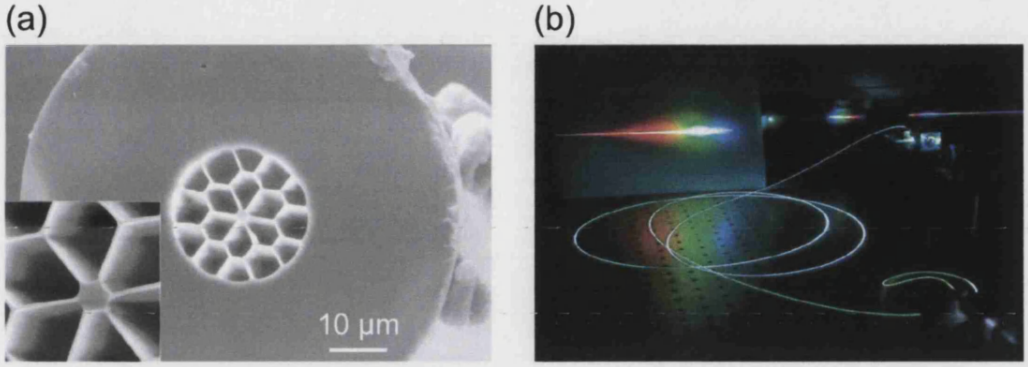

Figure 2.14: (a) a scanning electron micrograph of a "cobweb" PCF. (b) the resultant supercontinuum generated using similar fibre when pumped with femtosecond pulses from a Ti:Sapphire laser

2.4 Measuring Dispersion

As dispersion plays an important role in optical fibres, the method used to measure the dispersion of all the PCFs presented in this thesis is included here for reference.

Dispersion becomes critical in the propagation of ultra short pulses. It is therefore essential to be able to measure it accurately, which is especially difficult when the dispersion is small. The method described here has proved particularly useful for PCF as only short sections of fibre are required and the measurement technique has a large operating wavelength window.

The dispersion profile of a fibre can be obtained from equation 2.21 by measuring the group delay, β_1, and then taking its derivative with respect to wavelength.

$$D = \frac{d\beta_1}{d\lambda} = -\frac{2\pi c}{\lambda^2}\beta_2 \tag{2.21}$$

Group delay may be determined by measuring how the optical path length through a fibre changes for different wavelengths. Differences in optical path length are easily measured using an interferometer.

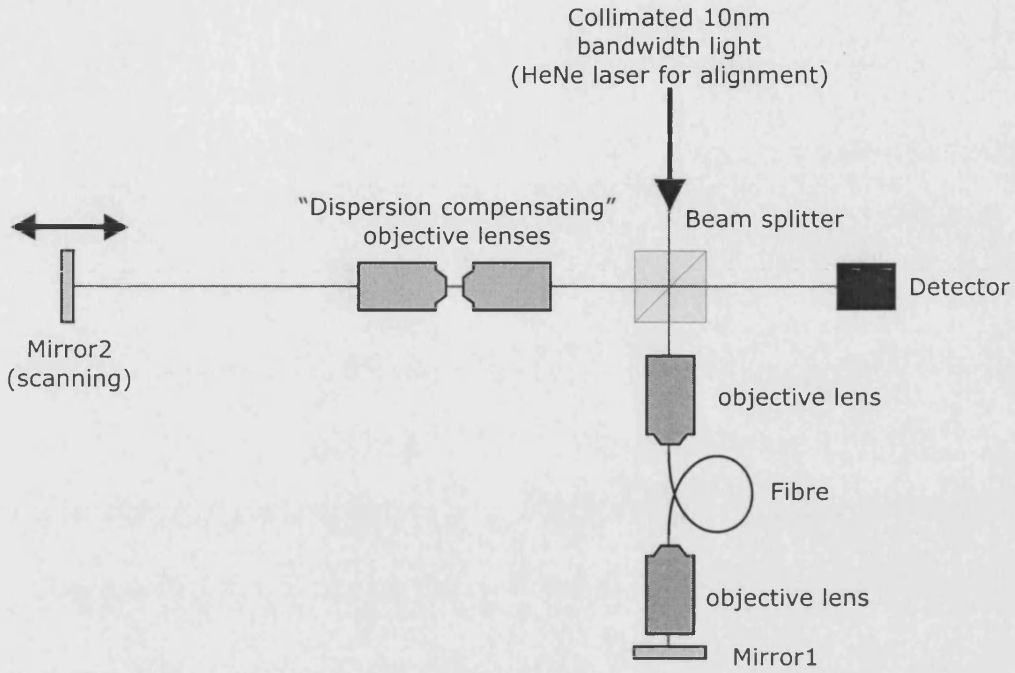

Figure 2.15: Schematic of the equipment, based on a Michelson interferometer, used to measure group delay with wavelength in optical fibres.

2.4.1 The interferometric technique

The technique described here is based on a low-coherence white-light interferometric method [30]. Figure 2.15 shows a schematic of the dispersion rig that employs a Michelson interferometer. One arm contains the fibre under test and a fixed mirror. The other, the free space arm, has a mirror mounted on a computer-controlled linear translation stage. This movable mirror compensates for the different optical path lengths (OPL) experienced by the different wavelengths. The coupling optics necessary for launching light into the fibre are reproduced identically in the free space arm to compensate for any dispersive effects they might introduce.

Initially red HeNe laser light is used to align the system, then 10nm band pass filters are placed in front of a white light halogen bulb, coupled into a single-mode fibre (in the wavelength range of interest) with which light is launched into the dispersion rig. Due to the low light levels used in the experiment, resulting from coupling white light into single mode fibre, the interferogram has to be measured by a femtowatt receiver with lock-in detection. A PC is used to record

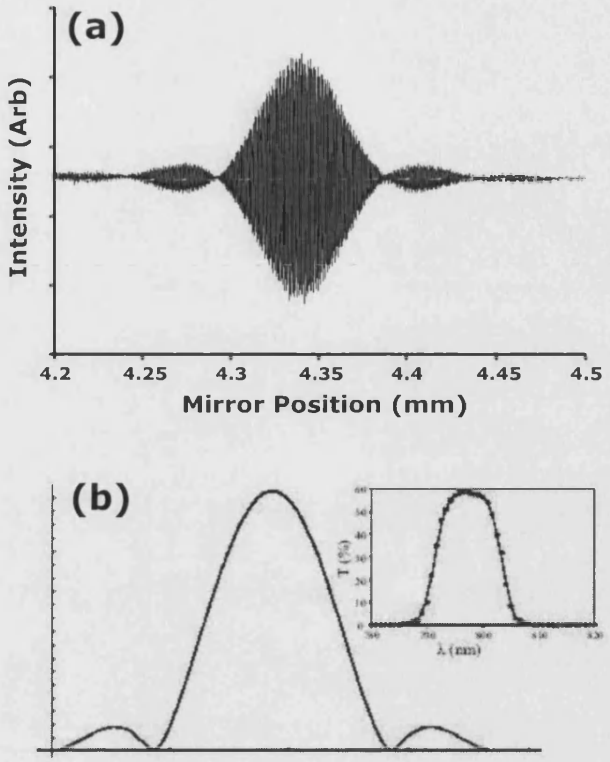

Figure 2.16: (a) A typical interferogram recorded using light with a bandwidth of 10 nm. (b) The Fourier transform of the filter's transmission profile (inset).

the variation of light intensity values with respect to mirror position.

The detected envelope of the fringe pattern is related to the fourier transform of the transmission profile against wavelength of the illuminating light source. A monochromatic source yields a fringe pattern for all positions of the travelling mirror whilst a narrow fringe packet appears for a large bandwidth. Light with a bandwidth of 10 nm produces a interferogram similar to that shown in figure 2.16(a). Figure 2.16 (b) shows the origin of the side lobes - the Fourier transform of the transmission profile resembles a sinc function. The center of the fringe packet is the mirror position at which the path lengths are equal.

Interferograms are taken for a number of filters with transmission profiles centered at a range of wavelengths. From the center positions of the fringe packets a plot of mirror position verses wavelength may be drawn. Figure 2.17 shows an example of one such plot.

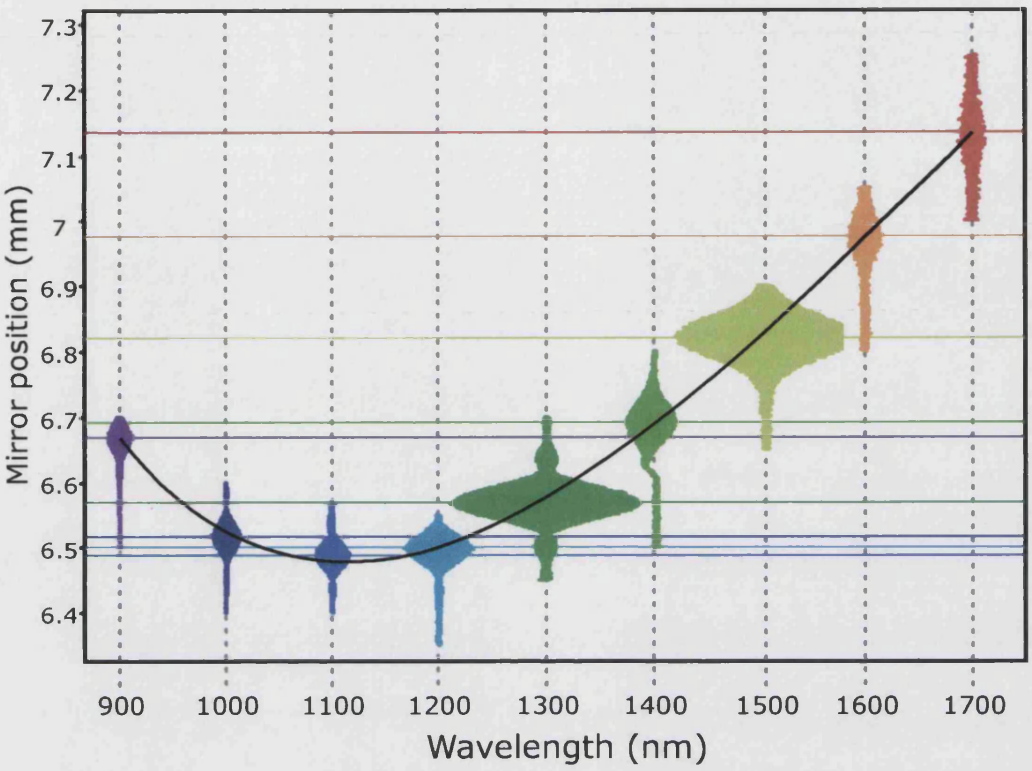

Figure 2.17: Fringes generated with a variety of 10 nm band pass filters centred at wavelengths from 900-1700 nm. The centre of each fringe packet signifies the mirror position at which the arms of the interferometer have the same OPL.

$$\beta_1(\lambda) = \frac{mirrorposition(\lambda)}{c} \cdot \frac{1}{fibrelength} \tag{2.22}$$

Thus, simply by dividing the 'mirror position' by the speed of light and the length of the fibre under test, figure 2.17 would become a plot of group delay with wavelength. From equation 2.21, a derivative with respect to λ yields the dispersion, D.

Figure 2.18 shows a dispersion curve generated from the derivative of the data presented in figure 2.17.

This technique is especially accurate when measuring fibres with large dispersion as the position difference between adjacent fringe packets is large. However, if the dispersion and dispersion slopes of the fibre are small for a broad wavelength range, as for the fibres described in chapter 5, the technique is not ideal. This

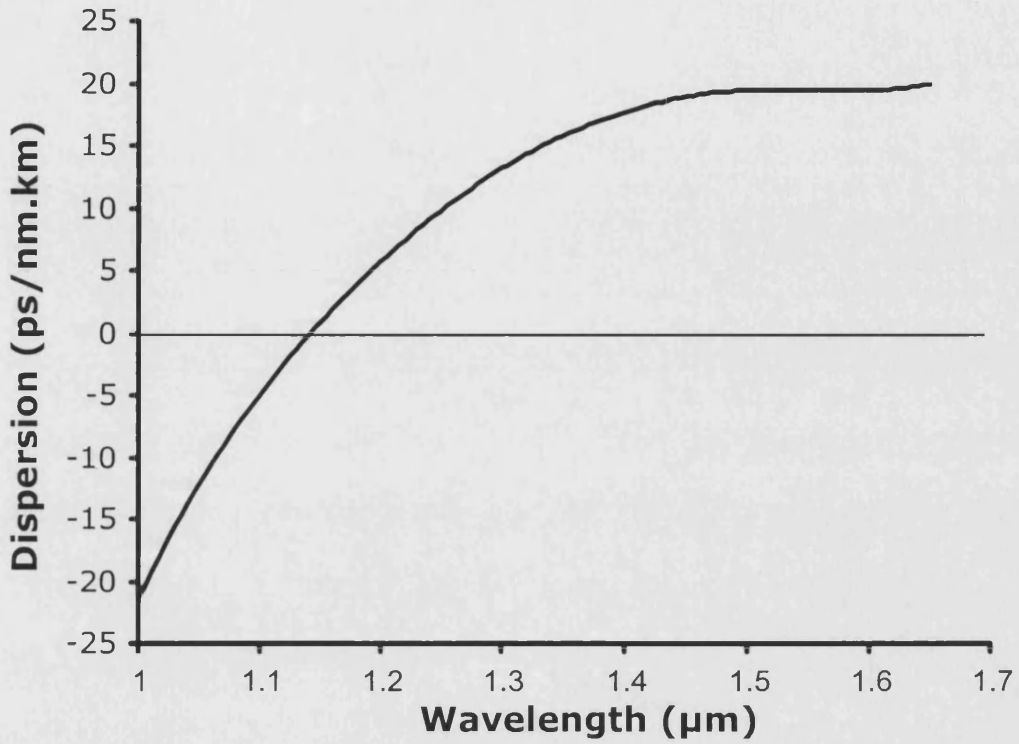

Figure 2.18: A dispersion plot calculated from the fringe position data shown in figure 2.17.

is due to the inability to distinguish the movement of the fringe packets, even for relatively long lengths of fibre, from wavelength to wavelength. Errors due to the 5 nm positional resolution of the mirror, experimental noise and the accuracy of determining the centre of the fringe packet are expected to be of the order of $\pm$ 0.25 ps/nm.km.

Chapter 3

PCF Fabrication

In a process akin to producing 'seaside rock', photonic crystal fibre (PCF) is made by reducing a relatively large, easily built, macro-structure down to a micro-structure with features in size comparable to the wavelength of light. The fabrication procedure for PCF differs radically from that used for conventional step index fibre as the micro-structure usually comprises of glass and air.

There are many variations on the PCF fabrication process that are dependant on the type of PCF to be fabricated. This chapter describes in detail work undertaken to produce the PCF investigated in later chapters.

3.1 Overview

Almost all photonic crystal fibres are fabricated using the 'stack and draw' technique that was developed by Knight *et al*[3]. Figure 3.1 shows a schematic of a typical PCF fabrication procedure.

Initially in a process called 'drawing', the tubes and rods are fed into the top of a furnace at one speed whilst being pulled out from the bottom at a faster speed. The relative speeds of the 'feeder' and the 'puller' set the diameter of the resultant capillaries and rods.

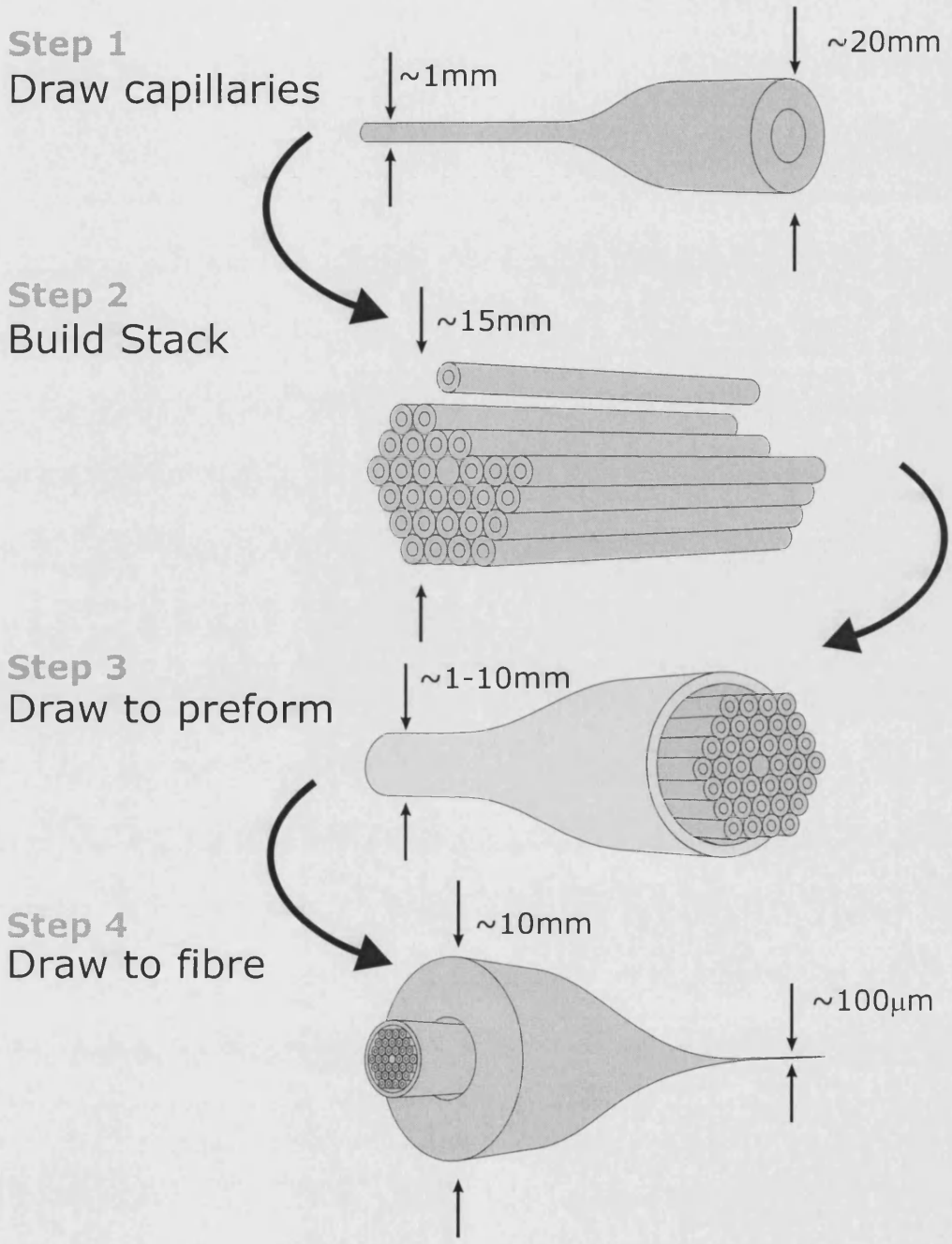

Figure 3.1: The basic stack and draw PCF fabrication technique. Silica capillaries and rods are stacked into a hexagonal array, and progressively reduced in diameter until the structure has the required waveguiding characteristics

In step two the capillaries are stacked into a hexagonal[1] array, placing a rod(s) instead of a capillary where a core(s) is needed.

Step three involves sliding the stack inside a tube and drawing the whole structure down in size, usually between 1 mm and 10 mm in diameter. This miniature version of the stack is called the 'preform'. In the final stage the preform is slid inside another tube and drawn once more into photonic crystal fibre.

The remainder of this chapter explains the fabrication procedure in detail.

3.2 PCF Design

The design and fabrication procedure for PCF must be thoroughly planned before any work is undertaken. A typical PCF design is shown in figure 3.2.

Standard conventional fibre is normally 125 μm in diameter and it is therefore advantageous for PCF to be fabricated to the same diameter for ease of cleaving and connecting to standard equipment. As the supplied silica tubes have a limited range of internal and outer diameters (IDs and ODs), the number of periods and wall thickness of the silica jacket must be appropriately selected for the final fibre diameter to reach the $\sim$ 125 μm without compromising the desired wave-guiding characteristics.

Additionally, the internal diameter (ID) to outer diameter (OD) ratio of the capillaries must be chosen to closely match the hole diameter to hole pitch (d/Λ) ratio of the final structure whilst allowing for the slight collapse of the holes that inevitably occurs every time the glass is passed through the furnace.

In step three of the fabrication procedure deformation at the stack/tube interface, caused by the fitting of a hexagonal structure in a round hole, can be avoided by removing the corners of the stack. The remaining space between the stack and the tube can be filled with small rods to further reduce any air gaps.

The interstitial air gaps between the capillaries may also be filled with rods to

[1]Although square arrays have also been fabricated

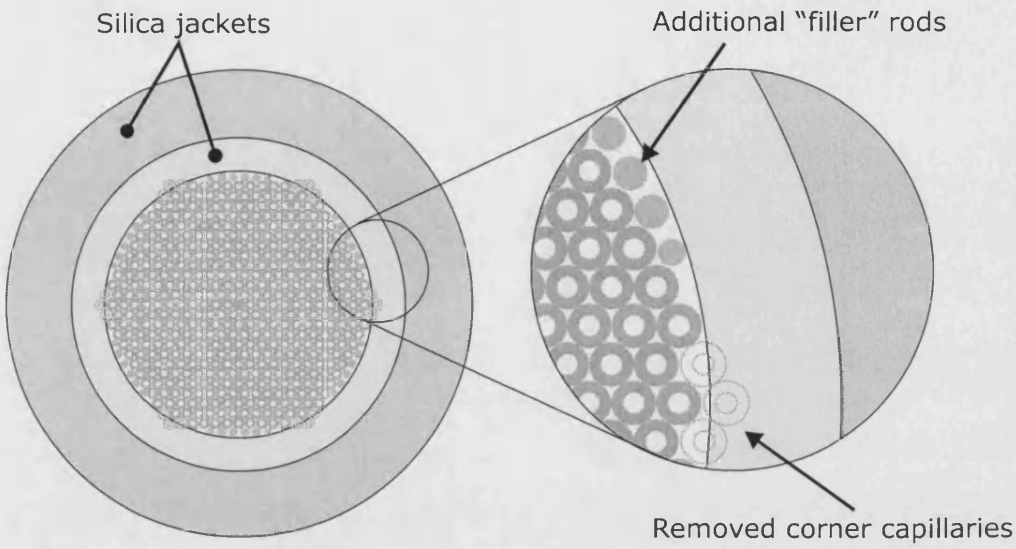

Figure 3.2: The design of a PCF. In this example the capillaries are 0.85mm in diameter and the silica jacket tubes are drawn so that the final fibre diameter is around 120 μm.

minimise any structure deformation. However, this is time intensive, especially when the number of periods becomes large, and is normally omitted.

Figure 3.2 shows a typical design for the Ultra flattened dispersion PCF described later in this thesis. The corner capillaries have been removed and external silica jackets added to make the external fibre dimension around 120 μm.

3.3 Initial preparation

The glass is supplied in the form of silica tubes and rods that are typically 20 mm in diameter. This glass is a water free synthetic quartz made by Heraeus Quartz Products Ltd. called Suprasil-F300. Before any capillaries or rods are drawn the tubes and rods are washed in a custom designed tube washer. The first stage of cleaning involves a rinse with deionised water at high pressure. Then a wash in a detergent solution, another rinse, and finally the rods and tubes are dried with nitrogen gas at 80^{o}C eliminating any drying stains that would have otherwise appeared.

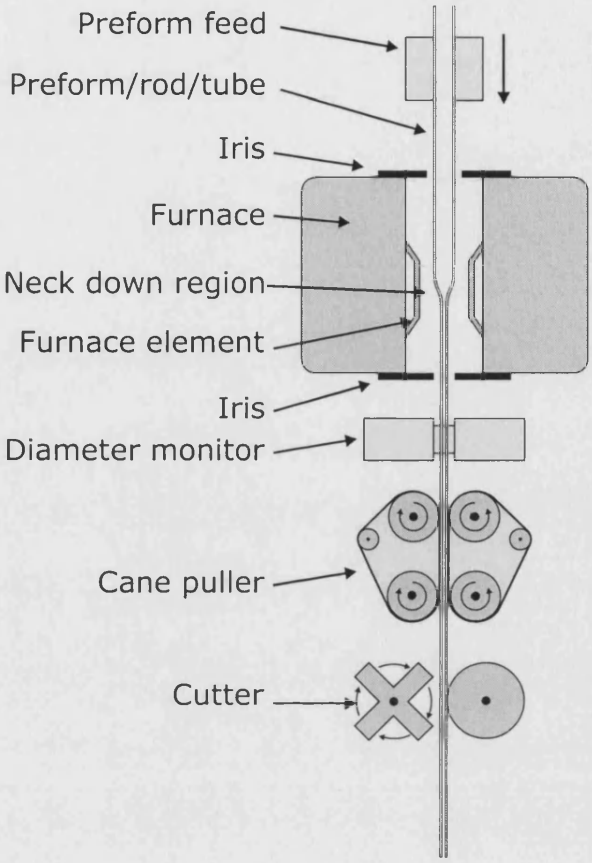

Figure 3.3: A schematic of the capillary, rod and preform 'drawing' procedure. Glass is fed into a furnace and is pulled out at a faster rate.

3.4 Capillary and rod drawing

Figure 3.3 shows a schematic of the capillary and rod drawing process and figure 3.4 shows a photograph of the equipment used at the University of Bath.

The 'preform feeder' comprises of a chuck, that holds the tubes and rods, mounted on a precision lead screw so that glass can be lowered into the furnace at finely controlled rates up to $\sim$ 10 cm/min.

The furnace is water cooled, and comprises of an electrically heated graphite element. The furnace chamber is purged with argon purified via a Getting furnace while irises and gas windows at the furnace entrance and exit prevent any atmospheric or other contamination. Glass drawing temperatures used are typically

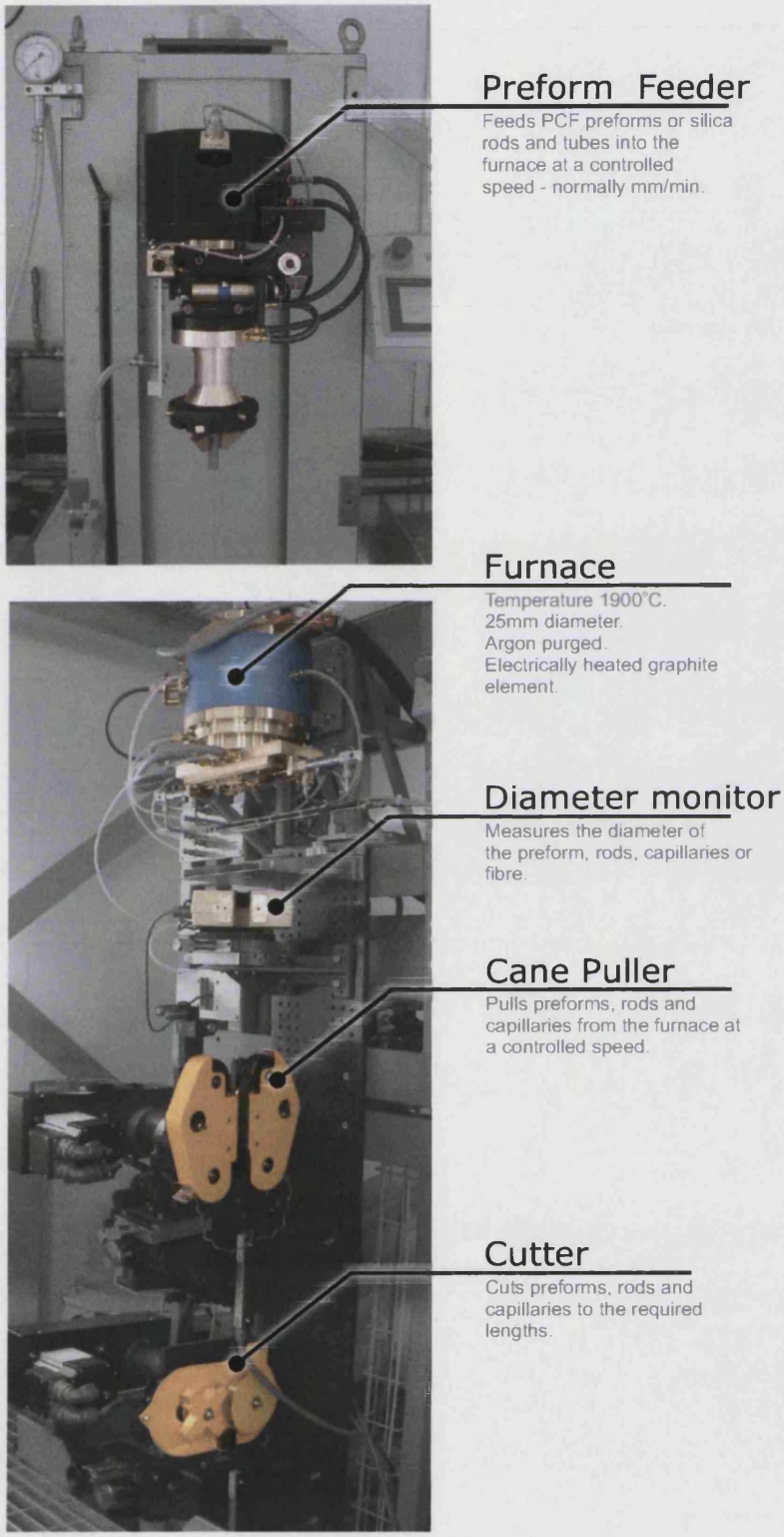

Figure 3.4: Fabrication facilities at the University of Bath for drawing capillaries and rods. See text for explanation.

between 1800 and 2100 °C.

The capillaries and rods are pulled from the furnace by two opposing rubber belts that form the 'cane puller'. The pulling speed can also be finely controlled and is normally around 1 m/min. The capillaries and rods are cut automatically into specified lengths of approximately 1 m. Clearly as the diameter of the capillaries becomes smaller, the more flexible they become. As a result they become increasingly difficult to handle and are often cut to shorter lengths to alleviate this problem. For example, capillaries of 0.7-0.8 mm in diameter have been cut to lengths of 75 cm for a marked improvement in the ease of cleaning and handling.

If the furnace temperature is set appropriately, around 1900°C, the ID to OD ratio of the capillaries will remain almost identical to that of the original tube. The glass will be viscous enough that surface tension effects cannot cause the holes to collapse.

A diameter monitor allows the precise control of the diameter of the glass being pulled from the furnace.

Although fairly crude in principle, the precise control of furnace temperature and feedback control of feed and pull rates allows as many as 650 capillaries, 75 cm length, with a diameter tolerance of ± 10 μm to be drawn from a 1 m long, 2.5 cm diameter, silica tube.

3.5 The preform

The freshly drawn rods and capillaries are washed and dried in the same way at the tubes in section 3.3.

The stack is then built by hand using a hexagonally shaped jig similar to that shown in figure 3.5. This jig can be adjusted to suit stacks up to a diameter of around 2.5 cm (the maximum diameter that can be drawn in the furnace). Capillaries are placed one row at a time and intentional guiding defects are placed during this stage. Static electricity can seriously hinder the stacking procedure,

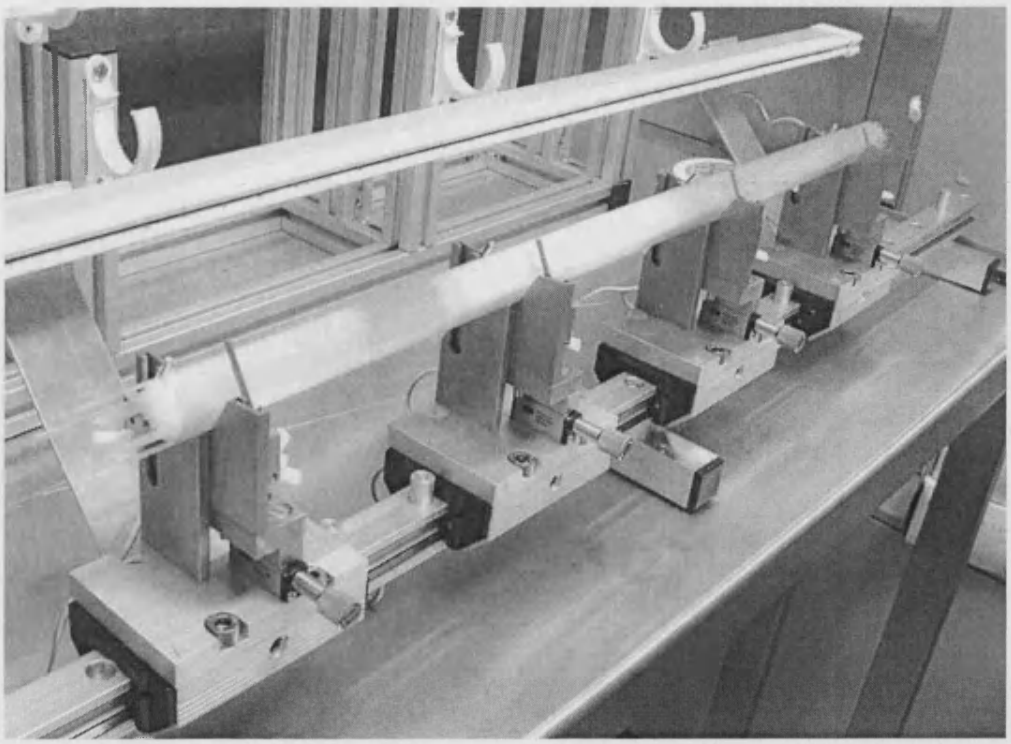

Figure 3.5: Equipment used to stack capillaries and rods into a hexagonal array. At the the rear of the jig a device creates a high voltage electric field that eliminates static buildup on the capillaries.

especially if the capillaries have thin walls and are therefore easily charged. A high voltage electric field can be applied to eliminate this static build-up using the device shown at the rear of the jig. The electric field creates a stream of ions that neutralise any charge on the capillaries.

Once the stack is complete one end is melted to hold one end together securely. This stage also stops the capillaries from falling from the stack when mounted vertically. It is then slid inside a tube that will eventually become part of the surrounding silica jacket. At this stage any additional 'filler' rods are inserted between the preform and the jacket.

The tube and preform are sealed to a chuck as shown in figure 3.6. A vacuum is then applied between the preform and the jacket. This vacuum aids the collapsing of the holes between the capillaries and rods, called interstitial holes, when the stack is drawn to preform in the next stage.

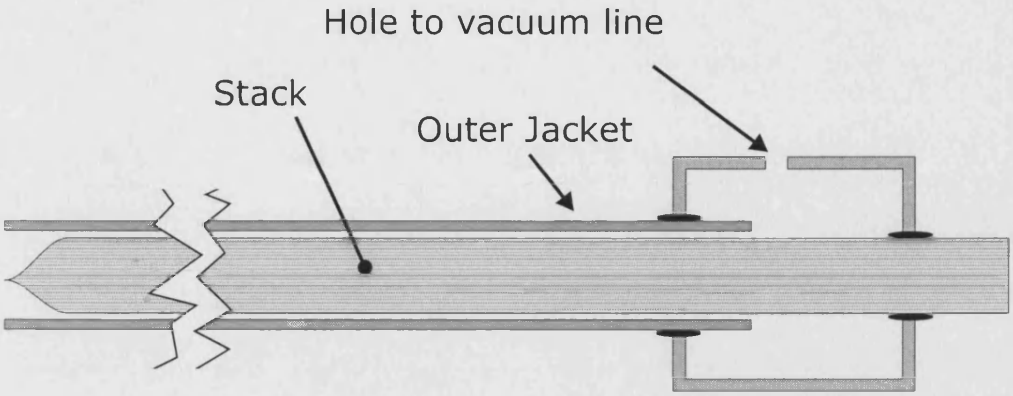

Figure 3.6: Schematic of a completed stack inside it's 1st silica jacket. The vacuum line aids in the removal of interstitial air holes when drawing the stack to preform.

In a process similar to that used in capillary drawing, the equipment previously shown in figure 3.4 is used to reduce the stack and jacket to a few millimeters in diameter. The furnace temperature and drawing speeds are set to ensure that the stack's structure is maintained whilst all the holes between the capillaries and rods collapse under vacuum. The air gaps between the stack and the jacket are also removed at this stage.

3.6 Fibre drawing

The preforms are slid inside their final outer silica jacket and mounted into the apparatus shown schematically in figure 3.7. Once again a vacuum is applied, this time to remove air gaps between the preform and outer jacket. The size of the air holes can be controlled to some extent by varying the pressure within them. This is achieved by using nitrogen line fitted to the top of the preform holder so that only the holes are pressurised.

The preform and outer silica jacket are then drawn to fibre using equipment similar to that used in capillary drawing except that the fibre is pulled from the furnace by a set of belts and wheels, called the capstan, that also measures the tension in the fibre. This gives a good indication of how the temperature is affecting the fibre structure. A low tension reading usually means that the

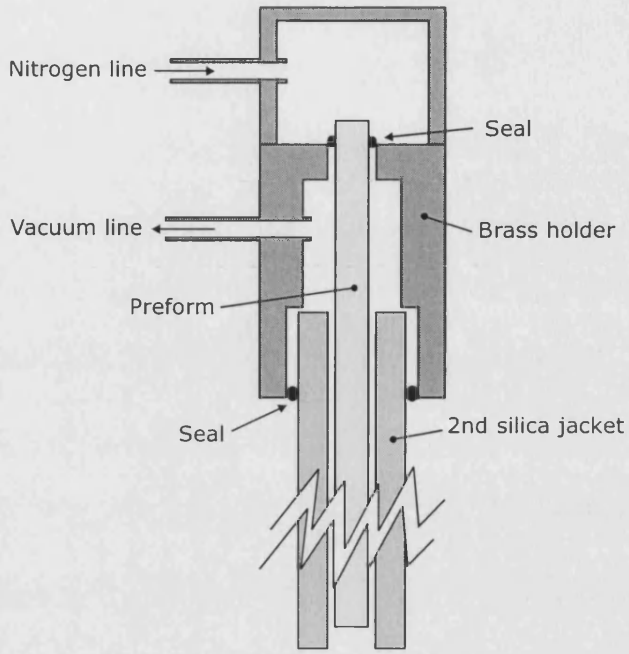

Figure 3.7: Apparatus for holding preform and jacket tube when drawing fibre. The vacuum line ensures removal of any gaps between the preform and the jacket.

temperature is too hot and holey structure is collapsing under surface tension. If the tension is too high the gap between the preform and the outer silica jacket may have not collapsed and/or the fibre could break. The tension is normally maintained at a set value, chosen by experience for each type of PCF, throughout the draw by varying the furnace temperature. For the fibres in this thesis the tension was set to 200 g.

Glass fibres are fragile when scratched. A protective coating must therefore be applied to the fibre if long lengths are to be drawn and stored on drums without breaking. Almost immediately after leaving the furnace the fibre is coated as is passes through a polymer filled cup. The coating is then cured immediately by UV exposure. A 'drum winder' takes up the polymer coated fibre once it leaves the 'capstan'. Figure 3.8 shows a photograph of this equipment in the University's cleanroom.

Providing the uniformity of the preform being drawn is sufficient, with feedback enabled on the preform feed and fibre pull rates, diameter fluctuations in the fibre can be less than ± 0.5 μm over many hundreds of meters.

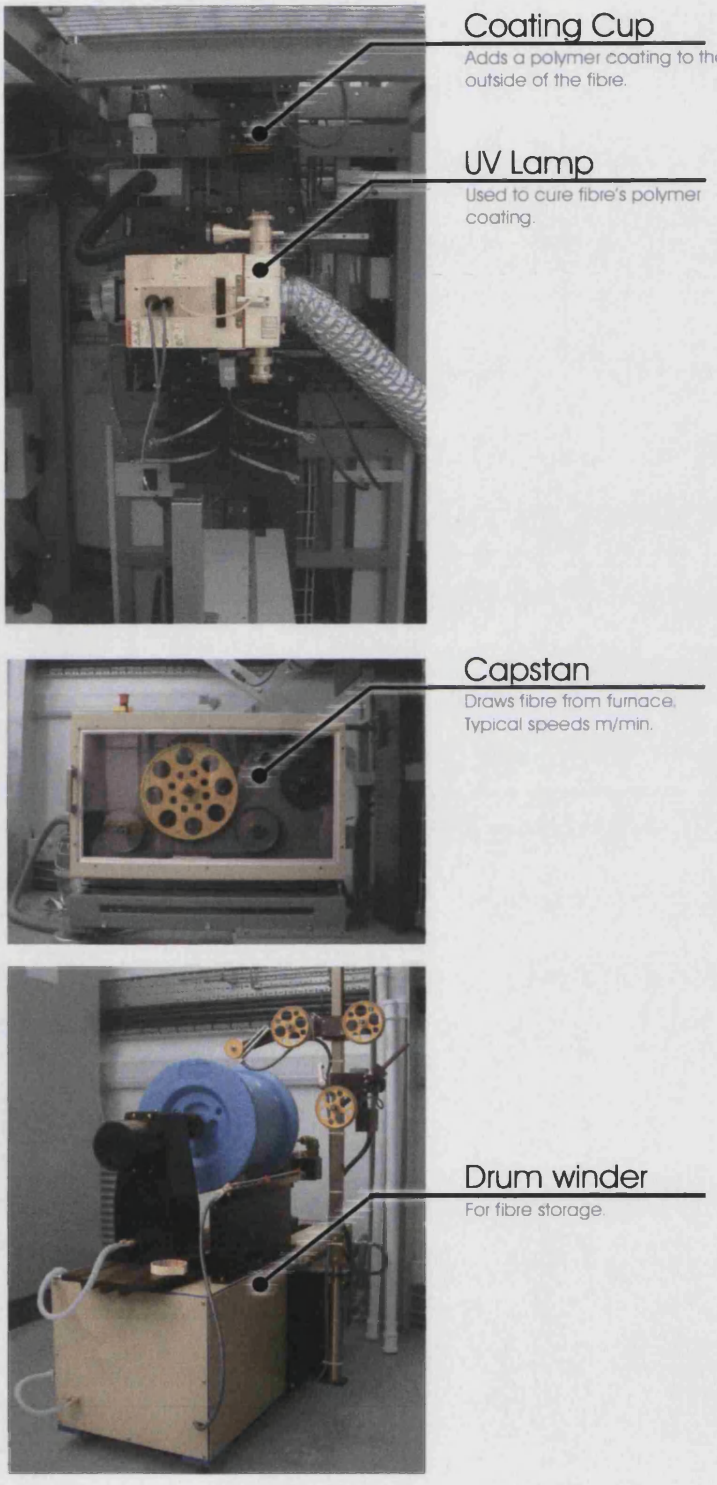

Figure 3.8: Equipment for drawing optical fibre at the University of Bath - see text for details.

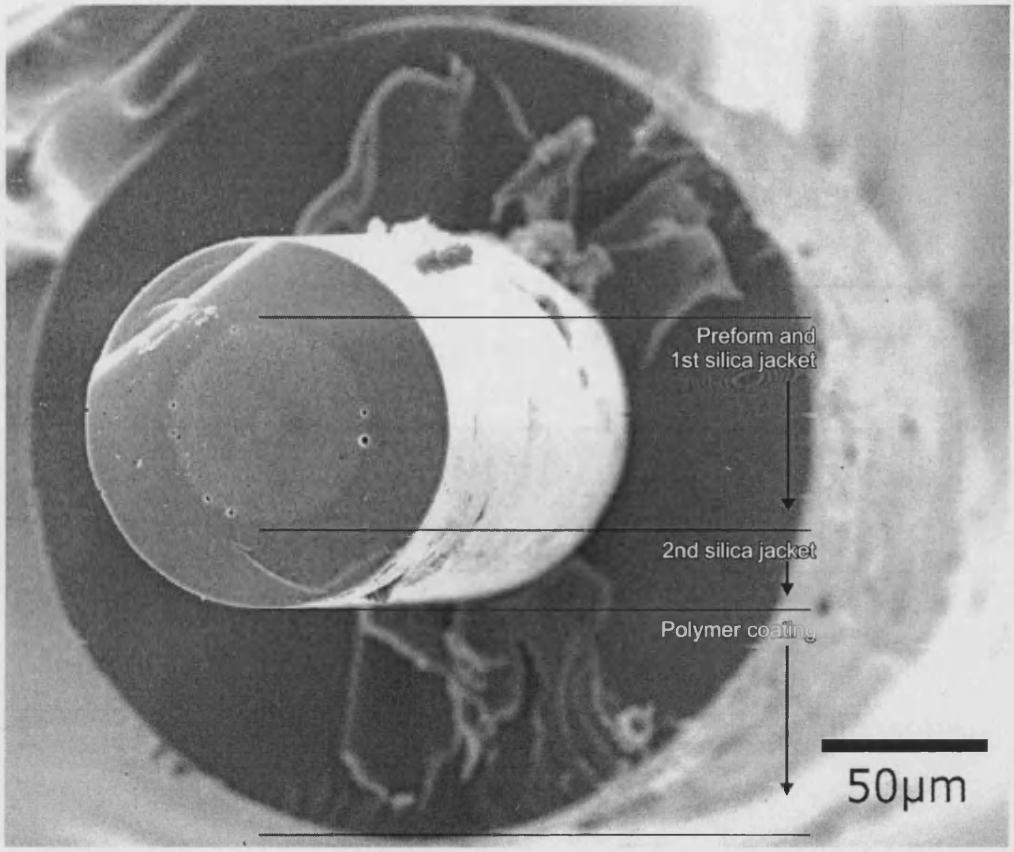

Figure 3.9: A scanning electron micrograph of a completed photonic crystal fibre and polymer jacket

The polymer coating also enables the fibre to be wound onto small drums for storage by using the University's rewinding facility. This is now essential as PCF is now routinely drawn to lengths in excess of 1 km.

Figure 3.9 shows a completed fibre including its external polymer coating.

Chapter 4

Review of nonlinear effects in optical fibre

4.1 Introduction

Silica, from which most PCF and conventional fibre is made, has a relatively small nonlinear refractive index compared to other materials (typically 2×10^{-20} m^2/W, one hundred times lower than the majority of significantly nonlinear materials). However, in addition to the nonlinear refractive index, nonlinear effects scale with light intensity and interaction length. Silica optical fibres are used extensively in the field of nonlinear optics as long-length fibres with small cores can be easily fabricated, which more than compensates for the small value of nonlinear refractive index.

This chapter is intended as an introduction to the field of Nonlinear optics in optical fibres and is based, in part, on material from 'Nonlinear fibre optics' by G.P. Agrawal[14]. In chapter 6, supercontinuum generation within flattened dispersion PCF is investigated. The theory relating to this is included here as an aid to understanding some of the processes that cause this supercontinuum generation.

4.2 The source of nonlinear effects

The response of any dielectric will be nonlinear if the intensities of the incident electromagnetic fields are large enough. These nonlinear effects stem from the anharmonic motion of the medium's bound electrons when perturbed by fields of high intensity. This results in a nonlinear total polarisation $\mathbf{P}$ induced by electric dipoles which satisfies the following relation:

$$\mathbf{P} = \varepsilon_0 \left(\chi^{(1)} \cdot \mathbf{E} + \chi^{(2)} : \mathbf{EE} + \chi^{(3)} \vdots \mathbf{EEE} + \ldots \right) \tag{4.1}$$

where ϵ_0 is the vacuum permittivity, $\chi^{(j)}(j = 1, 2, \ldots)$ is the jth order susceptibility, and the vertically-aligned dots denote tensor index contraction through implicit summation. Note that in general $\chi^{(j)}$ is a tensor of rank (j+1).

χ_1 is the linear susceptibility and has the largest contribution to $\mathbf{P}$. Its effects are manifested through the refractive index n and its associated attenuation constant α (which are related to each other via the Kramers-Kroning relations)[12].

χ_2 is the second order susceptibility that occurs in media that do not have inversion symmetry at the molecular level, and is responsible for second-harmonic generation (or frequency doubling). Fused silica is inversion-symmetric, so χ_2 is zero in most optical fibres. However, it is possible to observe second-order nonlinear effects in optical fibres when they are under the influence of external fields and/or contain non-inversion-symmetric impurities.

χ_3 is the third-order susceptibility and is responsible for the lowest-order nonlinear effects in optical fibres such as four-wave mixing(FWM), third-harmonic generation (THG), and nonlinear refraction. The fibre acts as a mediator for the interactions of FWM and THG and plays no active role in these processes. The fibre properties must therefore be favourable for these effects to be efficient. This implies that the dominant contribution to the nonlinear effects in optical fibres is through the nonlinear refractive index n_2, which is responsible for self-phase-modulation (SPM) and-cross-phase-modulation (XPM).

$$n_2 = \frac{3}{8n} \mathrm{Re}(\chi^{(3)}_{xxxx}) \tag{4.2}$$

where Re is the real part and the optical field is assumed to be linearly polarised so that only one component $\chi^{(3)}_{xxxx}$ of the fourth-rank tensor contributes to the refractive index.

Nonlinear processes can be classified into two categories: those involving 'elastic' (photon energy conserving) interactions such as FWM and SHG, and those involving 'inelastic' interactions such as stimulated Raman and Brilloun scattering, in which some energy is lost to phonons in the medium.

The remainder of this chapter outlines some of these nonlinear effects in more detail.

4.3 Inelastic processes: Stimulated Raman and Brillouin scattering

Inelastic scattering processes can perform frequency conversion via non elastic interactions with medium. The Photon - phonon (quanta of vibrational energy) interactions responsible for frequency conversion are of two different types due to the two types of vibrational modes possible, acoustic and optical[31].

An acoustic mode (acoustic-phonons) is one in which all the ions within a primitive cell move in phase as a unit and the dynamics are dominated by the interaction between cells. Conversely, an optical mode (optical-phonons) is one in which the ions within the cell are in what is essentially a molecular vibratory mode, which is broadened out into a band of frequencies due to the intercellular interactions.

The Raman effect is a result of photon-optical phonon interactions whilst the Brilloun effect involves photon-acoustic phonon interactions.

In both cases, the general form of the most likely interaction is as follows:

$$\underset{(high\ energy)}{\text{Photon}} \longrightarrow \text{Phonon} + \underset{(low\ energy)}{\text{Photon}} \tag{4.3}$$

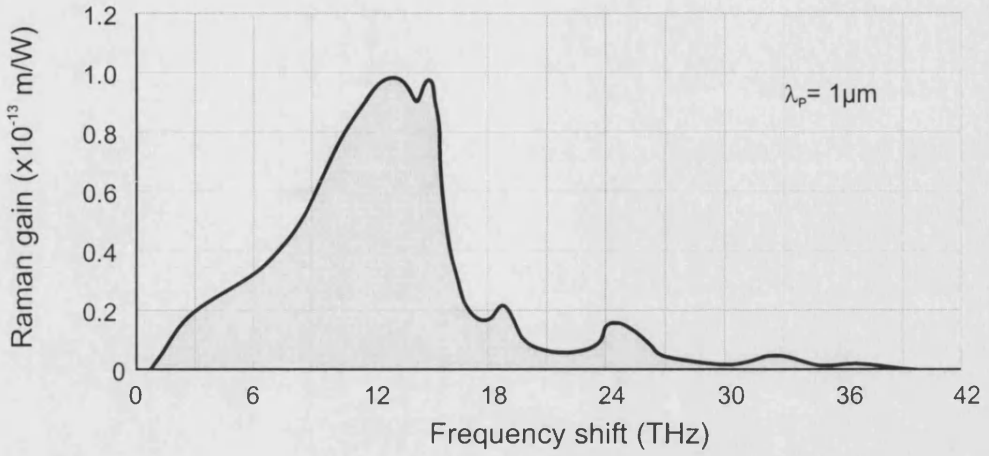

Figure 4.1: The Raman gain spectrum for silica at a pump wavelength of 1 μm.

This interaction converts light to the 'Stokes' frequency - red shift. Additionally, if a phonon with the appropriate energy is available a higher energy photon can be created at the 'anti-Stokes' frequency:

$$\underset{(low\ energy)}{\text{Photon}} + \text{Phonon} \longrightarrow \underset{(high\ energy)}{\text{Photon}} \tag{4.4}$$

This is less likely to occur, however, as phonon with the appropriate energy has to be present (unlike the 'Stokes' case where there is no such requirement).

The Raman gain spectrum of silica is very broad. Figure 4.1 shows an example gain curve for a pump wavelength of 1μm. This is due to the amorphous nature of glass, where the molecular vibrational frequencies spread out into bands and create a continuum. In most other molecular media the Raman gain only occurs at a set of well-defined frequencies.

If no other signals are present, when pump exceeds a threshold intensity value, dependent on the Raman gain coefficient g_R and fibre losses, these frequency conversion processes become self-stimulating according to:

$$\frac{dI_s}{dz} = g_R I_P I_s \tag{4.5}$$

where I_s is the Stokes intensity, the z axis is along the fibre length, and I_P is the pump intensity. Although Raman scattering generates photons within the entire gain bandwidth, the frequency component for which g_R is at maximum will build

up most rapidly. As a result, SRS leads to the generation of a Stokes wave at a frequency determined by the maximum of the Raman gain spectrum. However, if a signal is coincident with the pump, the fibre will act as an amplifier provided that the frequency difference between the pump and the signal lies within the non-zero Raman-gain frequency range.

Stimulated Brilloun scattering (SBS) can also lead to similar effects although the gain spectrum is much narrower, typically $<$ 100 MHz, due to the relatively short lifetime of the acoustic phonons.

4.4 Elastic processes

4.4.1 Parametric processes

Nonlinear processes in which the fibre plays a passive role and merely mediates the interaction of a number of optical waves are called 'parametric'. They are either second or third-order depending on their relationship to either χ^2 or χ^3 respectively. Since in silica glass χ^2 is zero, only χ^3 processes will be discussed here.

Third-order parametric processes generally involve the nonlinear interactions of four optical waves, and conditions for their occurrence can be expressed as follows:

As χ^2 in silica optical fibres is zero the nonlinear polarisation from equation 4.1 can be reduced to the following approximate form:

$$\mathbf{P}_{\mathrm{NL}} = \varepsilon_0 \chi^{(3)} \vdots \mathbf{EEE} \tag{4.6}$$

where $\mathbf{E}$ is the electric field and ε_0 is the vacuum permittivity.

If $\mathbf{E}$ comprises four waves at frequencies of ω_1, ω_2, ω_3 and ω_4, the total electric field can be written as:

$$\mathbf{E} = \frac{1}{2}\hat{x} \sum_{j=1}^{4} E_j \exp\left[i\left(k_j z - \omega_j t\right)\right] + \text{c.c.} \tag{4.7}$$

where all four waves are travelling in the same direction, $k_j = n_j\omega_j/c$, and n_j is the refractive index. By substituting equation 4.7 into equation 4.6 and using $\mathbf{P}_{\mathrm{NL}}$ in a form similar to equation 4.7 we obtain:

$$\mathbf{P}_{\mathrm{NL}} = \frac{1}{2}\hat{x}\sum_{j=1}^{4} P_j \exp\left[i\left(k_j z - \omega_j t\right)\right] + \text{c.c.} \tag{4.8}$$

This results in P_j having a large number of terms involving the products of the amplitudes of three electric fields. As an example P_4, can be expanded to give:

$$\begin{aligned} P_4 &= \frac{3\varepsilon_0}{4}\chi^{(3)}_{xxxx}\left[|E_4|^2E_4 + 2\left(|E_1|^2 + |E_2|^2 + |E_3|^2\right)E_4 + \right. \\ &\quad \left. + 2E_1E_2E_3\exp(i\theta_+) + 2E_1E_2E_3^*\exp(i\theta_-) + \ldots\right] \end{aligned} \tag{4.9}$$

where θ_+ and θ_- are defined as

$$\theta_+ = (k_1 + k_2 + k_3 - k_4)z - (\omega_1 + \omega_2 + \omega_3 - \omega_4)t \quad \text{and} \tag{4.10}$$

$$\theta_- = (k_1 + k_2 - k_3 - k_4)z - (\omega_1 + \omega_2 - \omega_3 - \omega_4)t \tag{4.11}$$

The first four terms in equation 4.9 account for SPM and XPM effects while the other terms result from four wave mixing (FWM) the effectiveness of which depends on the phase mismatch between E_4 and P_4, governed by θ_+ and θ_- or other similarly defined phase angles.

FWM only occurs when the phase mismatch is near zero, which requires matching of both the frequencies and the wavevectors. The energy and momentum must, of cause, be conserved in any interaction. With SRS and SBS this occurs automatically as a result of the active participation of the nonlinear medium (ie. phonon generation). However, this is not true for parametric processes since the total energy can only be carried by photons in these processes.

There are two types of FWM corresponding to θ_+ and θ_- in equation 4.10. The θ_+ term corresponds to the case where three photons are annihilated to produce a single photon at $\omega_4 = \omega_1 + \omega_2 + \omega_3$. If $\omega_1 = \omega_2 = \omega_3$ this is known as third harmonic generation (THG), else if $\omega_1 = \omega_2 \neq \omega_3$ it is known as frequency conversion. The θ_- term corresponds to the case where two photons ω_1 and ω_2 are annihilated to produce two new photons ω_3 and ω_4 with the condition that

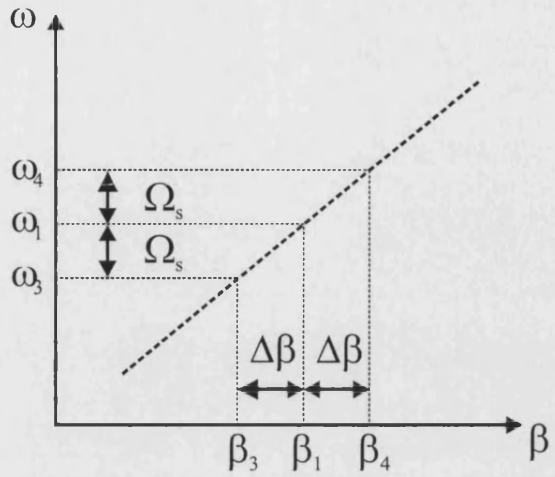

Figure 4.2: ω - β plot for a fibre with zero GVD over a wide frequency range.

$\omega_1 + \omega_2 = \omega_3 + \omega_4$. The phase matching requirement for this to occur is:

$$\Delta k = k_3 + k_4 - k_1 - k_2 = (n_3\omega_3 + n_4\omega_4 - n_1\omega_1 - n_2\omega_2)/c = 0 \tag{4.12}$$

Phase matching for the case where $\omega_1 = \omega_2$ is comparatively easy and is the most relevant for optical fibres. In an energy conserving interaction, two pump photons at ω_1 can create, two sidebands with frequencies equally spaced either side of the pump (called Stokes and anti-Stokes bands by direct analogy with Raman scattering.):

$$\Omega_s = \omega_1 - \omega_3 = \omega_4 - \omega_1 \tag{4.13}$$

In order for this conversion to occur equation 4.12 must also be satisfied. This is achieved when $\beta_1 - \beta_3 = \beta_4 - \beta_1 = \Delta\beta$. A trivial way for this condition to be satisfied (for low powers) is shown in figure 4.2 where β varies linearly with ω, ie. the GVD is zero over the frequency range of interest.

The overall phase matching condition can be broken down into three components:

$$\kappa = \Delta k_M + \Delta k_W + \Delta k_{NL} = 0 \tag{4.14}$$

where Δk_M and Δk_W represent the mismatch arising from material dispersion (related to the refractive index of the material) and waveguide dispersion (related to the change in refractive index imposed by the waveguide). Δk_{NL} accounts extra nonlinear phase shift and only becomes significant at high powers (when it is always positive) and will not be discussed further in this section.

If the effective indices are written as:

$$\tilde{n}_j = n_j + \Delta n_j \tag{4.15}$$

where Δn_j is the change in index due to waveguiding, Δk_M and Δk_W can be expressed as[14]:

$$\Delta k_M = \left[n_3\omega_3 + n_4\omega_4 - 2n_1\omega_1\right]/c \tag{4.16}$$

$$\Delta k_w = \left[\Delta n_3\omega_3 + \Delta n_4\omega_4 - 2\Delta n_1\omega_1\right]/c \tag{4.17}$$

in the partially degenerate case where $\omega_1 = \omega_2$. In order to obtain phase matching at least one of the contributions to $\Delta\kappa$ in equation 4.14 must be negative. In conventional single mode fibres $\Delta k_W \approx 0$ because the index contrast is small however, the structure of PCF can be chosen so that a larger contribution of Δk_W is obtained (for example, cobweb PCF where the GVD zero is shifted to shorter wavelengths). This is advantageous as Δk_W can be engineered to cancel Δk_M and thus to provide an increased extent of phase matching (Δk_M is negative in the anomalous dispersion regime). For example, the fibres presented later in this thesis have regions of flattened and near zero GVD over a wide frequency range.

4.4.2 Solitons

Group velocity dispersion

Group velocity dispersion (GVD) is a linear phenomenon and was introduced in section 2.2.2. Chromatic dispersion (ie. the variation of GVD with wavelength) makes the different spectral components of the pulse travel at different velocities. The phase angle at a given time T and propagation distance z is different, in general, for each spectral component of which the pulse is composed. The time derivative is approximately the frequency difference from ω_0 (the central frequency of the pulse):

$$\delta\omega(T) = \frac{\mathrm{sgn}(\beta_2)(2z/L_D)}{1+(z/L_D)^2}\frac{T}{T_0^2} \tag{4.18}$$

If $\beta_2 > 0$ red components arrive first (blue if $\beta_2 < 0$) and there is a frequency change, which varies linearly with T across the pulse, called chirp. GVD alters

the pulse shape but has no effect on the pulse spectrum; it merely spreads-out the frequency components in time, resulting in broadened pulses.

Self phase modulation

Self phase modulation (SPM) is a nonlinear effect and it causes an intensity-dependent phase shift in optical pulses. SPM causes the phase shift through the intensity dependance of the refractive index.

$$\tilde{n}(\omega, I) = n(\omega) + n_2 I \tag{4.19}$$

The phase of an optical field due to nonlinear effects is:

$$\phi_{NL}(L,T) = |U(0,T|^2(L_{eff}/L_{NL}) \tag{4.20}$$

where $U(0,T)$ is the field amplitude at $z = 0$ and L_{eff} is the effective interaction length defined as follows:

$$L_{eff} = \frac{1 - \exp(\alpha L)}{\alpha} \tag{4.21}$$

where α is the fibre loss coefficient. L_{NL} is the nonlinear length, which provides a scale for which nonlinear effects become important, and is defined by:

$$L_{NL} = \frac{1}{\gamma P_0} \tag{4.22}$$

where γ is the nonlinear parameter and is defined by:

$$\gamma = \frac{n_2 \omega_0}{c A_{eff}} \tag{4.23}$$

The maximum value of phase shift is to be found at the pulse centre, where the intensity is largest, and it is given by:

$$\phi_{max} = \frac{L_{eff}}{L_{NL}} = \gamma P_0 L_{eff} \tag{4.24}$$

SPM can induce spectral broadening as a consequence of the time-dependence of ϕ_{NL} and the induced frequency chirp that increases in magnitude with the propagated distance. New frequency components are therefore generated continuously

as the pulse propagates along the fibre.

Solitons: the combination of GVD and SPM

In the anomalous dispersion regime it is possible for the phase shifting effects of the GVD to compensate those of SPM. The two chirp contributions nearly cancel in the central portion of the pulse when $L_D = L_{NL}$ and form the fundamental soliton.

Solitons of higher-order can also form and the order N of a soliton can be found using the following relation:

$$N^2 = L_D/L_{NL} \tag{4.25}$$

where L_D is the dispersion length, which provides a scale on which dispersive effects become important, and can be expressed as:

$$L_D = \frac{T_0^2}{|\beta_2|} \tag{4.26}$$

The power P_0 required to generate a soliton of order N in a medium with anomalous dispersion can be expressed as:

$$P_0 = \frac{N^2|\beta_2|}{\gamma\tau_0^2} \tag{4.27}$$

where τ_0 is the initial pulse width.

There is an infinite set of higher-order solitons but an important subset consists of those which have an initial sech shape. These have periodic variations in shape with propagation distance. These soliton forms are known as 'breathers' and have a spatial soliton period z_0 of

$$z_0 = \frac{\pi}{2}L_D = \frac{\pi}{2}\frac{T_0^2}{\beta_2} \tag{4.28}$$

As an example, figure 4.3 shows the evolution of the third order soliton over approximately three soliton periods[1]. The plot on the left shows evolution of

[1]Data provided by Mr. F. Biancalana

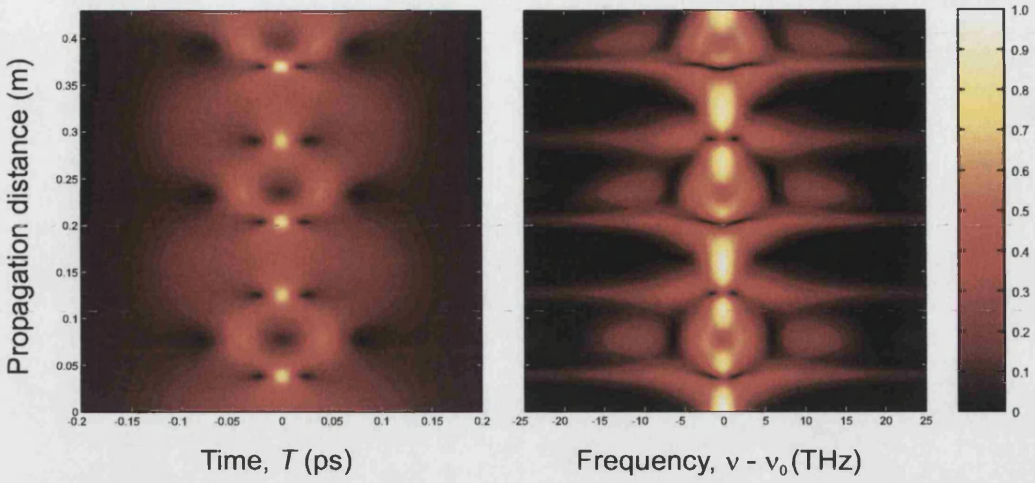

Figure 4.3: An example of the temporal (left) and spectral (right) evolution of a higher (2nd) order soliton with propagation distance plotted on a linear intensity scale.

temporal profile with propagation distance. The plot on the right shows the associated spectral profile for the same propagation distance.

4.4.3 Higher order effects

The effect of higher order dispersion

When β_2 is small, the third order dispersion (TOD) becomes more important and it affects the SPM-induced spectral broadening. When β_3 is positive, oscillations form on the trailing edge of the pulse. Conversely, oscillations form on the leading edge of the pulse with negative β_3. With increasing values of β_2, these oscillations become progressively damped and eventually become a smooth tail. For large values of β_2 the tail becomes insignificant.

For solitons propagating relatively far from λ_D it can be shown that TOD does not affect amplitude, frequency or phase but simply delays the soliton peak by an amount that increases with distance.

Fibres with flattened dispersion profiles have small values of β_3. Should β_2 also be small, β_4 must be considered as it will become the dominant dispersion term.

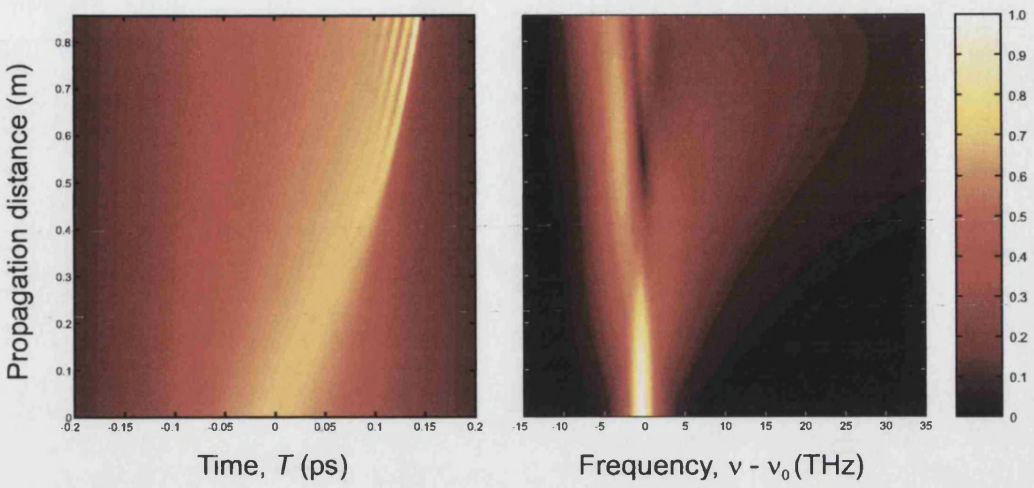

Figure 4.4: An example of the temporal (left) and spectral (right) evolution, with propagation distance, of a pulse experiencing the buildup of optical shock plotted on a linear intensity scale.

Self-steepening

Group velocity is dependent on intensity, resulting in the slower propagation of more intense pulse components. Should the centre of the pulse be delayed so that it attempts to arrive after the trailing edge of the pulse, an optical shock wave is created, as the pulse intensity envelope cannot be multi-valued. Figure 4.4 shows an example of this, for which equation 4.29 was solved[2] whilst excluding Raman effects and where β_2 was set equal to zero. The temporal plot clearly shows the buildup of a shock front and the frequency plot shows that self-steepening causes an asymmetric broadening and red-shifting of the pulse.

Soliton self frequency shift

Soliton self-frequency-shift (SSFS) was discovered in 1986 when Mitschke *et al* and Gordon studied sub-picosecond pulses in a single-mode, polarisation-maintaining optical fibre[32, 33]. They observed a continuous (rather than discrete) shift in the optical frequency of a soliton as it travelled along a fibre.

If pulses are sufficiently short (ie. if they have broad spectral profiles) and if their

[2]Data provided by Mr. F. Biancalana

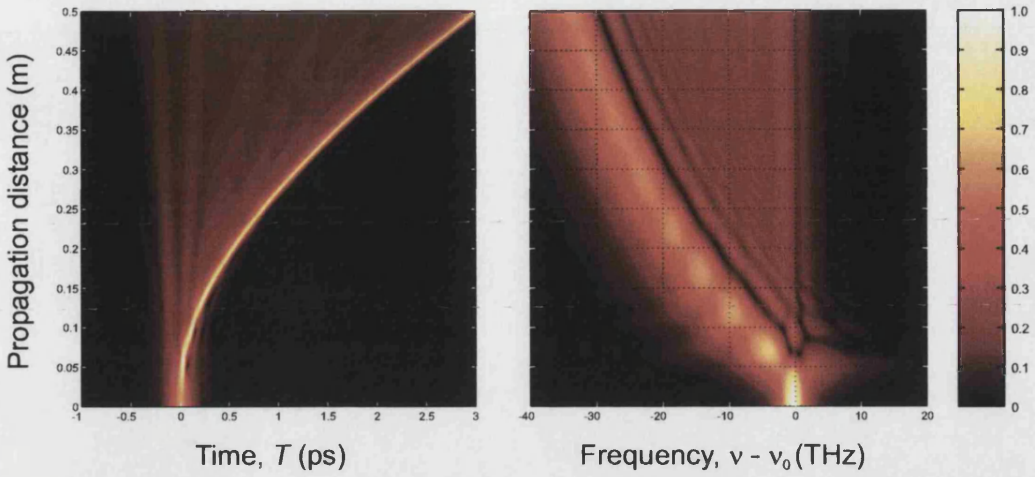

Figure 4.5: An example of the temporal (left) and spectral (right) evolution, with propagation distance, of a soliton experiencing self-frequency-shift plotted on a linear intensity scale.

intensities are sufficiently high, they have the potential to experience SSFS. The pulse spectrum's higher-frequency components can act as a Raman pump for the lower frequencies, depending on the profile of the Raman gain spectrum (which will be similar to figure 4.1). The conversion is not 100 % efficient and energy is lost from the soliton in the form of non-solitonic dispersive waves. Figure 4.5 shows an example of this[3] from modelling where optical shock is neglected and β_2 is negative and constant. The temporal plot clearly shows the delay of the soliton and the loss of energy that constitutes non-solitonic radiation. The frequency plot shows the frequency shift of the soliton and the continuum of the dispersive waves. One interesting feature is the series of 'steps' that appear in the frequency plot. These are discussed in detail in chapter 6.

[3]Data provided by Mr. F Biancalana

4.5 Supercontinuum generation

When combinations of the aforementioned nonlinear effects occur, optical pulses in fibres may spectrally broaden into a super-continuum.

PCF have received much attention in this field as they can be very efficient in generating supercontinua due to the small effective modal areas possible, coupled with an excellent degree of control over the waveguide dispersion. This increases the attainable nonlinearity of the fibre and allows pumping of the fibres near their ZDWs.

The low pulse energies required for continuum generation (for example, more than two octaves from 5 nJ, 200 fs-long pulses[6]), it's coherently pulsed nature, and the high spatial brightness in the fundamental mode make PCF continuum sources ideal for many applications such as femtosecond-pulse phase stabilization[34], optical coherence tomography[35], ultrashort pulse compression, spectroscopy and fibre characterisation. Additionally, since the PCF are pumped using a periodic pulse train from a mode-locked laser (also described in the frequency domain as a comb of equidistant modes) the supercontinuum is also a frequency comb of equally spaced frequencies separated by the repetition rate of the laser. This feature has been used extensively in the field of frequency metrology[34, 36, 37, 38].

Many papers (for example [39, 40, 41, 42, 43, 44]), both theoretical and experimental, have been published with the aim of understanding the processes involved in generating supercontinua. Convincing evidence suggests that Raman scattering leads to the fission of higher order Solitons and that the energy lost from the solitons in this breakup is non-solitonic radiation that continuously shifts to shorter wavelengths than the pump, due to phase-matching-selected FWM processes. As the power is increased, the bandwidth of the supercontinuum grows and its intensity spectrum becomes flatter.

4.6 Modelling pulse propagation in optical fibre

If pulse propagation in optical fibres is to be modelled accurately, all of the aforementioned linear and nonlinear effects must be accounted for. The equation that is usually solved, using the split-step Fourier method[14], is called the 'Generalised' or 'Extended Nonlinear Schrödinger Equation' (GNLSE):

$$\overbrace{i\partial_z A(z,T)}^{1} + \overbrace{\sum_{m\geq 2} \frac{i^m}{m!}\frac{L_{D2}}{L_{Dm}} sgn(\beta_m)\partial_T^m A(z,T)}^{2} + \\ + \underbrace{N^2\left(1+\frac{i}{\omega_0 T_0}\partial_T\right)}_{3}\underbrace{\left[A(z,T)\int_{-\infty}^{\infty} R(T')A|(z,T-T')|^2 dt'\right]}_{4} = 0 \qquad (4.29)$$

where A is the amplitude of the pulse envelope, T is measured in a reference frame moving at the group velocity such that $T = t - z/v_g$, and ω_0 is the pump frequency. Gaussian pulses are considered in this discussion where T_0 is the initial duration and $T_{FWHM} \approx 1.763T_0$. Fibre losses are omitted here as the experiments in chapter 6 were conducted on short lengths of fibre. The numbered terms in equation 4.29 will now be described in turn:

Part 1 accounts for the evolution of the envelope of the pulse with propagation distance. In this case, backward-propagating waves are neglected.

Part 2 accounts for the total dispersion in the fibre. If pulses are long, ie. $T_0 >$ 0.1 ps, the light can be considered monochromatic and only a constant value of β_2 is required - the slowly varying envelope approximation (SVEA). However, as the pulses become shorter in time and broader in frequency the dispersion must be specified more precisely. β_m is the m$^{\text{th}}$ order dispersion coefficient from the Taylor expansion of dispersion for short pulses (equation 2.9). L_{Dm} is the m$^{\text{th}}$ order dispersion length defined as $L_{Dm} = T_0^m/|\beta_m|$. Dispersion also determines the phase mismatch which affects parametric processes such as four wave mixing (FWM) and third harmonic generation (THG).

The time derivative in part 3 accounts for self-steepening and shock formation at the pulse edge.

Part 4 accounts for the Raman effect. $R(T')$ is the Raman response function

which includes instantaneous and delayed contributions. Instantaneous effects arrise from interactions with electrons, whilst the delayed contributions are from nuclear interactions:

$$R(T) = (1 - f_R)\delta(T) + f_R \frac{\tau_1^2 + \tau_2^2}{\tau_1 \tau_2^2} e^{-T/\tau_2} \sin\left(\frac{T}{\tau_1}\right) \Theta(T) \qquad (4.30)$$

where f_R is a coefficient that represents the relative importance of the delayed Raman response with respect to the nonlinear polarisation P_{NL}. f_R is usually taken to be 0.18. τ_1 and τ_1 are empirical adjustable parameters chosen to provide a good fit to the actual Raman gain spectrum and are normally set to be 12.2 and 32 femtoseconds respectively. $\Theta(T)$ accounts for causality and is the Heavyside step function.

Chapter 5

Design, Fabrication and characterisation of ultra-flattened dispersion PCF

The large variety of structures available to the PCF designer allow an unprecedented extent of control over the waveguide dispersion. This is a significant benefit as dispersion plays a fundamental role in optical fibres, especially when propagating short pulses.

One particular dispersion profile of interest is one with a small slope over a wide wavelength range. Significant dispersion flattening has been achieved using step-index fibre technology, but this chapter presents evidence of the first PCF with *ultra-flattened* dispersion to be fabricated.

5.1 Motivation

Flattened dispersion fibres have enabled the development of large-bandwidth telecommunications. The reduction of pulse spreading in such fibres has allowed the propagation of ultra-short pulses in multiple channels, resulting in a bandwidths in excess of tens of Gbits of data per second. If the value of the flattened dispersion is close to zero, new frequencies can be generated via phase-matched

parametric processes such as four-wave mixing (see Chapter 4). These types of fibre can be used to generate supercontinuua[10, 45] and can strengthen signals though parametric amplification[46, 11]. Conversely, fibres used in WDM telecommunications are made with non-zero values of flattened dispersion to suppress crosstalk between channels that can be caused by phase-matched processes.

In conventional optical fibres, dispersion-flattening is achieved by introducing additional doped glasses between the core and the cladding in concentric rings. The simplest example has one additional ring of glass around the core with refractive index lower than both the core and the cladding, the so-called 'W' fibre.

A number of papers investigate this type of fibre and the design of a maximally flat dispersion profile. These papers are, however, constrained by the condition that the fibres must remain single mode within the standard telecommunications wavelength bands. Lundin *et al*[47] present a fibre that is single-mode in the range 1.2 to 1.6 μm, with values of dispersion of -5 ps/nm.km at 1.2 μm, just above 0 ps/nm.km at 1.4 μm, and -3 ps/nm.km at 1.6 μm.

Lee *et al*[48] designed dispersion flattened fibres for the C and L communication bands. Their fibre has a dispersion of 3.94 ps/nm.km at 1.53 μm, 4.18 ps/nm.km at 1.55 μm with a slope of 0.015 ps/nm^2.km, and 4.18 ps/nm.km at 1.565 μm. The fibre had a mode-field diameter of 7.7 μm and a single-mode cutoff at 1.1 μm.

Provided the d/Λ ratio is less than 0.4, PCF is endlessly single mode[27]. This advantage coupled with the greater control over waveguide dispersion, suggests that PCF should be able to provide flatter dispersion profiles over a much wider wavelength range than that of modified conventional fibre.

5.2 Designs

5.2.1 Design 1: wide wavelength range

In 2000 and 2001, Ferrando *et al* proposed a range of PCF designs with ultra-flattened dispersion profiles[49, 50]. The strategy used to design these fibres

was based on the approximation that the total dispersion is equal to sum of the geometric (waveguide) and material dispersion. Control over the geometric dispersion in PCF is greater than for conventional fibre due to the large range of structures and large core/cladding effective refractive index contrasts achievable. In order to flatten the dispersion profile they simply matched the geometric dispersion slope with the signed-negated material dispersion slope in the wavelength range of interest. In their Optics Letters paper[49], they present examples of two possible fibres. One fibre had a dispersion of ± 1 ps/nm.km over a wavelength range of 543 nm centered at approximately 1520 nm ($d \approx 0.73$ μm, $\Lambda \approx 3.02$ μm). By choosing a narrower wavelength range (of width 482 nm) of flattened dispersion, a fibre with a dispersion of ± 0.5 ps/nm.km was proposed ($d \approx 0.63$ μm, $\Lambda \approx 2.64$ μm). Initially, the second of these two designs was singled-out for re-examination in an effort to establish the extent to which the modelling results are repeatable.

Modelling issues and validity of the plane wave expansion method

Modelling was undertaken, using existing code written by Dr. Jesus Arriaga, in order to verify their result. Both modelling methods find the propagation constant of the guided modes by solving Maxwell's equations by expressing the solution as a linear combination of plane waves. However, their results could not be reproduced.

Our code is known to be accurate for fibres with hole diameters of the order of a few microns. For the sub-micron hole diameters specified by Ferrando *et al.* a large number of plane waves were required for convergence. Figure 5.1 shows the results of numerous calculations for a fixed pre-specified fibre structure using various numbers of plane waves. Unfortunately, the number of plane waves required for convergence was large due to the small hole sizes, ≈ 0.5 μm, requiring a high spatial resolution.

Ferrando *et al.* suggest that for $d = 0.63$ μm and $\Lambda = 2.64$ μm the flattened dispersion region is centered at 0 ± 0.5 ps/nm.km. Using our model we find larger values of dispersion and a different slope.

The discrepancies between our model and that of Ferrando *et al.* are likely to

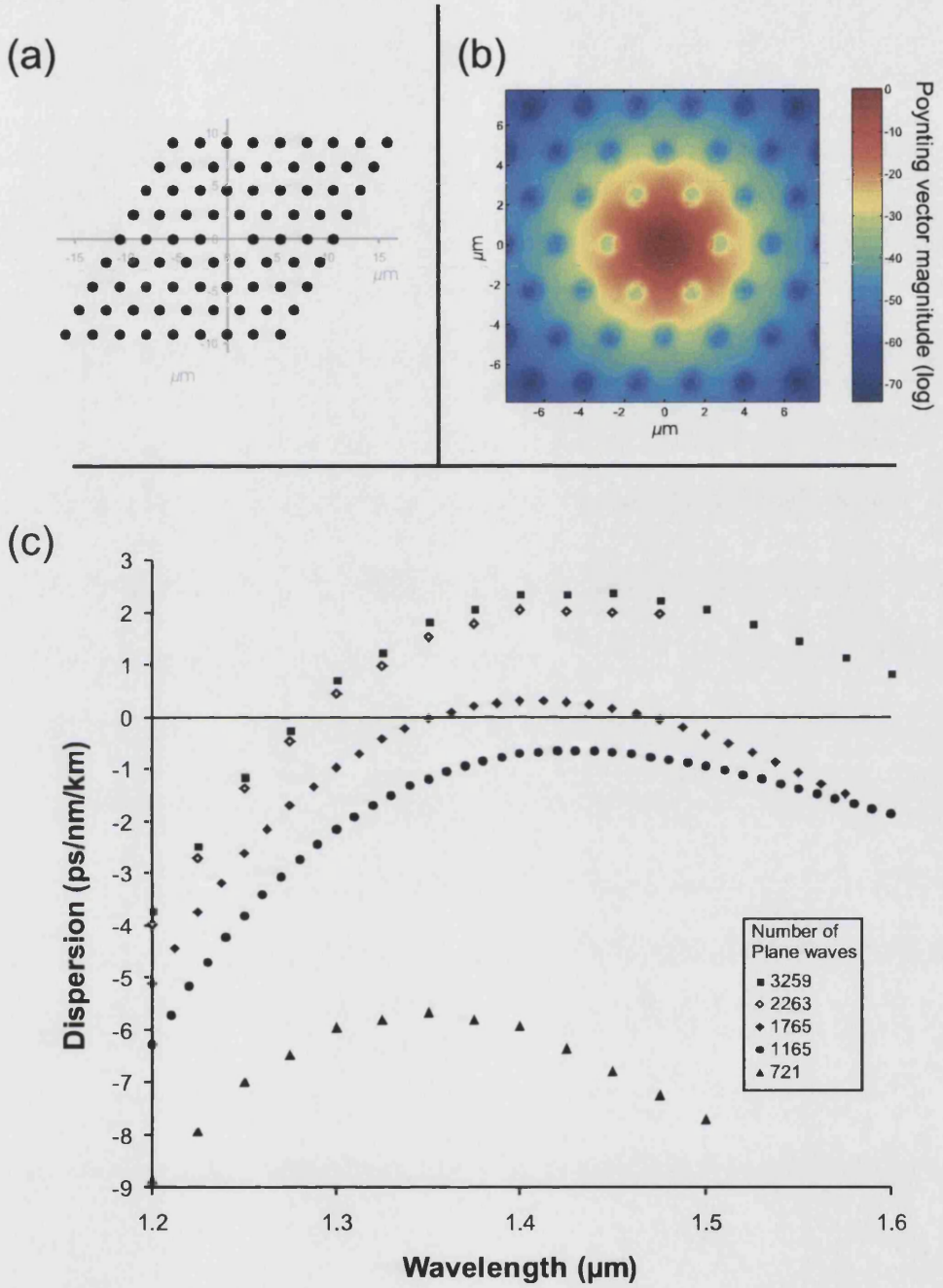

Figure 5.1: (a) The super cell used to calculate the dispersion profiles in (c). For this case $d = 0.63$ μm and $\Lambda = 2.64$ μm. (b) The magnitude of the Poynting vector at 1.5 μm calculated using 1165 plane waves. (c) Dispersion profiles calculated by varying the number of plane waves used in the expansion. The solution for this particular problem appears to converge for linear combinations of more than 2263 plane waves.

be due to the definition of the supercell and the number of plane waves used. For example, the relatively poor confinement of the light to the fibre core meant that large numbers of periods had to be incorporated into the supercell in order to reduce unphysical modal overlap between adjacent cells. It is unknown how many periods Ferrando *et al.* used.

The modelling of PCF with small holes using plane wave expansion is perhaps less accurate than for other methods unless very large numbers of periods and many plane waves are used. However, the results from this modelling technique were sufficient for initial fibre fabrication.

5.2.2 Design 2: maximally flat dispersion PCF at 1550 nm

Once the fabrication procedure was optimized another design was attempted: fibres with maximally flat dispersion profiles. These profiles would ideally have zero dispersion slope at 1.5 μm and be flattened in an approximate 2-300 nm range.

Due to the discrepancies with the plane wave expansion method, an alternative modelling technique was used to determine the required hole diameter and pitch for these fibres. This modelling was undertaken by Dr. John Roberts of Blaze Photonics[1], and was based on the Multipole method[25, 51]. The data generated from these calculations is shown in figure 5.2. (a) shows the calculated dispersion at 1550 nm for PCF with a range of hole radii and pitches. (b) shows the calculated dispersion slope at 1550 nm for the same PCF parameter range. The desired parameters for maximally flat dispersion slope fibre are therefore approximately $d = 0.59$ μm ($a/\Lambda \approx 0.116$) and $\Lambda = 2.56$ μm, at the intersection of zero dispersion and dispersion slope.

It can be seen that small changes about this point in the ratio of radii/pitch result in a large variation in the value of the dispersion and slope at 1550 nm. However, simply scaling the structure by a few percent has a only a small effect on the dispersion slope and dispersion. These two plots proved invaluable when fabricating the ultra-flattened dispersion PCF.

[1] A 'spin-off' photonics company from the University of Bath's optoelectronics group - for more information see www.blazephotonics.com

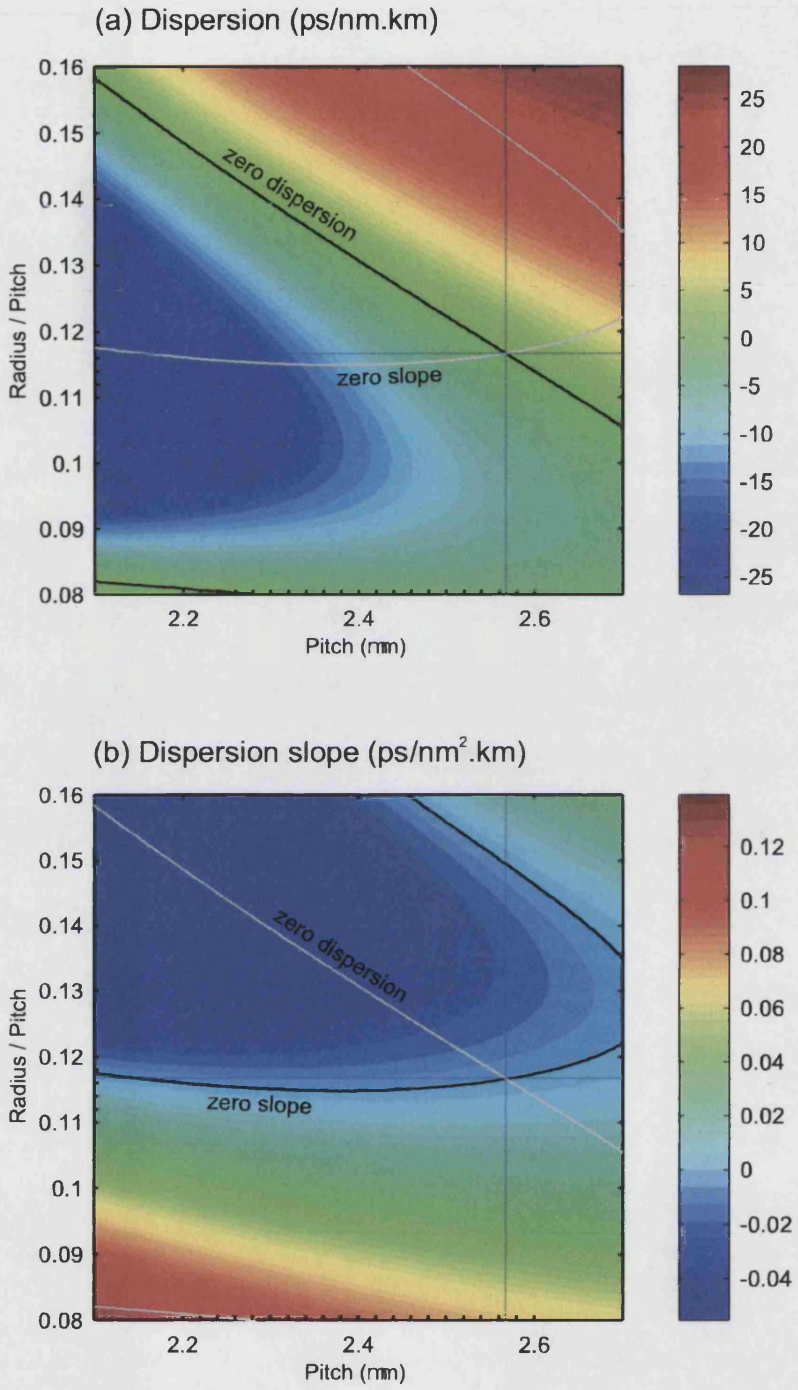

Figure 5.2: (a) Calculated dispersion at 1550 nm for PCF, against pitch and hole radius/pitch. The locus of zero dispersion slope is represented as a grey line for reference. (b) Calculated dispersion slope at 1550 nm for PCF, against pitch and hole radius/pitch. The locus of zero dispersion is represented as a grey line for reference.

5.3 The fibres

The basic fabrication procedure for making fibres with structures similar to those required for flattened dispersion is outlined in Chapter 3. However, it is non-trivial for these cases for a number of reasons, which will now be described.

The holes are sub-micron in diameter and this in itself causes a number of problems. The interstitial holes between the capillaries of the stack are of comparable diameter to the required holes. Normally a negligible effect in cobweb or large-hole PCF, the interstitial holes tend to deform the structure when they collapse during fabrication.

Whilst approximations could be made with an optical microscope, the low tolerance on the hole diameter (see figure 5.2) required more accurate measurements to be made by scanning electron microscopy (SEM). This meant that adjustments to the fibre drawing parameters could not be made while drawing and resulted in a substantial increase in fabrication time.

Although confinement loss was expected to be large, it was hoped that two periods of holes with $d = 0.63\ \mu$ and $\Lambda = 2.64\ \mu$ would affect the waveguide dispersion sufficiently. It was hoped that the addition of outer periods with a d/Λ ratio of 0.4 would reduce confinement loss. The software package "BeamProp", manufactured by Optima Research, was used to model the fundamental mode of this design. Figure 5.3(b) shows the theoretical profile of the fundamental mode at 1550 nm. (a) shows a scanning electron microscope image of the fibre, and (c) shows the near-field intensity pattern at 633 nm recorded using a CCD camera.

Unfortunately the fibre had very large losses, too high for dispersion measurements to be made. It was concluded that more periods were required to reduce this loss.

A fibre with seven complete periods (eight with the corners removed corresponding to 186 holes) was therefore fabricated, again with the target $d = 0.63\ \mu$m and $\Lambda = 2.64\ \mu$m. These target values were obtained iteratively through both structural measurements made on SEM images, and by measuring the fibre's dispersion using the low coherence interferometric technique described in Section 2.4.1. Figure 5.4 shows a SEM of one particular fibre.

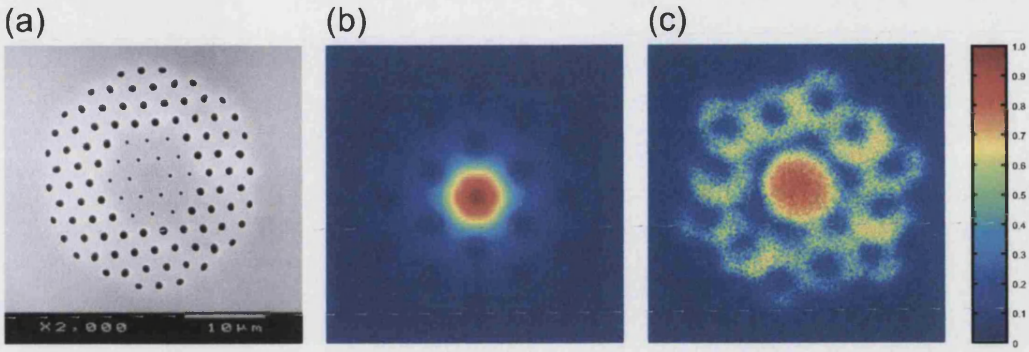

Figure 5.3: (a) A SEM of a flattened dispersion PCF with a pitch of 2.5 μm and two different hole diameters of 0.5 μm and 1 μm. (b) Theoretical (at 1550 nm) and (c) Measured (at 633 nm) nearfield profiles of the fundamental mode from the fibre shown in (a). The scale for (b) and (c) is arbitrary and linear (shown on the right).

Figure 5.4(b) shows the measured dispersion for a selection of different PCFs. Even though the hole size and pitch for some of the fibres were measured to be within a few percent of the ideal dimensions (for example $d \approx 0.63$ μm, $\Lambda \approx 2.55$ μm), the measurements of dispersion did not match those predicted by Ferrando *et al.*

A suggested explanation for the discrepancy in GVD was that the guided mode was still not sufficiently well confined. Modelling by John Roberts suggested that in order for the dispersion to converge towards that of a PCF with an infinite cladding, 8 or more rings would be needed.

In order to test this hypothesis yet another fibre was made, this time with 455 holes (corresponding to 11 complete periods between the core and the external jacket). Figure 5.5(a) shows an SEM of this PCF.

Figure 5.5(b) shows the dispersion profiles for two PCFs with similar structures. The fibre with the larger dispersion slope (blue curve) had a measured Λ of 2.47 μm. The value of d varied over the microstructure and an average diameter of 0.57 μm was measured over the first 6 periods with standard deviation 0.06 μm. The fibre with the larger flattened range has $\Lambda = 2.59$ μm and an average d of 0.58 μm with a standard deviation of 0.05 μm.

Even though the values of dispersion were near to the predicted values in the

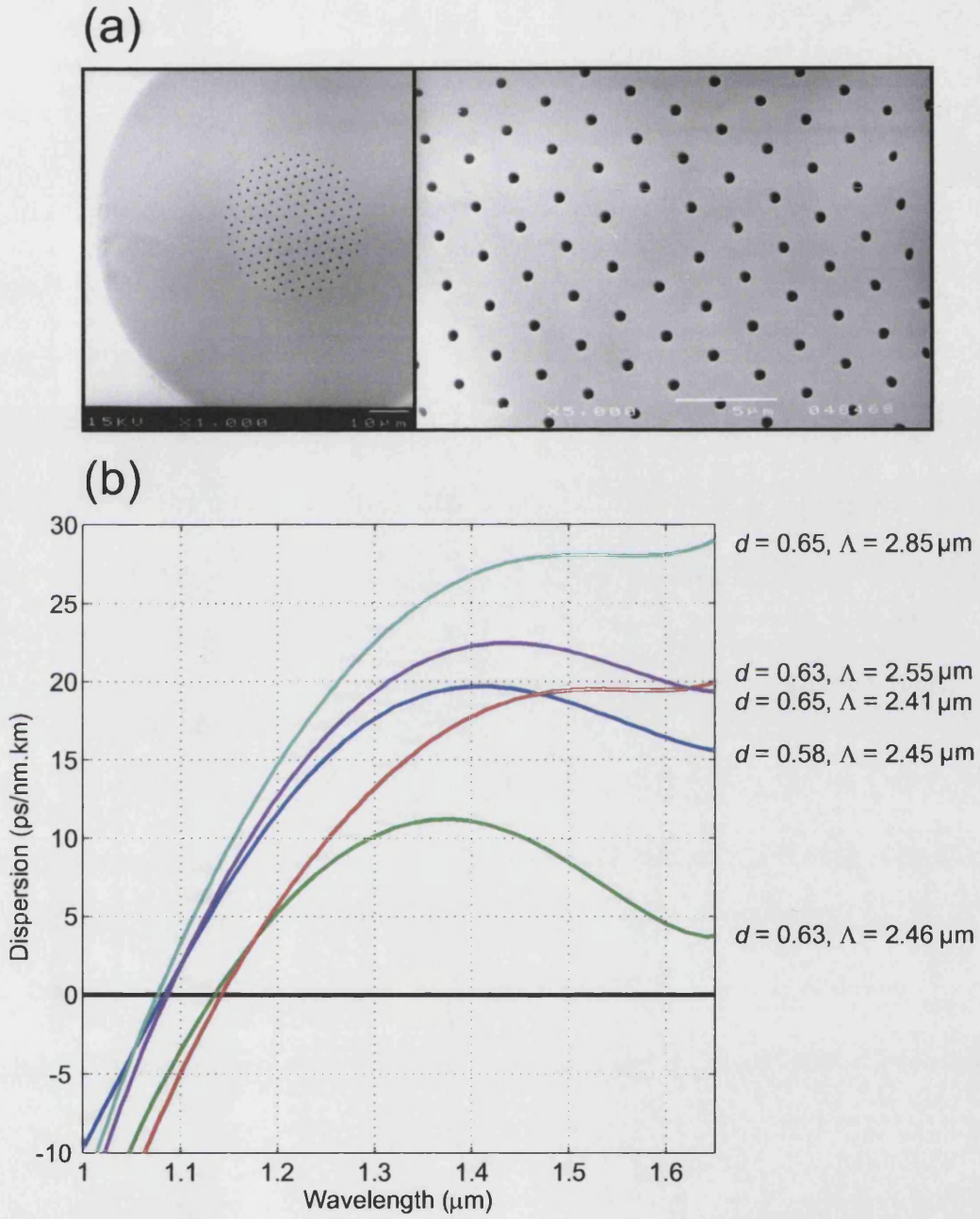

Figure 5.4: (a) A dispersion flattened photonic crystal fibre with 7 periods in the cladding and with $\Lambda \approx 2.5$ μm and $d \approx 0.5$ μm. (b) Measured dispersion profiles for a number of fibres with similar structures.

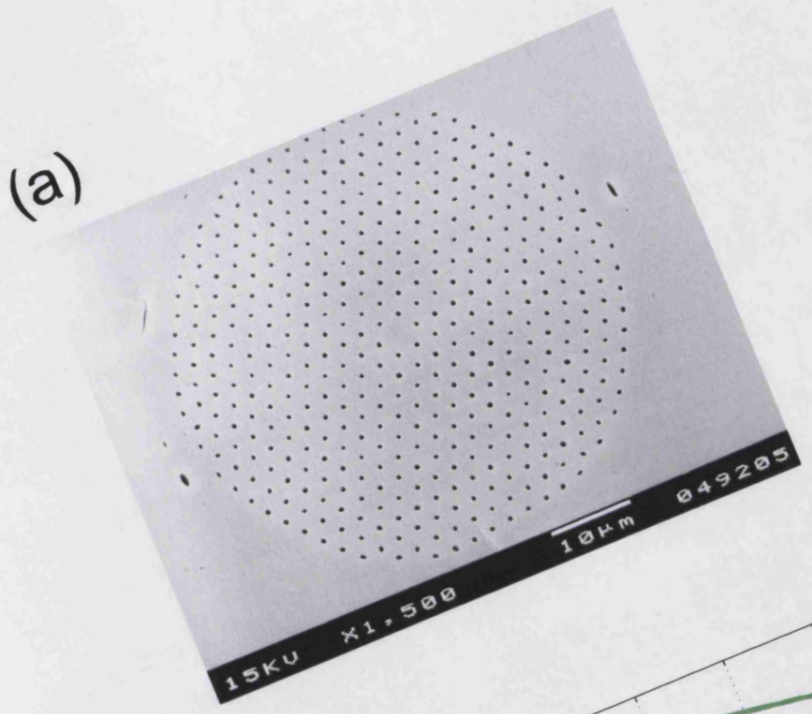

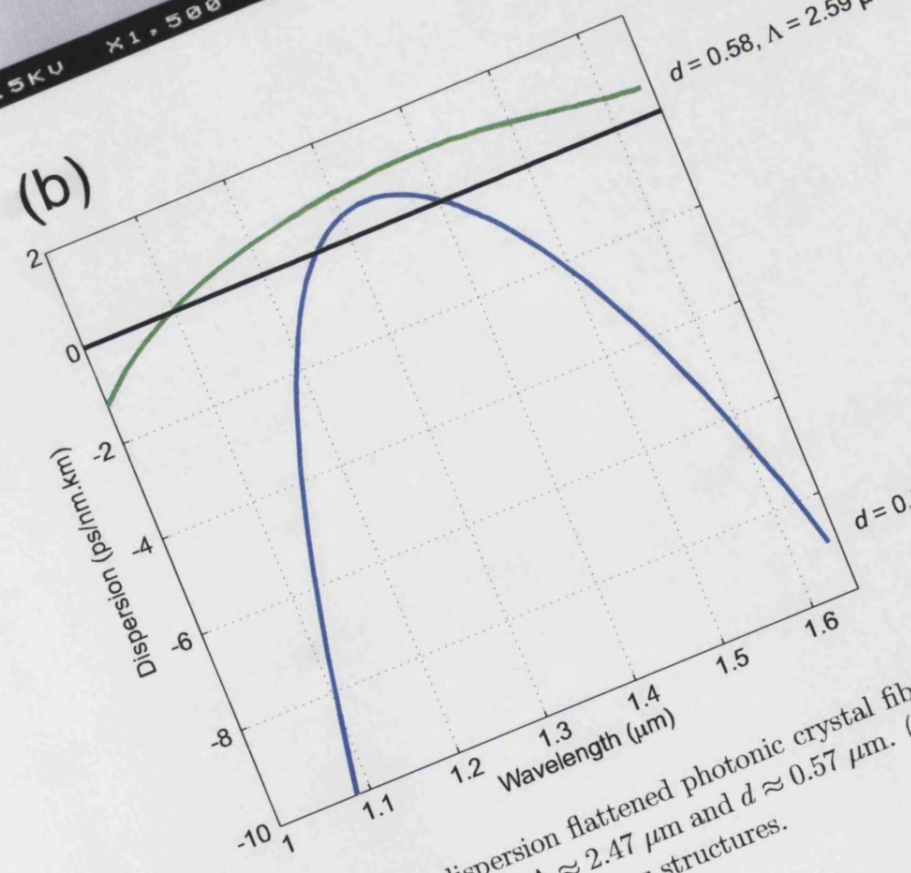

Figure 5.5: (a) A dispersion flattened photonic crystal fibre with eleven periods in the cladding and with $\Lambda \approx 2.47$ μm and $d \approx 0.57$ μm. (b) Measured dispersion profiles for two fibres with similar structures.

wavelength range between 1.2 and 1.5 μm, the dispersion slope differed greatly. Additionally, the difference between the dispersion profiles of the two fibres was large when compared to the physical difference in their structures. The cause of this discrepancy was attributed to the fluctuations in d and Λ along the length of the fibres. This suggested that various problems with the fabrication procedure had to be addressed.

Normally in each stage of fabrication, the fibre's d/Λ ratio falls due the collapse of the holes under surface tension. Small holes collapse at a proportionally faster rate than large holes. In the case of the exceptionally small d required by flattened dispersion PCF design, fibre drawing required a cold, fast draw. Preforms were small in diameter and therefore fed into the furnace at the fastest rate possible to reduce the cumulative amount of time in which the glass resided in the hot zone. For all of the fibres previously described, this resulted in fibre being drawn at 2-4 m/min, far outside of the operating specifications of the capstan and the fabrication tower (built in the 1970s and donated to the University by British Telecom). The resultant fibre fluctuations were of the order of $\pm$15 % in 120 μm.

In order to overcome this problem a technique developed by Blaze Photonics was implemented, namely the addition of pressure to the holes (typical values of tens of kPa) whilst drawing the fibre. With the constraints on preform diameter and draw speed thus removed, larger preforms could be used and hundreds of meters of polymer coated fibre could be drawn on the University's new fibre pulling tower (manufactured by Heathway - illustrated in figures 3.4 and 3.8).

Another stack was built, this time with as many periods as possible to reduce confinement loss to a minimum. The limits on the size of the stack were the diameter of the furnace and the ability of the fabricator to stack capillaries of sufficiently small diameter. As a general rule, for stacks of around 80-100 cm in length, capillaries larger than 3/4 mm must be used otherwise stacking becomes very difficult. The image in figure 3.2 showed the design for this stack.

Using the Heathway drawing tower has many advantages. The preform feed and fibre drawing motors are more reliable and are feedback controlled with respect to fibre diameter. Previously, setting the temperature of the furnace was somewhat arbitrary and it was maintained at a constant value throughout each draw. The Heathway tower is fitted with a fibre tension monitor allowing the

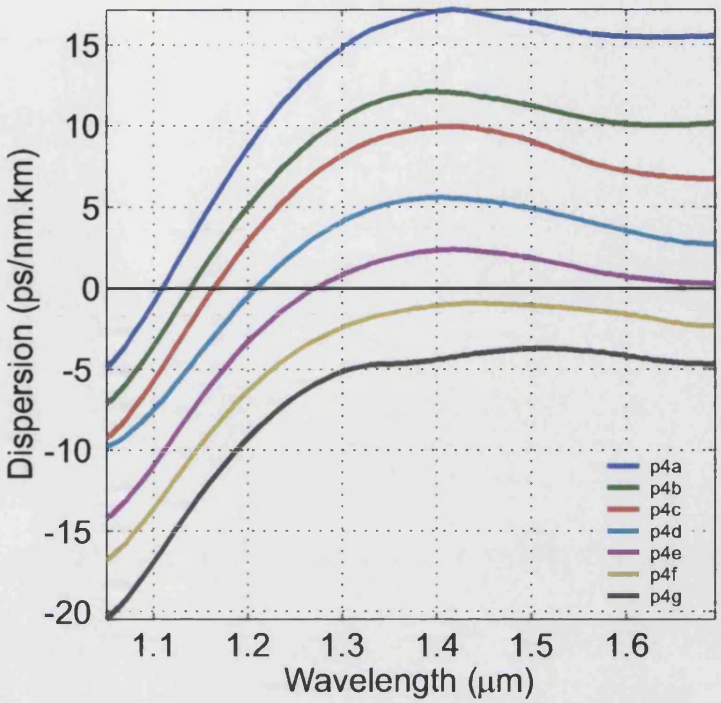

Figure 5.6: Dispersion profiles of the P4 set of fibres. As hole size is decreased the value of dispersion in the flattened region falls.

dynamic adjustment of temperature to maintain constant viscosity of the glass.

New fibres were drawn at a fixed tension of around 200 g. The diameter was set to a constant 118 μm in order to obtain the desired pitch for the maximally flat dispersion profile. Pressure on the holes was set at a high value and then reduced every 150 m for each fibre draw, thus generating a range of fibres with identical Λ but varying d. Figure 5.6 shows the resultant dispersion curves for one such draw. This set of fibres is referred to as 'P4' (preform 'P', draw number 4). 'P4a' has the largest holes and the largest dispersion. 'P4g' has the smallest holes. From SEM images, the difference in d from 'P4a' to 'P4g' is only 140 nm while Λ remained approximately 2.4 μm throughout the draw.

These experimental results appear to be in reasonable agreement with the calculation results shown in figure 5.2. Using the calculation of dispersion at 1550 nm and selecting $\Lambda = 2.4$ μm, a difference in dispersion from +15 to -5 ps/nm.km corresponds to a change in d of 144 nm, which is in excellent agreement with the measured value. For the same range of d and Λ the calculation of dispersion slope yields values that are small and negative at 1550 nm, also in good agreement with

experiment.

In order to produce fibres with flatter dispersion profiles the modelling results shown in figure 5.2 were used as a guide. The graphs suggested that in order to increase the dispersion slope to zero at 1550 nm, the pitch should be increased by drawing the fibres to a slightly larger diameter. The experimental results shown in figure 5.6 suggested that in order to obtain fibres with values of dispersion closer to zero at 1550 nm, pressures located between those used to draw fibres P4e and P4f should be used. The implementation of these changes resulted in the fabrication of a set of fibres referred to as 'P7' and their dispersion profiles are shown in figure 5.7.

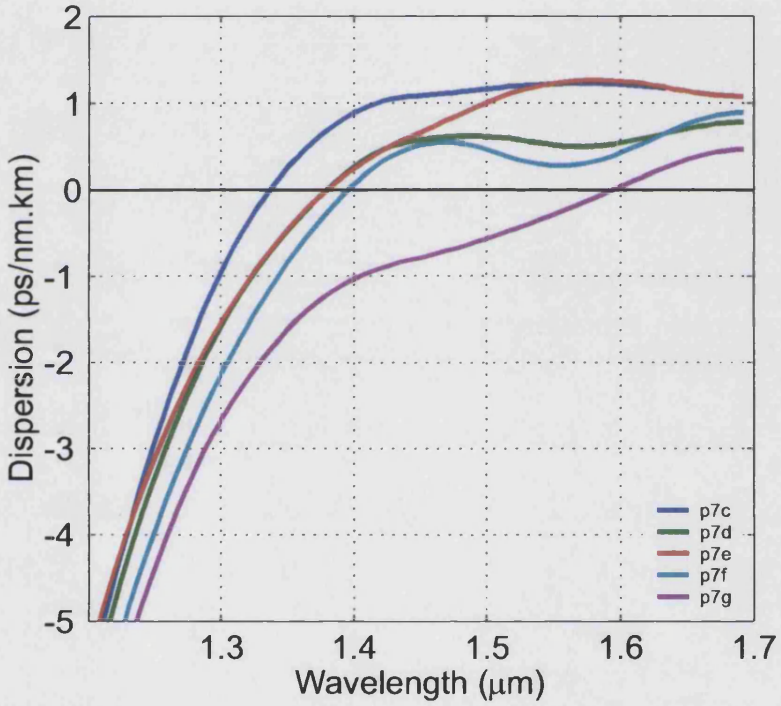

Figure 5.7: Dispersion profiles of the P7 set of fibres. As hole size is decreased the value of dispersion in the flattened region falls. Note that the error in dispersion slope is likely to be large due to the small quantity and relatively low accuracy of the experimental data points.

The apparent abnormalities in the shapes of the dispersion profiles are unlikely to be physical as the combination of material and waveguide dispersion cannot produce some of the rapid changes in slope seen here. The resolution limit of the dispersion measurement method is estimated to be slightly less than $\pm$ 0.5 ps/nm.km for the lengths of fibre under test (235 mm). Therefore we can conclude that dis-

persion measurements on these fibres are inherently inaccurate.

Figure 5.8 shows a small selection of dispersion slopes calculated from the data shown in figures 5.6 and 5.7. As can be seen from these graphs, the value of dispersion slope typically remains smaller than ± 0.02 ps/nm^2.km from 1.36μm to at least 1.7μm. Additionally, the slopes of the fibres P7e and P7f are smaller than ± 0.007 ps/nm^2.km within a wavelength range of at least 260 nm from 1.44 to 1.7 μm.

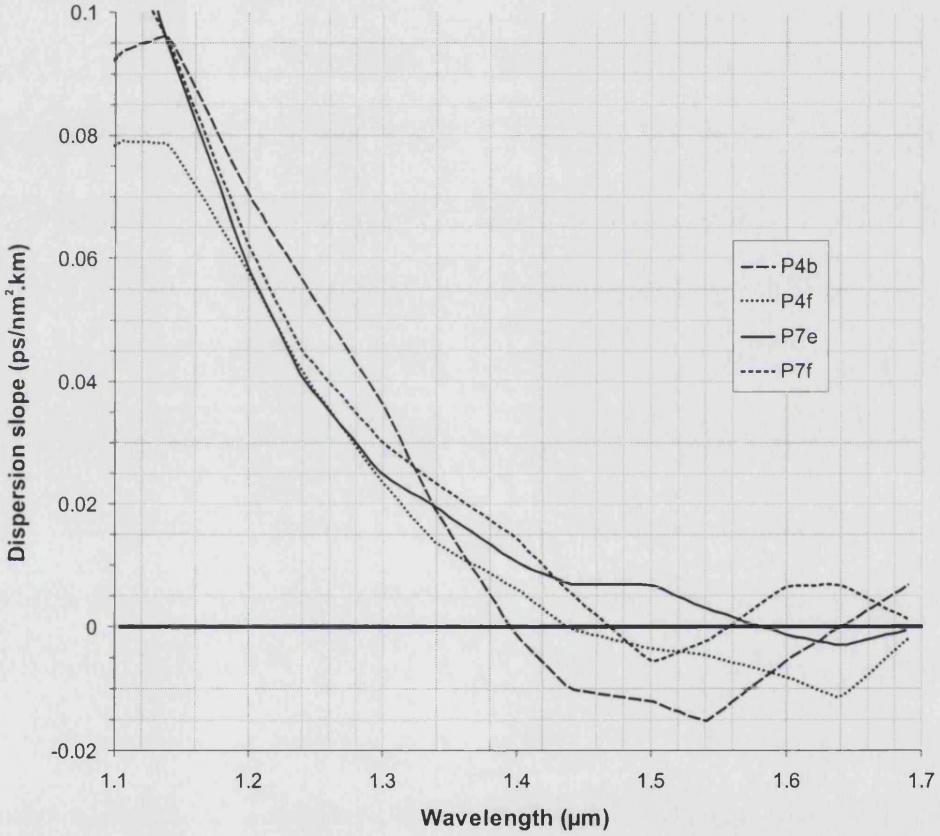

Figure 5.8: Dispersion slope calculated from the data shown in figures 5.6 and 5.7 for a small selection of UFD-PCF.

The fabrication of flattened dispersion PCF was suspended at this point as a satisfactory 'proof of principle' had been obtained. Long lengths of fibre with near-zero dispersion and dispersion slope had been fabricated by this stage. However, with further optimisation of d and Λ aided by an improved dispersion measurement method, fibres with smaller dispersion slope could conceivably be fabricated.

5.4 Characterisation results

The remainder of this chapter presents the results of some of the characterisation measurements made on the flattened dispersion fibres. As some of these measurements were destructive, and the fibre lengths drawn were short, some experiments were made on fibres drawn immediately before the 'P4' set. These 'P3' fibres, drawn from the same preform, had almost identical draw parameters but the dispersion profiles were further from optimal than the 'P4' or 'P7' sets.

A short study of the fibre diameter fluctuations and the resultant effect on dispersion is also presented.

5.4.1 Losses

A "cut back" loss measurement was made on 'P4e' where white light was coupled into 100 m of the fibre and the output spectrum was measured using an optical spectrum analyser. 99 m was then cut from the original length and the spectrum from the remaining meter length taken. The overall loss of the fibre, shown in figure 5.9, was calculated by taking the difference of these two traces and dividing by the length cut from the fibre.

The attenuation at 1380 nm was too large to measure over this length. This loss is attributed to the presence of water but was expected as no attempt to remove water was made during the fabrication process. As expected, it appears that the Rayleigh scattering and IR Si-O resonance loss mechanisms dominate for wavelengths shorter than 600 nm and longer than 1600 nm respectively. Attenuation at 1550 nm is approximately 35 dB/km.

A bend-loss measurement was made on the fibre 'P7f' by wrapping the fibre around a mandrel of various diameters five times. White light was launched into the fibre and recorded at the output using an optical spectrum analyser (OSA) manufactured by Ando. The short wavelength cut-off was determined to be the wavelength at which the light was attenuated by 10 dB.

Figure 5.10 shows how the cut-off wavelength varies with bend radii and confirms

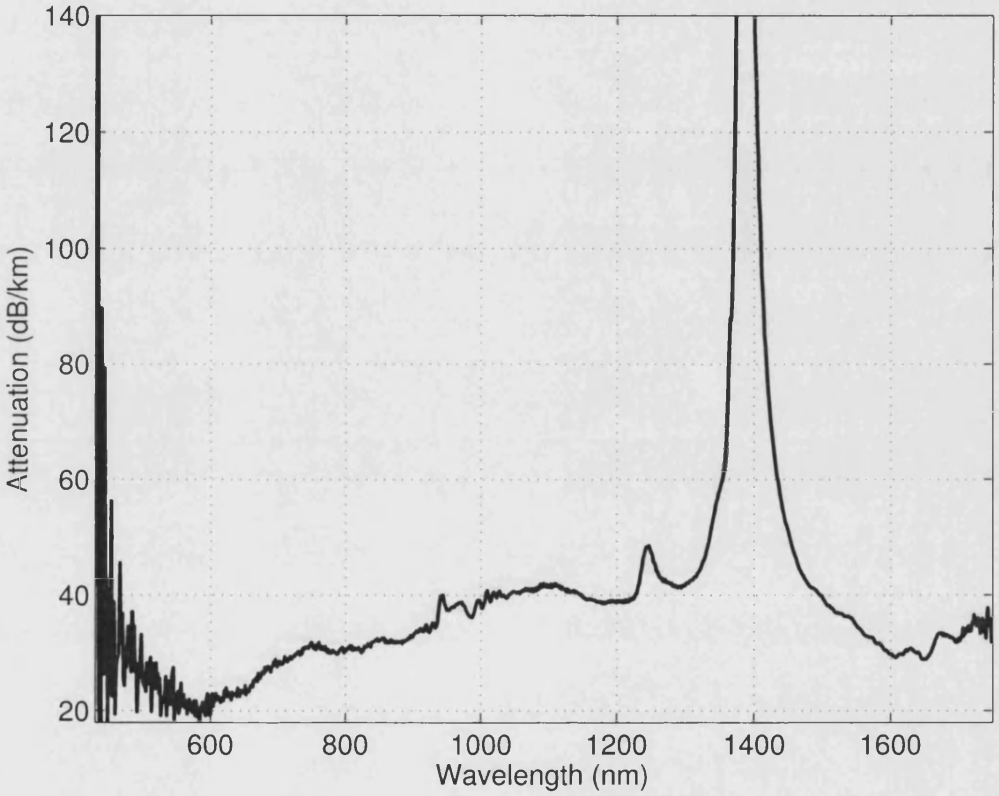

Figure 5.9: A cutback measurement of attenuation against wavelength made on an ultra-flattened dispersion PCF. An attenuation value of 35 dB/km is obtained at a wavelength of 1550 nm.

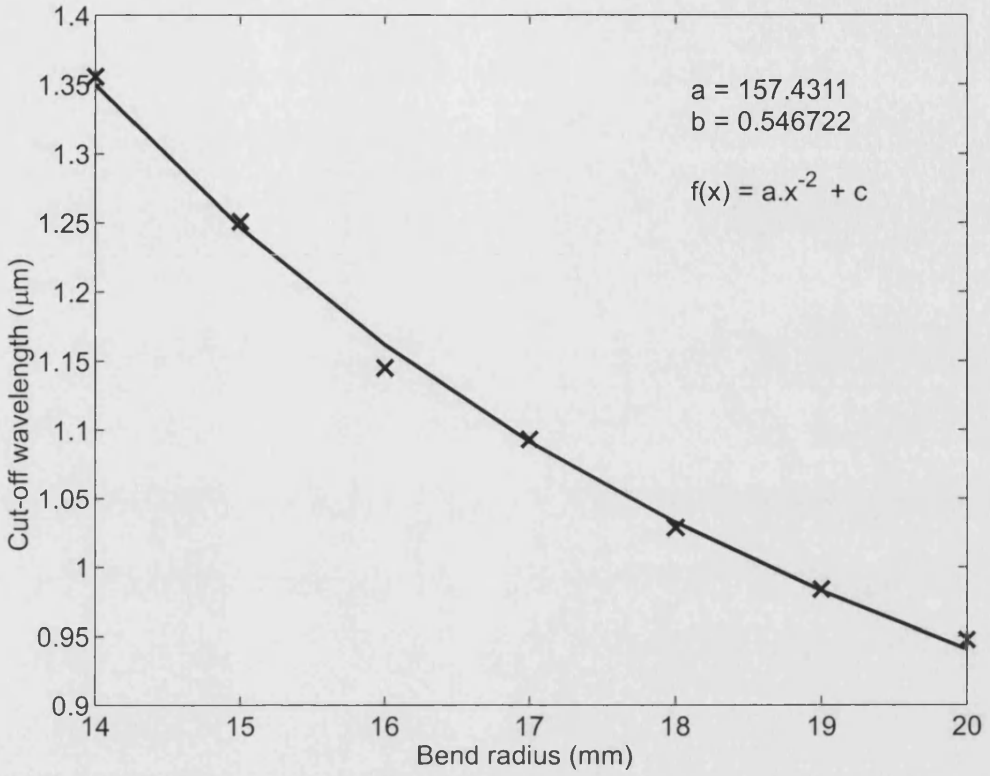

Figure 5.10: Results of a bend loss measurement made on the fibre 'P7e'.

that these fibres have acceptable bend losses in the wavelength range of interest and, if the traditional inverse-square relation is assumed to hold, the critical bend-radius for a wavelength of 600 nm is 24 mm.

5.4.2 Fibre diameter fluctuations

The fibre tower is equipped with a data-logging PC that records numerous parameters as they change during the draw. Figure 5.11 shows the deviation of fibre diameter from the set value with time for the 'P3' set of fibres. The 'P4' and 'P7' fibres had similar diameter variations.

As can be seen, the fibre has nominal diameter fluctuations of ± 0.5 μm (± 0.42 %). However, larger variations occur with a period of tens of seconds and can be almost as large as 4 μm and last for around a second. The draw speed was set to 60 m/min (feedback controlled) so this corresponds to abberations spanning

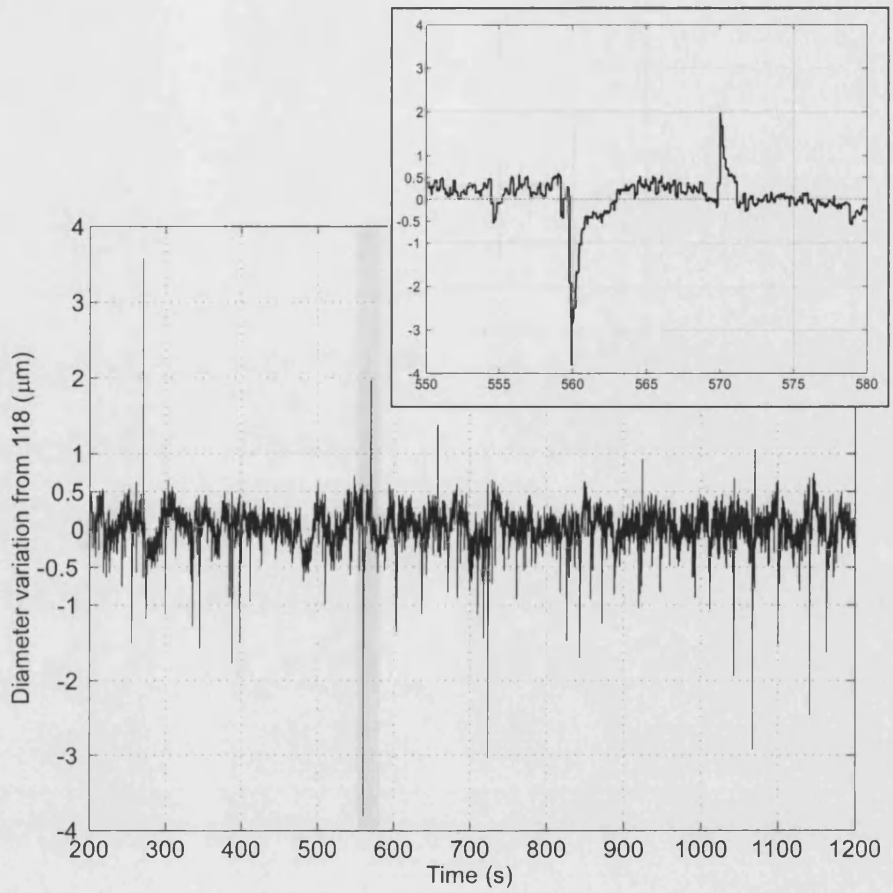

Figure 5.11: Fibre diameter deviation during the drawing of the 'P3' fibres. The inset shows a blowup of the grey shaded region in the main plot. The drawing speed was $\approx$ 60 m/min, so seconds in time correspond directly to meters in length.

a meter in length with spatial periods of the order of tens of meters.

To investigate the effect of the diameter variations on the dispersion in a typical fibre, 235 mm segments of the fibre P3D were removed at 10 m intervals from a 100 m length. The dispersion of each section was then measured using the interferometric method described in section 2.4.1. The mean GVD at 1550 nm was 4.91 ps/nm.km with a standard deviation of 0.24 ps/nm.km - comparable to the error of the measurement technique. Figure 5.12 summarizes these findings.

This small variation in dispersion is to be expected. Referring back to figure 5.2, since to a first approximation fibre diameter fluctuations only change the pitch

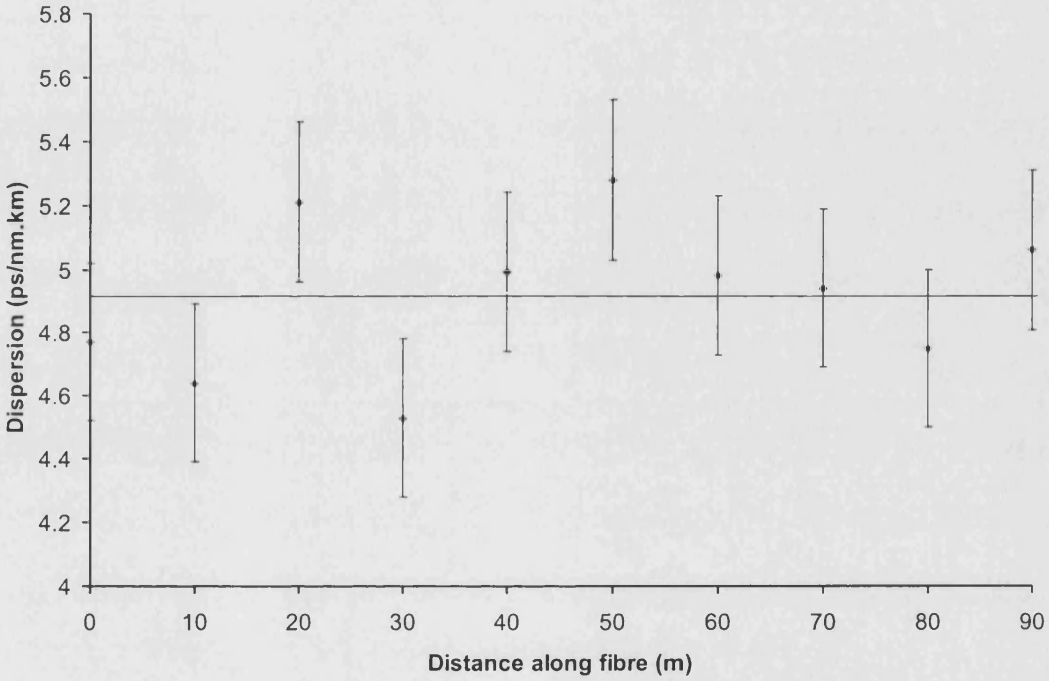

Figure 5.12: Measurements of GVD at 1550 nm taken at 10 m intervals along a 100 m length of UFD-PCF. Each measured section was approximately 235 mm long. The mean GVD was 4.91 ps/nm.km (black line). The error on the measurement is estimated to be $\pm$ 0.25 ps/nm.km.

while the hole radius/pitch ratio remains constant, the dispersion in the locality of our chosen parameter set is insensitive to fluctuations in the fibre diameter. This is advantageous as the dispersion and dispersion slope change less rapidly with this parameter, implying that the dispersion profile is tolerant to small changes in fibre diameter. However, the large fluctuations in fibre diameter that occur in figure 5.11 may not have been sampled during this experiment. There is therefore a possibility that the dispersion may vary more significantly in fibre with a diameter 4 μm larger or smaller than the set value.

5.4.3 Scanning electron microscopy analysis

During the fabrication process no attention was paid to the variation of hole diameter throughout the structure and only the results from the dispersion measurements were used to optimise the fibres. This is justified by the argument in the preceding subsection.

With the aid of computer software borrowed from Blaze Photonics, the variation in hole size throughout the structure was analysed from SEM images. Figure 5.13 shows two examples of the SEMs used.

Although not immediately apparent, there is a gradual hole diameter variation throughout the structure. The holes increase in diameter with increasing distance from the core. This is almost certainly due to the temperature gradient experienced by the glass at the fibre drawing stage. The glass towards the edge of the preform is hotter and therefore less viscous than that of the centre. The pressure applied to the holes is constant throughout the structure and the holes are therefore able to expand with increasing ease towards the periphery of the fibre.

Figure 5.14 shows a plot of average hole diameter for each period in the fibre, period number '0' being the core.

In order to see how this variation in structure affected the dispersion from the "ideal" global macrostructure, the average d of 0.58 μm and Λ of 2.45 μm (r/Λ ratio of 0.12) for the fibre 'P7f' was used in conjunction with the calculations shown in figure 5.2. This resulted in a theoretical dispersion of approximately

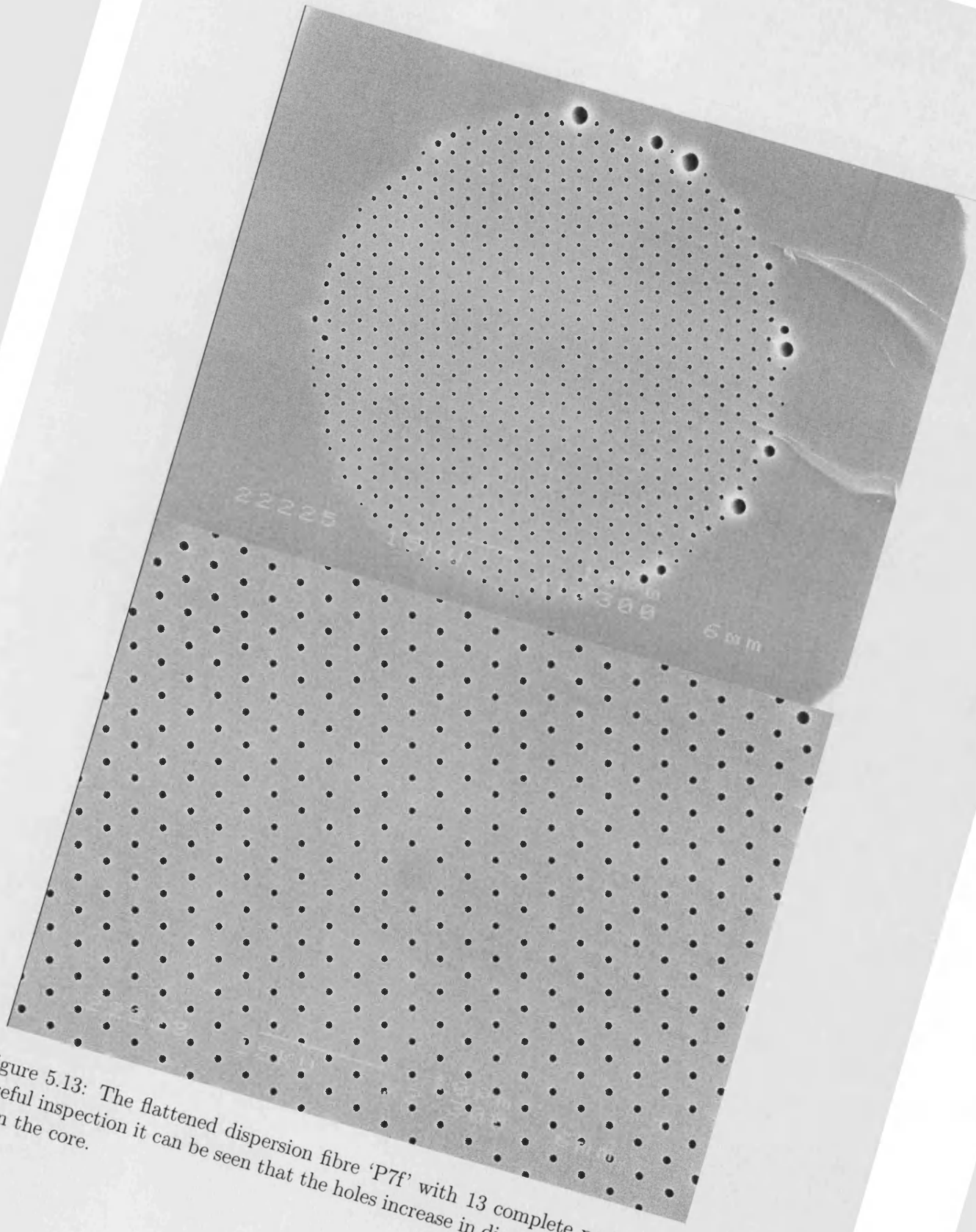

Figure 5.13: The flattened dispersion fibre 'P7f' with 13 complete periods. On careful inspection it can be seen that the holes increase in diameter with distance from the core.

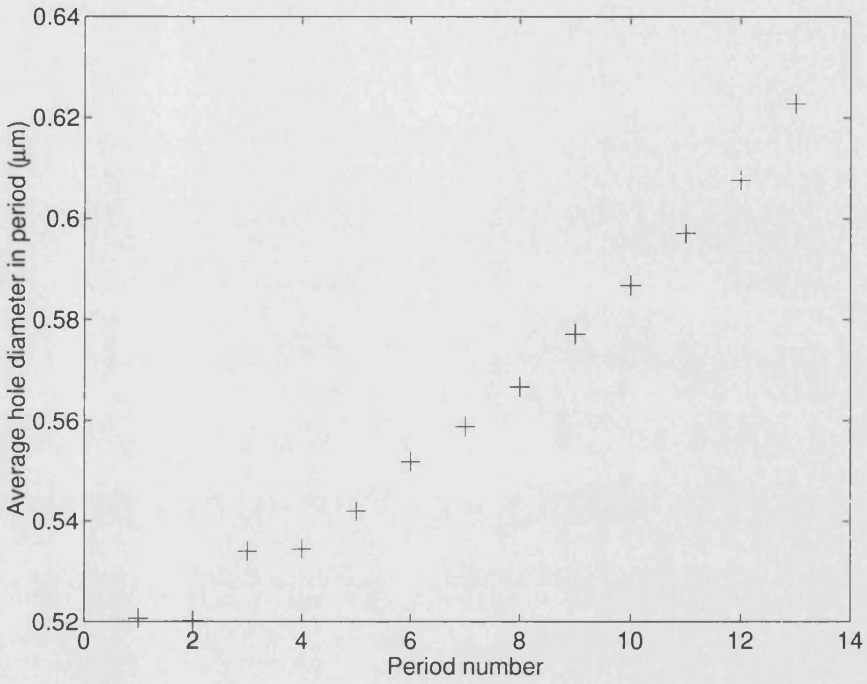

Figure 5.14: The variation of hole hole diameter for each period of fibre "P7f".

-2.5 ps/nm.km at 1550 nm, in contrast to the measured value of 0.5 ps/nm.km.

Clearly, in order for flat-dispersion fibres with sub-micron hole diameters to be modelled accurately the whole structure must be taken into account. However, the benefits of this may not warrant the required additional computation time as there is another source of error to be considered - the error associated with measuring sub-micron features using a scanning electron microscope. In practice an assumption regarding the exact location of the glass/air interface has to be made due to charging effects of the glass by electrons from the microscope. The adjustment of SEM brightness and contrast can also affect the measurement.

Luckily, there is no such uncertainty in the determination of Λ. Furthermore this measurement can be made over the entire cladding, and in the case of the "P" preform this entails that an average over 26 periods can be made. Using this information, the iterative fabrication process and an improved dispersion measurement method, it should be possible to further optimise the structure to produce fibres with even flatter dispersion in future.

5.5 Conclusions

PCF have been fabricated by means of an iterative fabrication procedure to produce fibres with low dispersion over a wavelength range of unprecedented width.

The goal of a fibre with zero dispersion and ultra flattened dispersion slope centered on a pre-specified wavelength was achieved and a range of ultra-flattened dispersion PCF with values of dispersion between 17 ps/nm.km and -5 ps/nm.km were fabricated. Dispersion slopes were typically smaller than $\pm$ 0.02 ps/nm^2.km in the range 1.36 to at least 1.7 μm. Some of the fibres had slopes smaller than $\pm$ 0.007 ps/nm.km in a range of at least 260 nm, from 1.44 to 1.7 μm.

These fibres are used in chapter 6 to investigate the effect of PCF waveguide dispersion on ultra-short pulse propagation.

In principle the flatness of the dispersion profiles is *not* limited by the basic fabrication procedure that we have adopted. With additional fibre draws and improvements to the dispersion measurement method it would be possible to fabricate fibres with even smaller dispersion slopes.

Fibre losses are relatively high ($\approx$ 35dB/km) but, with the exception of confinement losses, no attempt to reduce this attenuation was made during fabrication. This loss could be reduced by reducing contamination of the preform during stacking through general cleanliness. Additional procedures during fabrication could be implemented to reduce the water content by, for example, drying the preform with chlorine and purging the glass tubes and preforms with nitrogen before and during drawing.

Chapter 6

Ultrashort pulse propagation in ultra-flattened dispersion photonic crystal fibre

6.1 Introduction

The fibres described in chapter 5 had ultra-flattened dispersion regions centered near 1550 nm. In order to investigate nonlinear properties and soliton formation in these fibres, a laser source near this wavelength was used to ensure pumping in the anomalous dispersion regime. The University of Bath did not have such a source, so this work was conducted at the Los Alamos National Laboratory (LANL), New Mexico USA.

6.2 Experimental apparatus

The fibres investigated were the 'P4' and 'P7' sets of fibres. Their almost constant dispersion profile shapes, differing only by vertical translation (to a good approximation) gave an opportunity to investigate the effect of dispersion on the nonlinear effects observed in optical fibres when pumped with ultra-short pulses.

All of the experiments were conducted with the experimental setup shown in figure 6.1.

Laser pulses were obtained from an 'Opal' optical parametric amplifier pumped by a 'Tsunami' Ti:Sapphire laser, all manufactured by Spectra Physics. The pulse length was approximately 110 fs, the repetition rate was 80 MHz and the average power was 240 mW (corresponding to a peak power of approximately 30 kW). The input laser power was controlled by using two crossed polarisers, and a 16× objective lens with an NA of 0.25 (close to the fibre's predicted NA of 0.2) was used to couple light into the fibres.

Although the fibres had minimal birefringence, a waveplate was nevertheless used to vary the input beam polarisation. The output power did not vary by more than a few percent for a full 180° of input rotation polarisation and the input polarisation was consistently chosen so that maxim power was recorded at the fibre output.

The spectra generated in the fibres were recorded at the fibre output using one of three devices: a Jobin-Yvon 'ISA 1100' spectrometer that had an operating wavelength range between 800 and 1650 nm (with data-recording in the range 800-1700 nm), an optical spectrum analyser manufactured by Ando that had an operating wavelength range between 350 and 1750 nm, and a monochromator with a cooled InGaAs detector extended the measurement wavelength range up to 2200 nm.

6.3 Experiment: the effect of laser intensity on fibre output spectra

The measurements presented in this section were taken with the Jobin-Yvon spectrometer for a number of powers recorded at the output of the fibre. The spectrum was recorded in sections (as the Jobin-Yvon spectrometer only had a 150 nm capturing window) and the data was digitised and recorded using a digital oscilloscope. This data was combined and scaled to cover the required wavelength range. Many data files were generated for each fibre and as an aid to viewing the data, two-dimensional colour plots were produced showing generated

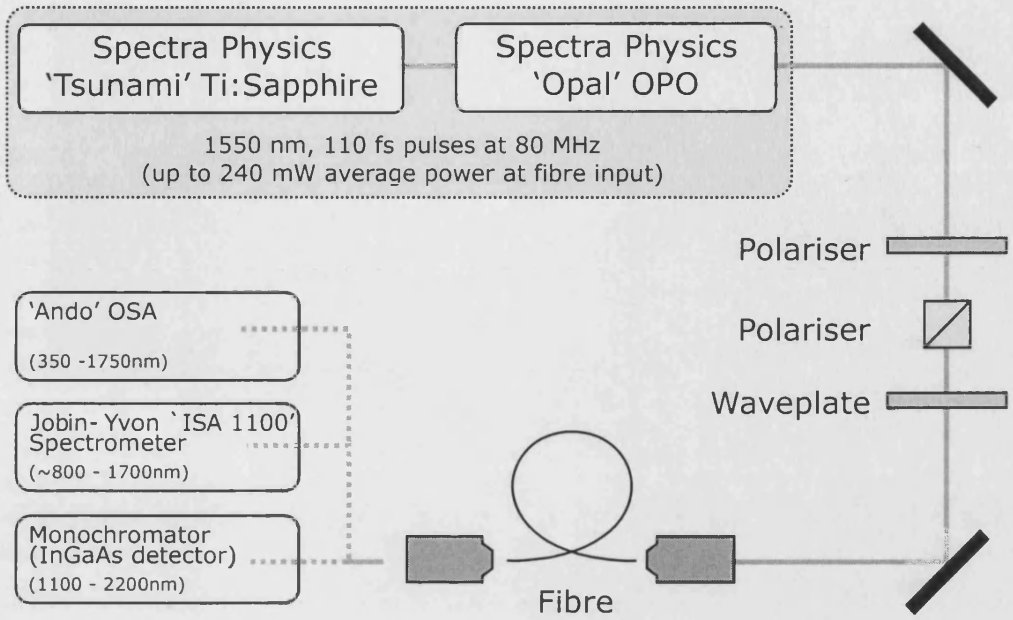

Figure 6.1: Equipment used at Los Alamos to investigate ultra-short pulse-propagation in UFD-PCF and extruded SF6 fibre.

spectra against output power (in which colour represents the light intensity).

6.3.1 Notes on measurement method

Conventional fibre (SMF28) was used to test the measurement method and figure 6.2a shows the resultant data. Figure 6.2b shows the same data, but in the form of an interpolated contour plot. However, care must be taken to disregard interpolation/sampling artifacts such as the crisscross feature present in the lower right-hand corner of (b). It is important to note that the 'steps' that appear in the light moving towards longer wavelengths at powers greater than 80 mW are not interpolation artifacts. These 'steps' are discussed in more detail later in this chapter.

In order to approximately gauge the amount of light being converted to wavelengths outside spectrometer range the total power recorded by the spectrometer over all wavelengths was plotted for each spectral measurement. Such wavelength conversions manifest themselves as dips in an otherwise straight line. Figure 6.3 shows one such plot for the SMF28 data depicted in figure 6.2. Additionally, this

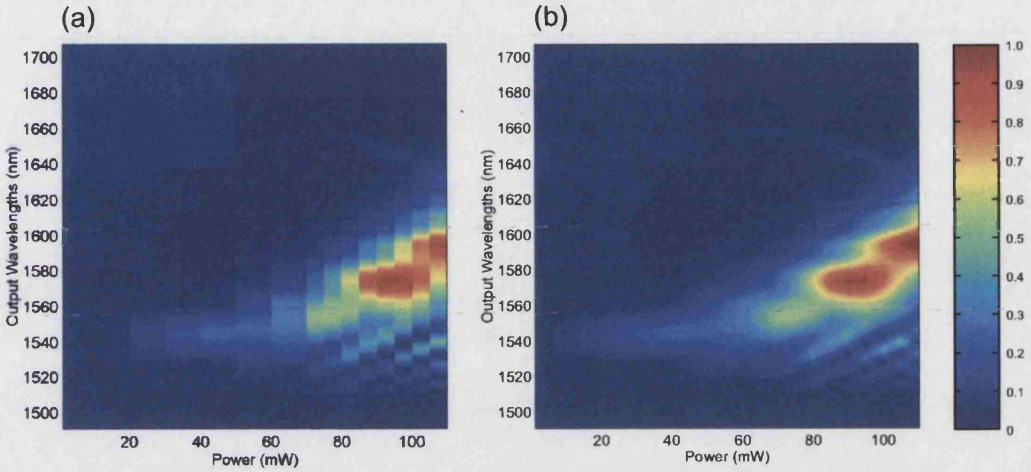

Figure 6.2: Generated spectrum with power from SMF28 when pumped with 110 fs pulses at 1550 nm. (a) without interpolation, and (b) with interpolation both plotted with a linear, arbitrary scale (shown on right).

plot can indicate whether or not the laser-power fluctuated during the series of experiments. However, it should be noted that plots of this type do not take the spectrometer's spectral response into account whereas the output power was measured using a thermal detector. This could be the reason why the curve in 6.3 becomes steeper with increasing output power.

From figure 6.3 we can conclude that almost all of the spectra generated by the fibre fall within the detectable range of the Jobin-Yvon spectrometer, as the trace approximates a straight line.

6.3.2 Results

Experiments were made on a large number of distinct UFD-PCF (see appendix A). However, figures 6.4 and 6.5 show a selection of data sets that illustrate the general trends relating to how dispersion affects the generated supercontinuua.

It should be noted that, to a first approximation, the dispersion profile is the only difference between these fibres. The structure and effective areas remain practically constant for all the fibres as the hole diameter of the fibre P4a to P4g

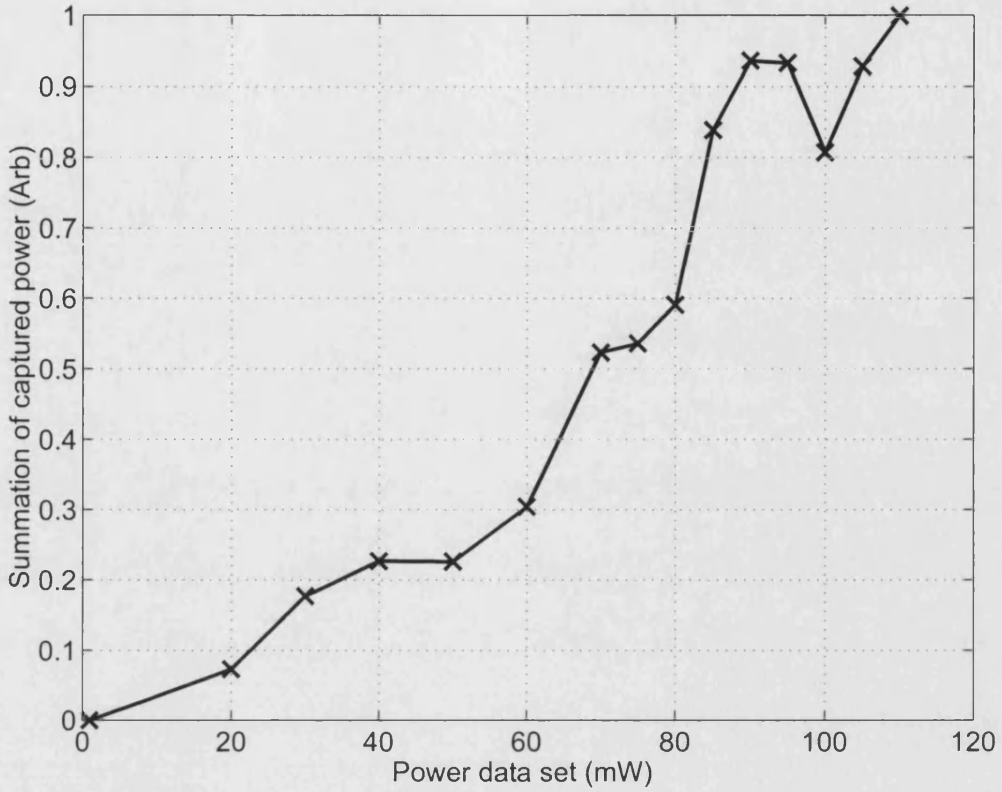

Figure 6.3: The total power recorded by the spectrometer for each measurement of spectra. Ideally, if no light is frequency shifted outside the wavelength of the Jobin-Yvon spectrometer, this plot should have the form $y = mx$.

only varies by ~ 140 nm.

6.3.3 Discussion

Unlike fibres with 'conventional' dispersion curves, the particular UFD-PCF that have flattened segments in the normal region have *no* portions of anomalous dispersion *throughout the measurable wavelength range* (such as P4g in figure 6.5). Solitons and the nonlinear effects acting on them play an important role in the production of new frequencies, fibres that have normal dispersion for all measurable wavelengths cannot support solitons (see Chapter 4). This has important implications for supercontinuum generation as in previous experiments (for example, [41]) pumping in the normal dispersion regime inevitably results in the

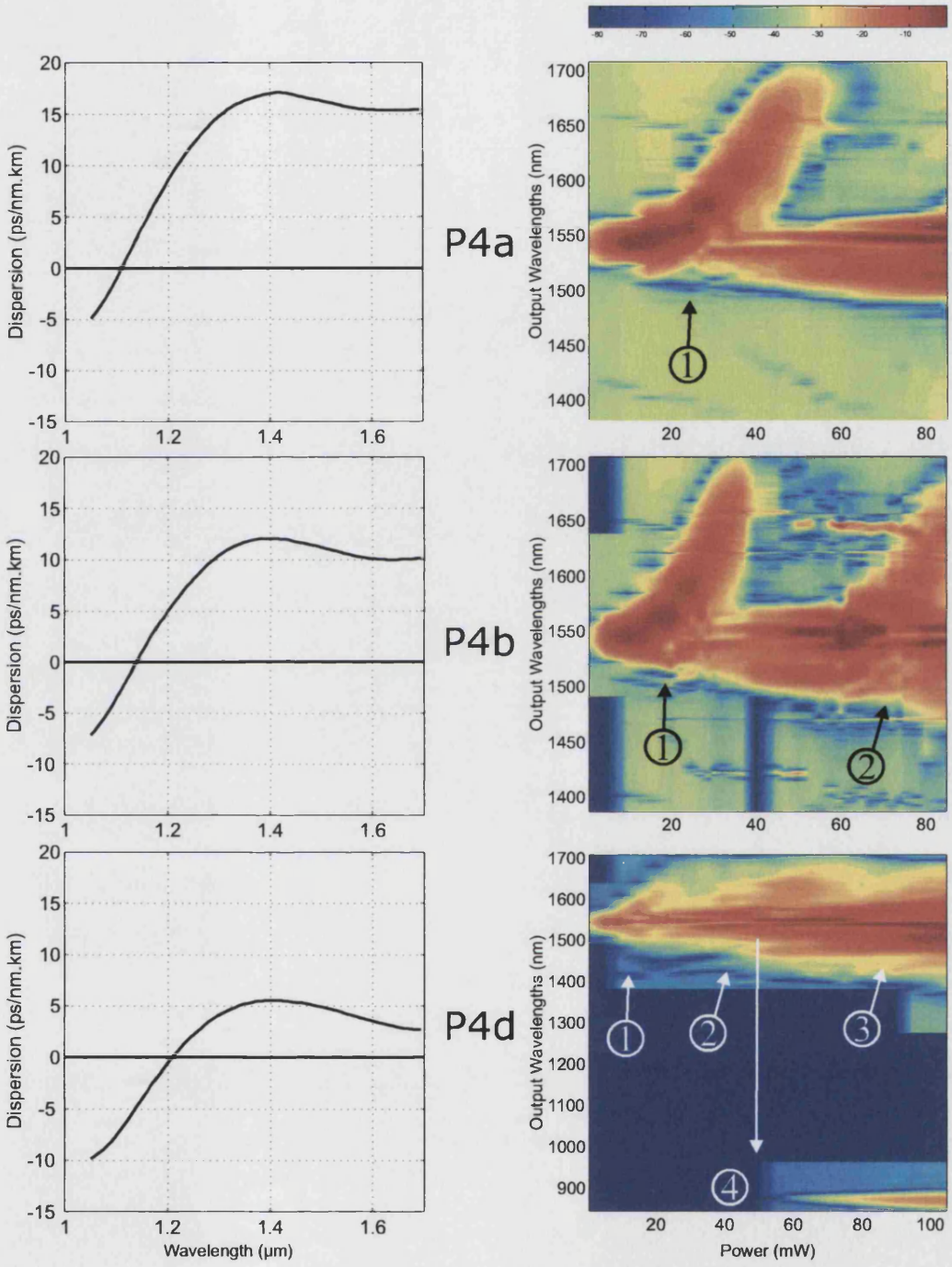

Figure 6.4: The dispersion profiles and generated spectra against power (logarithmic scale) for 1 m lengths of the UFD-PCF P4a, P4b and P4d. The numbered points are referred-to within the discussion section.

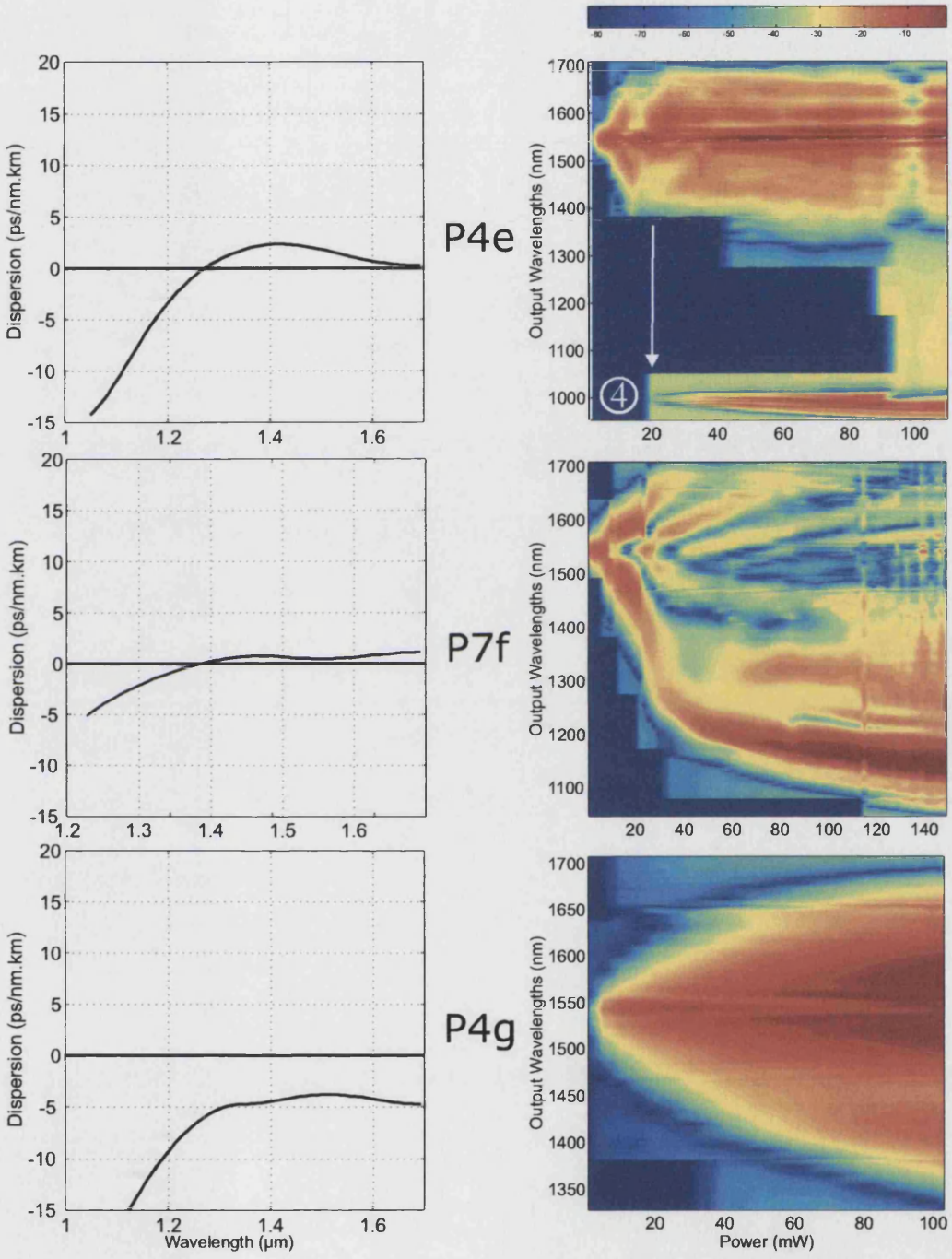

Figure 6.5: The dispersion profiles and generated spectra against power (logarithmic scale) for 1 m lengths of the UFD-PCF P4e, P7f and P4g. The numbered points are referred-to within the discussion section.

generation of wavelengths in the anomalous dispersion regime through processes such as SPM. This light is then able to form solitons. With enough power a supercontinuum with spectral features similar to those generated by pumping in the anomalous dispersion regime can be generated.

This cannot happen in the UFD-PCF with normal dispersion 'everywhere' and, as a result, these fibres exhibit markedly different spectral features from those with regions of anomalous dispersion (and fibres with 'conventional' dispersion curves pumped in the normal dispersion regime).

UFD-PCF with anomalous dispersion

The first feature of interest for UFD-PCF with anomalous dispersion is the first peak that shifts to longer wavelengths with increasing power (figure 6.4 note 1). This is most apparent in fibres with large anomalous dispersion, for example fibres P4a and P4b, at powers between approximately 10 and 50 mW. This feature is attributed to the formation of a soliton and its subsequent shift to longer wavelengths with increasing power, via the Raman-assisted soliton-self-frequency-shift (SSFS)[14]. Fibres with decreasing values of positive dispersion require less power to create the soliton and to initiate the self frequency shifting. This is because less SPM, and consequently less power, is required to compensate the dispersive effects. However, for fibres with very small dispersion this trend is much less apparent as SPM broadening becomes dominant (see appendix A).

The response of the spectrometer accounts for the apparent loss in intensity towards long wavelengths (the operating range was specified to extend to 1650 nm, however, the precise spectral response of the spectrometer was not available).

Interestingly, the peak of the SSFS only appears at certain discrete values of wavelength. These 'step-like' features imply that the associated values of wavelength/frequency are quantised. Confirmation that the steps were not sampling artifacts was found when spectrometer readings were taken at more closely spaced power intervals. It should be noted that these steps also appear in the case of conventional SMF28 fibre (figure 6.2b).

One probable cause for the 'steps' is based on the supposition that a higher-order

soliton is formed rather than the fundamental soliton. Such solitons have intensity profiles that are periodic in time, caused by the interplay between GVD and SPM, and are called 'breathers' (see Chapter 4). Figure 4.3 showed an example of one such higher order soliton. As the pulse spreads in time the peak intensity falls. When the pulse is at its broadest, intensity is at its lowest and SSFS is likely to be small. Accelerated SSFS could occur when the pulse is temporally short. This effect could be seen with propagation distance and possibly with increasing power. However, it is believed that higher-order solitions are not responsible for the steps for the following reason.

In fibres such as P4b and P4d a 2nd and even 3rd spectral feature deviating towards longer wavelengths can be seen (figure 6.4 notes 2 and 3). These features can be attributed to the formation, and subsequent frequency-shifting, of higher-order solitons. The power required to create a soliton can be calculated from the following[14]:

$$P_0 = \frac{N^2|\beta_2|}{\gamma\,\tau_0^2} \tag{6.1}$$

where P_0 is the pulse peak power, N is the soliton order and τ_0 is the pulse width.

This means that the 2nd-order soliton requires four times, and the 3rd-order nine times, the power of the fundamental to be formed in a given medium. This is in good agreement with the experimental data, for example, in figure 6.4 fibre 'P4d' has three distinctive spectral features thought to correspond to the formation of solitons (labelled 1,2 and 3). These features start at powers of approximately 10, 40 and 90 mW, implying that the solitons are of the fundamental, second and third order respectively. This also implies that the fundamental soliton is always formed first, implying that the step-like features can not be attributed to the breathing of higher-order solitons. Using equation 6.1 the average powers required to form the fundamental, second and third order soliton in fibre P4d are approximately 2.5, 10, and 23 mW respectively. From the experiment (figure 6.5) solitons form at values of *output* powers of approximately 10, 40 and 90 mW, in good agreement to theory where the discrepancy could be attributed to the approximate values of γ and τ_0 used in the calculation.

A possible cause of the 'steps' that can be immediately discounted is that of frequency-chirp on the input pulses. The combination of SPM chirp and the input pulse chirp disturbs the balance between the GVD and SPM necessary for

soliton formation. Initially, an oscillation occurs where the pulse is compressed in time, is then broadened and is eventually compressed a second time[14]. However, no such chirp was introduced during the theoretical modelling for figures 4.5 and the 'steps' still appear. While chirp on the input pulse could be a contributory factor, it is not the main cause. Interestingly, theory shows a step-like shifting (with length not power) for a fundamental soliton in a region of small and constant β_2 with no other non-linear effects included (figure 4.5). So perhaps this step-like shifting is a previously unnoticed feature of SSFS.

Another interesting feature associated with our solitons is the formation of a peak at short wavelengths, for example figures 6.4 and 6.5 label 4.

It is probable that this peak is due to soliton break-up and FWM and can be explained as follows: The apperance of the peak coincides with the formation of the first higher order soliton (figure 6.4 label 2). This soliton is not stable and it breaks up into its constituent fundamental solitons, releasing energy in the form of non-solitonic radiation. This radiation can then be converted to shorter (and longer) wavelengths via FWM. The corresponding long wavelengths are generated outside of the operating range of the spectrometer (eg. for a peak forming at 1 μm the associated, energy conserving, long wavelength peak is at 3.4 μm).

Experimentally, this explanation seems plausible, as the peaks always occur at around the same power as the higher-order soliton (figure 6.4 fibre P4d and figure 6.5 P4e). If this is indeed true, a blue peak should occur in the spectra for fibre P4b at a power of approximately 70 mW (figure 6.4). As no such peak was recorded it was hypothesised that the peak resided outside of the spectral range of the Jobin-Yvon spectrometer.

To test this hypothesis, figure 6.6a was plotted, showing the summation of the total power of each spectral measurement recorded by the spectrometer for the fibre P4b. It can be seen that there are two substantial losses of power. The first occurs at around 35 mW and corresponds to the SSFS towards longer wavelengths. The second occurs at around 70 mW, near the formation of the second-order soliton, and is likely to be due to the blue-shifting of radiation outside the spectral range of the spectrometer.

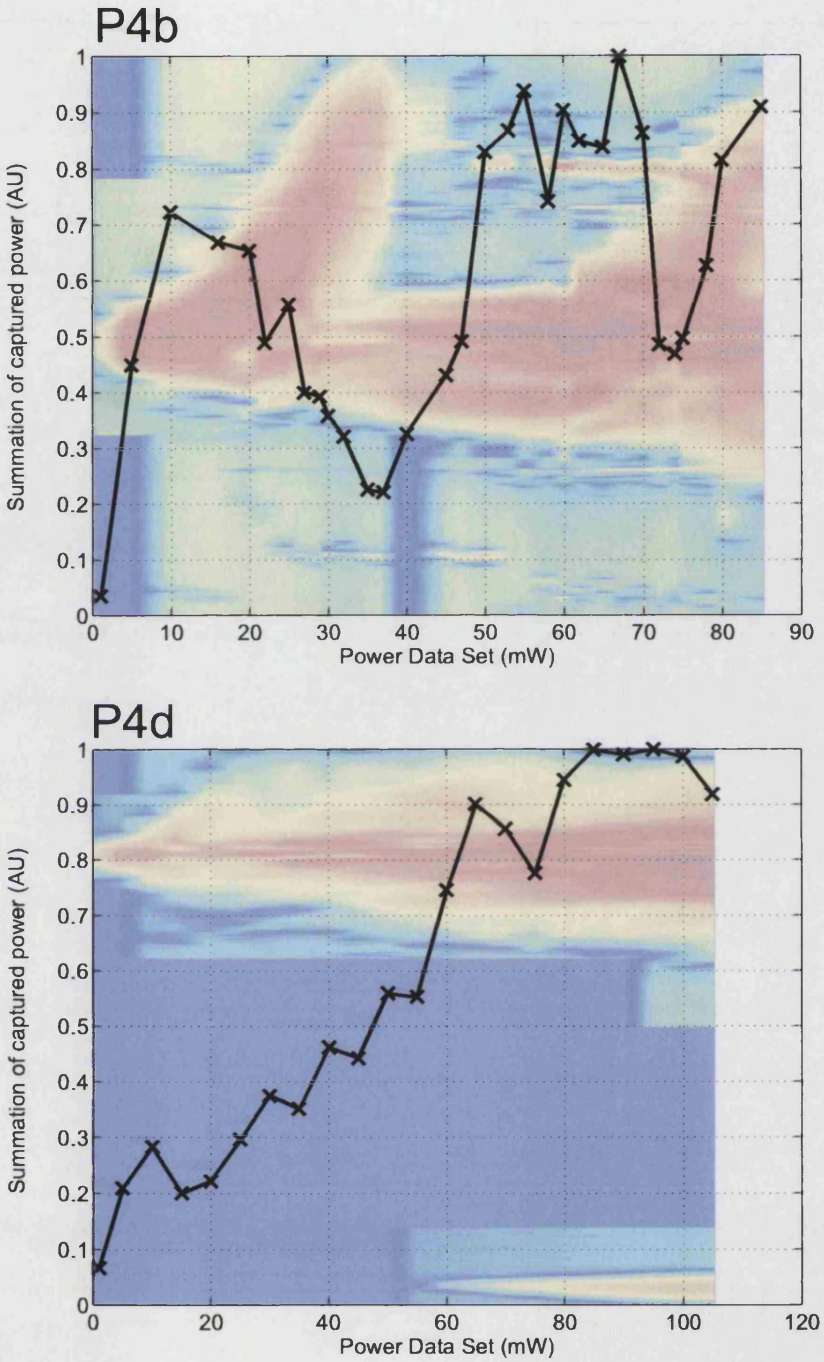

Figure 6.6: Power loss in P4b (top) with spectra shown in background. The second dip in recorded power is probably due to higher-order soliton breakup and the generation of wavelengths outside the range of the spectrometer. The power loss in P4d is shown below for comparison. For this fibre the blue peak appears within the wavelength range of the spectrometer and no large associated loss can be seen.

With the exception of P7f, all the fibres with anomalous dispersion have a large spectral component centered around the pump wavelength. The majority of this light is likely to be non-solitonic radiation not used in the formation of solitons and residual radiation left during SSFS (see figure 4.5).

UFD-PCF with normal dispersion

The fibres that have normal dispersion for all measurable wavelengths (for example P4f, P4g and P4h) share a common spectral feature: increasing spectral broadening with power. As a result, no solitons can form in these fibres and therefore the only prominent spectral feature is SPM-induced spectral broadening.

The maximum change in frequency for SPM broadening $\delta\omega$ can be estimated using the following[14]:

$$\delta\omega_{max} = 0.86\Delta\omega_0\phi_{max} \tag{6.2}$$

where $\Delta\omega_0$ is the spectral width of the pulse and ϕ_{max} is the maximum value of the phase shift as defined in equation 4.24.

For the UFD-PCF fibres typical parameters are $A_{eff} = 44\ \mu\text{m}^2$, $\Delta\omega_0 = 8$ THz and $n_2 = 2.2 \times 10^{-20}\ \text{m}^2/\text{W}$, so the maximum change in frequency is $\delta\omega_{max} = 0.145$ THz either side of ω_0. This corresponds to a spectrum that extends from approximately 1.38 to 1.76 μm, which is in good agreement with the experimental data for fibres with normal dispersion (such as P4g as shown in figure 6.5).

Comparison with modelling results

Dr. D.V Skryabin and Mr. F. Biancalana modelled the propagation of 100 fs pulses in a selection of the ultra-flattened dispersion fibres[52] using dispersion data plotted in figures 5.6 and 5.7.

They solved the generalised nonlinear Schrödinger equation, as described in section 4.6, using a fast Fourier transform method to integrate the linear part and a second-order Runge-Kutta algorithm for the non-linear part. The input pulses

were chosen to have hyperbolic-secant profiles in time and to be chirp-free.

Considering the complexity of the nonlinear processes involved, and the numerical model's reliance on the accuracy of the measurement of the fibre's dispersion profile, modelling results can be considered to be in extremely good agreement with the experiment. Figure 6.7 shows for fibres p4c, p7e and p4g. Almost all of the spectral features are accounted for and their locations in power, wavelength and intensity are all similar to experiment.

The discrepancies are partly due to the omission of loss in the calculation and the uncompensated spectral response of the spectrometer (for wavelengths greater than 1650 nm). Large spectral discrepancies, like the absence of light near the pump frequency in the modelling for (b), are likely to be a result of limited knowledge of the higher order dispersion of the measured dispersion profiles. The dispersion becomes paramount for small β_2, as the higher order dispersion terms then become more important. However, the value of β_n becomes less accurate with increasing n, as higher-order derivatives of the measured data curves (from the dispersion measurement method detailed in section 2.4.1) are required.

6.4 Comparison of spectra from UFD-PCF with different values of dispersion

An Ando OSA was used to record the spectra at the output of the fibre for maximum input power, and a monochromator in conjunction with an InGaAs photodiode was used to extend the wavelength range up to 2200 nm.

Combining a selection of the resultant traces into a single plot, figure 6.8, allows some insight into the effect of dispersion on the supercontinuum generated in each fibre at constant power and pump-wavelength.

The most striking features in figure 6.8 are the two large peaks at short wavelengths in fibres P4b to P7f, marked (a) and (b). The longer-wavelength peaks (a) are probably due to the breakup of the second-order soliton and subsequent FWM allowed by phase matching (as they occur at the same wavelengths as the peaks in figures 6.4 and 6.5 note 4).

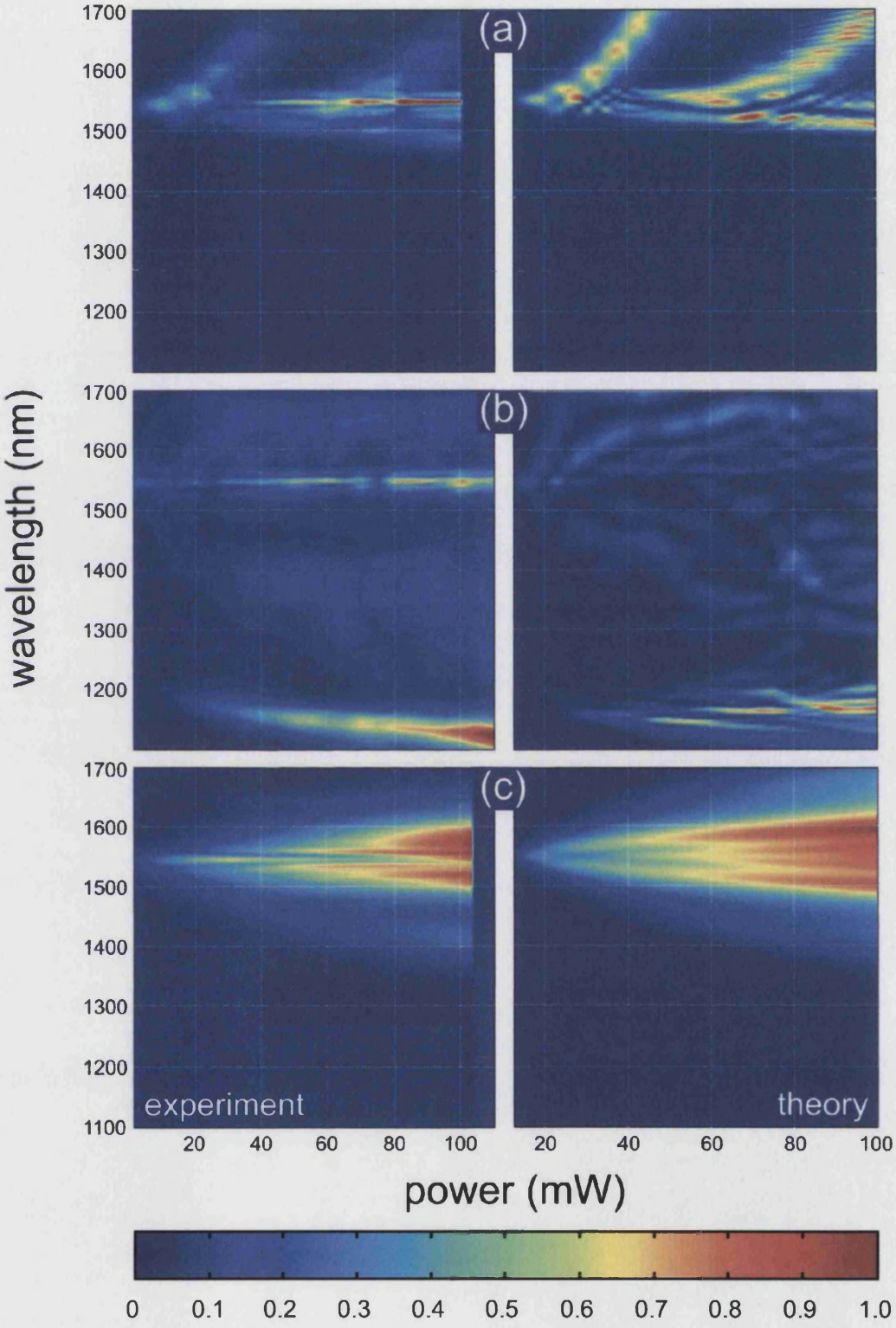

Figure 6.7: Experimental (left) and theoretical (right) spectra for three PCF with flattened dispersion profiles. Fibre (a) is P4c, (b) P7e and (c) P4g. All plots shown on an arbitrary, linear scale.

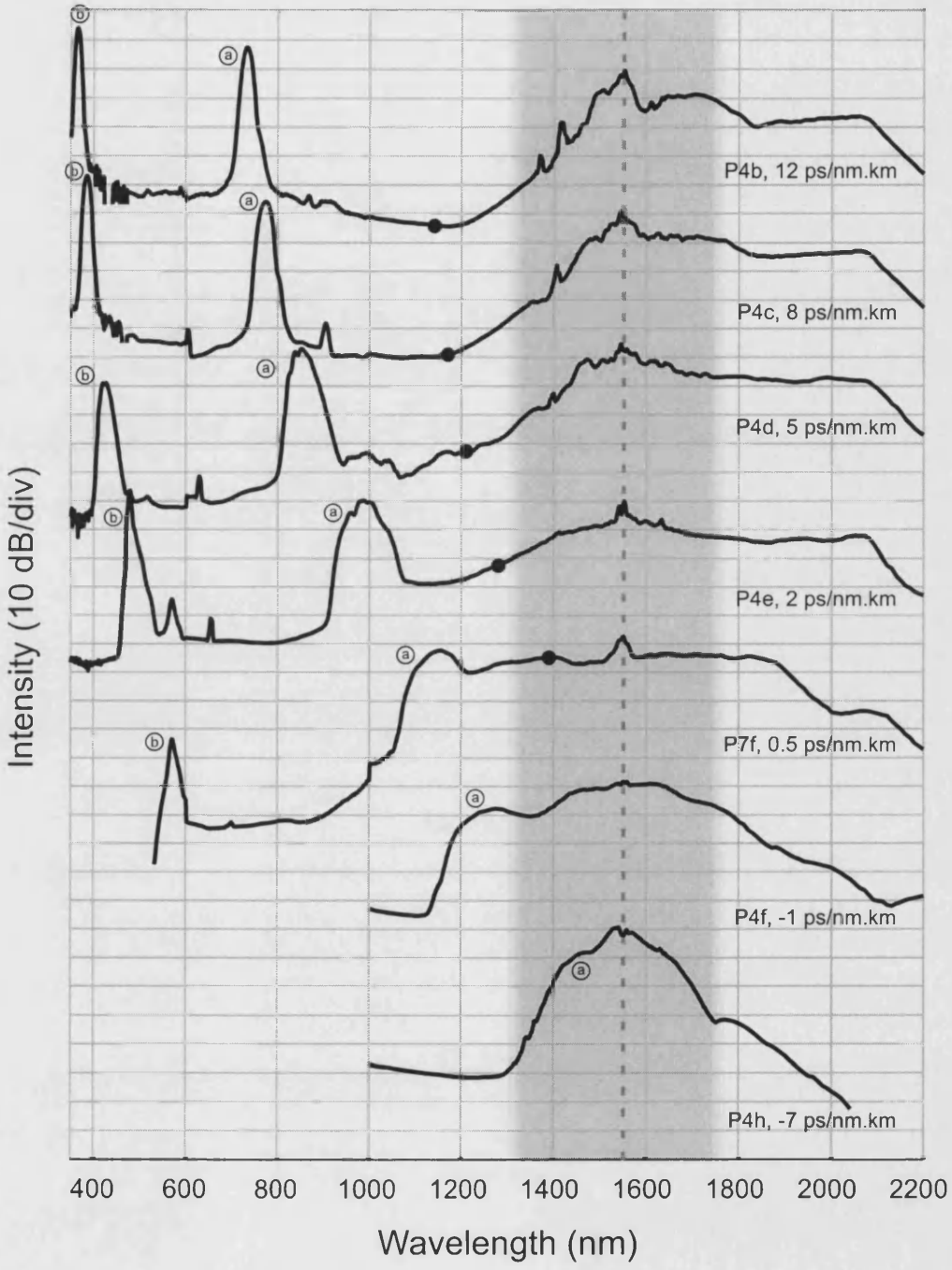

Figure 6.8: Recorded spectra for a range of ultra-flattened dispersion photonic crystal fibres. The vertical dotted line corresponds to the pump wavelength and the shaded gray area is the approximate extent of the flattened-dispersion region. The black circles denote the zero-dispersion wavelength of the fibre.

The following general trend can be observed in these fibres: the smaller the value of dispersion, the longer the zero-dispersion wavelength. This results in a shift of the (a) peaks to longer wavelengths due to the changing phase matching condition. (Unfortunately, phase-mismatch graphs could not be included here due the unavailability of dispersion data for wavelengths longer than 1.7 μm).

The shorter-wavelength peaks (b) are always twice the frequency of the first and are speculated to be a measurement artifact generated from the overlap of grating orders within the Ando OSA. However, the peaks have different spectral profiles (as can be clearly seen for fibre P4e) so it is possible that these peaks are real. Unfortunately this was not investigated during experimentation at Los Alamos due to time restrictions. However, verification would simply require the direct viewing of the light emerging from the fibre P4d. If the light is blue/green then the peak is real, in which an alternative explanation must be sought.

Figure 6.8 also shows that at the transition between the anomalous and normal dispersion regimes there is no discontinuity in the output spectra. Interestingly, the phase-matching peaks formed from soliton-breakup seem to occur (to some extent) in fibres with negative values of dispersion. In fibres with progressively larger values of normal dispersion, the peaks appear to broaden and merge with the SPM spectral broadening. This apparent continuity could be due, in part, to fibre non-uniformities (eg. small sections of fibre may vary sufficiently size to make part of the dispersion profile anomalous). However, in a fibre with a dispersion-flattened region with a value of approximately -7 ps/nm.km, the remnant of the peak is still visible as a step at approximately 1450 nm.

Figure 6.8 shows that the generation of broad flat supercontinuua is possible in UFD-PCF. For example, the fibre P7f has a continuum the extends from 1.1 to 1.9 μm with a power variation of only 10 dB.

6.5 Experiment: generated spectra with fibre length

To examine the effect of fibre-length on the spectra generated, a cutback measurement was performed on the fibre P7e (with a very similar dispersion profile

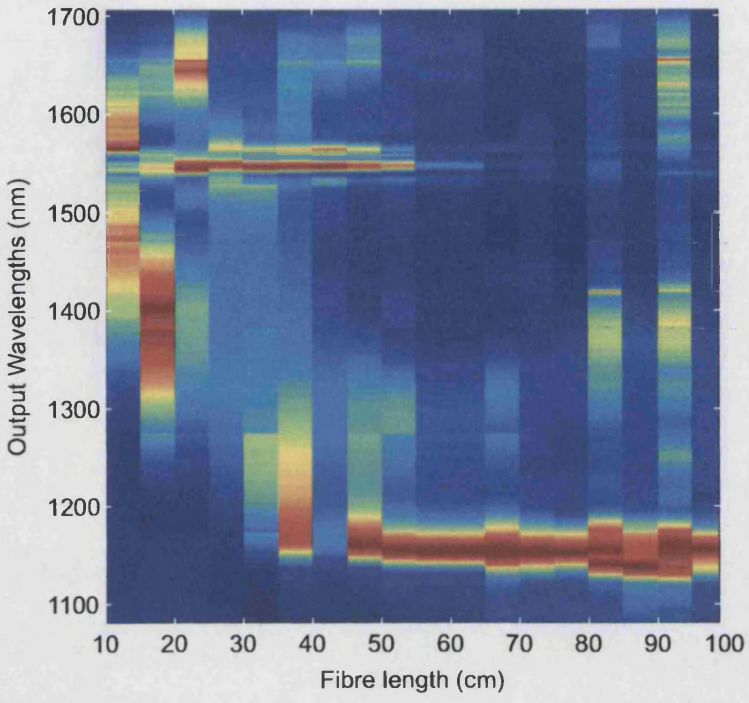

Figure 6.9: The spectra generated using the maximum ($\sim$ 240 mW average input) pulse power for various lengths of the fibre P7f.

to P7f). A 1 m section of fibre was cut back every 5cm to final length of 10 cm. The output spectrum was recorded for each length, for the maximum input power available (approximately 240 mW). Figure 6.9 shows the results of this experiment. The data is shown without interpolation as not many points were taken and is also normalised for each measurement. Fibre input coupling was not altered during the experiment however, output coupling into the spectrometer inevitably varied each time the fibre was cleaved. It is believed that this, together with small laser power fluctuations, caused the data to be noisy.

From this plot it is interesting to note that the dominant peak at around 1150 nm appears after approximately 35-40 cm of propagation.

Figure 6.10 presents modelling results showing that soliton formation occurs at a propagation distance of approximately 40-50 cm. This is in good agreement with the experiment as the large peak centred at approximately 1150 nm in figure 6.9 starts to become prominent at this length.

Figure 6.11 shows measurements, of spectra against power, made on the fibre

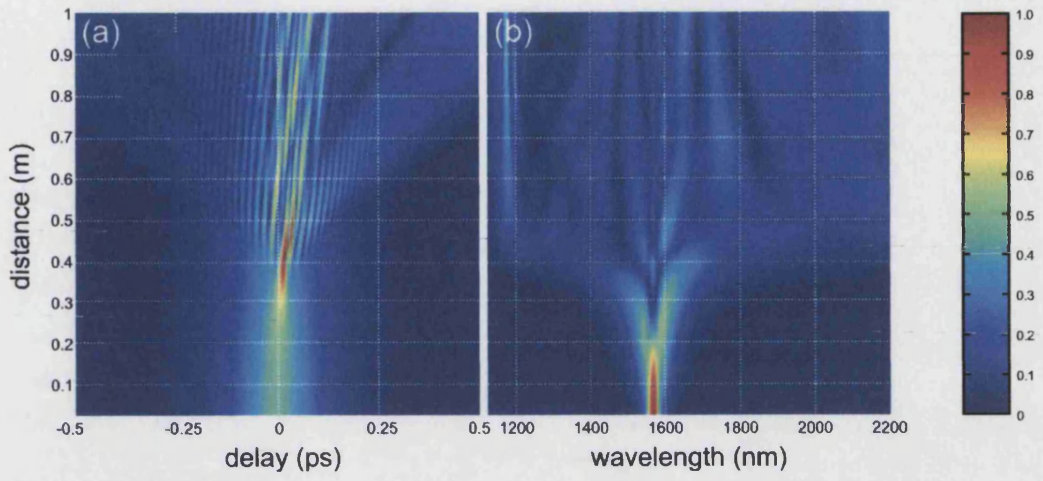

Figure 6.10: The theoretical pulse evolution with propagation distance for fibre P7e. (a) shows pulse delay and (b) the spectrum. both plots shown on an arbitrary, linear scale.

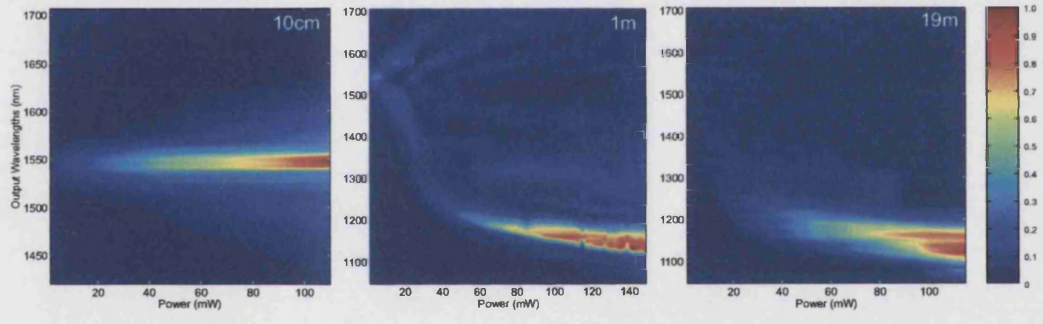

Figure 6.11: Generated spectra against power for 10 cm, 1 m and 19 m of the fibre P7F plotted on a arbitrary linear intensity scale.

P7F with lengths of 10 cm, 1 m and 19 m respectively.

As the data in figure 6.9 suggests, no soliton forms within a length of 10 cm and only a small amount of spectral broadening occurs. With a 19 m length of fibre the plot looks similar to that obtained from the 1 m-length segment. However, the effect of the additional length only appears to smooth-out the spectra and obscure the fine features. However, the additional length has no effect on the phase matching condition, resulting in the dominant peak remaining centered at 1150 nm. Further broadening of the spectra due to SSFS may occur in the IR but is not detectable by the spectrometer.

6.6 Summary and conclusions

By varying the laser power in a range of PCF with ultra-flattened dispersion profiles it can be clearly seen how intensity and dispersion govern the nonlinear processes responsible for supercontinuum generation. The solution of the GNLSE has proved to be extremely accurate when modelling pulse propagation in these fibres considering the complexity of the nonlinear interactions and the model's reliance on the accuracy of the fibre's dispersion profile. Discrepancies are likely to be caused by the experimental error of the measured dispersion profiles of the various fibres.

An interesting feature was found in the spectra generated using the UFD-PCF (and also in SMF28). The Raman-induced frequency shift of the soliton does not appear to be continuous with increasing power. Modelling has shown that these 'steps' appear even in the simple case where dispersion is set to a constant and optical shock is neglected. It is proposed that the step-like shift is a feature (for special cases as it is not discussed in the literature) of SSFS.

Even though solitons cannot form in fibres with normal dispersion, the transition from the anomalous to normal dispersion regimes appears to affect the spectra in a continuous manner, and there is no abrupt change in the spectral profile of the supercontinuum. In fact, the spectral features corresponding to higher-order soliton breakup seem to gradually merge with the SPM broadened spectra. Additionally, the generation of broad flat supercontinuua was shown to be possible in UFD-PCF. For example, the fibre P7f has a continuum that extends from 1.1 to 1.9 μm with a variation of only 10 dB.

More generally, we can conclude that nonlinear effects can be selectively enhanced and controlled not only by increasing the effective nonlinear coefficients of the material, but also by manipulating the dispersion profile over a wide wavelength range.

Chapter 7

Ultra short pulse propagation in SF6 extruded fibre

This chapter investigates supercontinuum generation in a PCF made from a high index glass called SF6. This fibre was made by Dr. V.V.R.K. Kumar and Mr. A.K. George by extruding the bulk material instead of the traditional PCF 'stack-and-draw' method. My role within this work involved measuring the dispersion of the fibres and to conduct the nonlinear experiments at the Los Alamos National Laboratory.

7.1 SF6 extruded fibre

The majority of photonic crystal fibre research concerns fibres made of silica fabricated using the stack-and-draw process. Recently PCF drawn from other glasses[53] and polymers [54, 20] have been reported. However, fabrication using the stack-and-draw process may not be suitable for such materials due to their availability and cost (stack-and-draw typically uses large quantities of glass) or melting properties. Fabrication of fibres by extrusion is an alternative technology and has recently been extended to the use of soft glasses[55].

Nonlinear applications of photonic crystal fibres require both a high nonlinearity (achieved by forming small cores and by using materials with large values

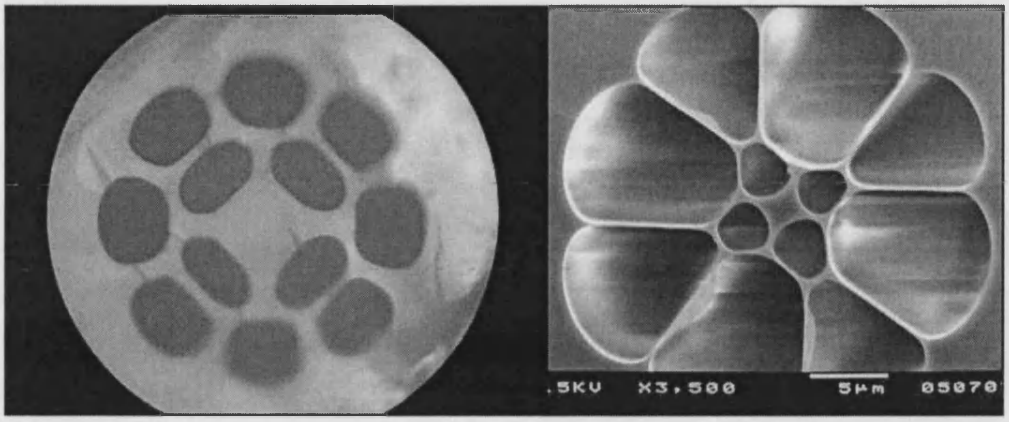

Figure 7.1: Preform (left, optical micrograph) and fibre (right, electron micrograph) fabricated from SF6 glass by extrusion. The preform (left) is 1mm in outer diameter, and was jacketed prior to drawing the fibre shown on the right. The fibre has a nominal 2.6 μm core diameter, and the glass strands in the second ring of air holes are 150 nm across and 6 μm in length.

of nonlinear refractive index n_2) and good control of the GVD. Previous work concentrated on optimizing the nonlinearity in PCF formed from soft glass[55].

Dr. Kumar and Mr. George of the University of Bath produced a range of microstructured fibre by extruding commercially available SF6 glass[19]. SF6 has a refractive index of 1.76 at 1550 nm[56], and has a nonlinear index $n_2 = 2.2 \times 10^{-19} m^2/W$[57]. Figure 7.1[1] shows images of the preform and one of the final fibres. The cores of the fibres were rectangular with a aspect ratio of about 1:2. Consequently the fibres had significant form birefringence.

Figure 7.2 shows the measured GVD curves for the fundamental mode in SF6 fibres with four different core sizes. Also included is the dispersion profile of the bulk SF6 material. Even though the fibre was multi-mode the dispersion measurement was relatively easy as light was launched into the interferometer via a single-mode fibre. Light was therefore only launched into the fibre's fundamental mode and this meant that additional fringe packets (corresponding to higher order modes) were not seen.

The two polarisation modes of the fibres were measured independently by using a polariser mounted in the input arm of the interferometer. The two polarisation

[1]Images courtesy of Dr. Kumar

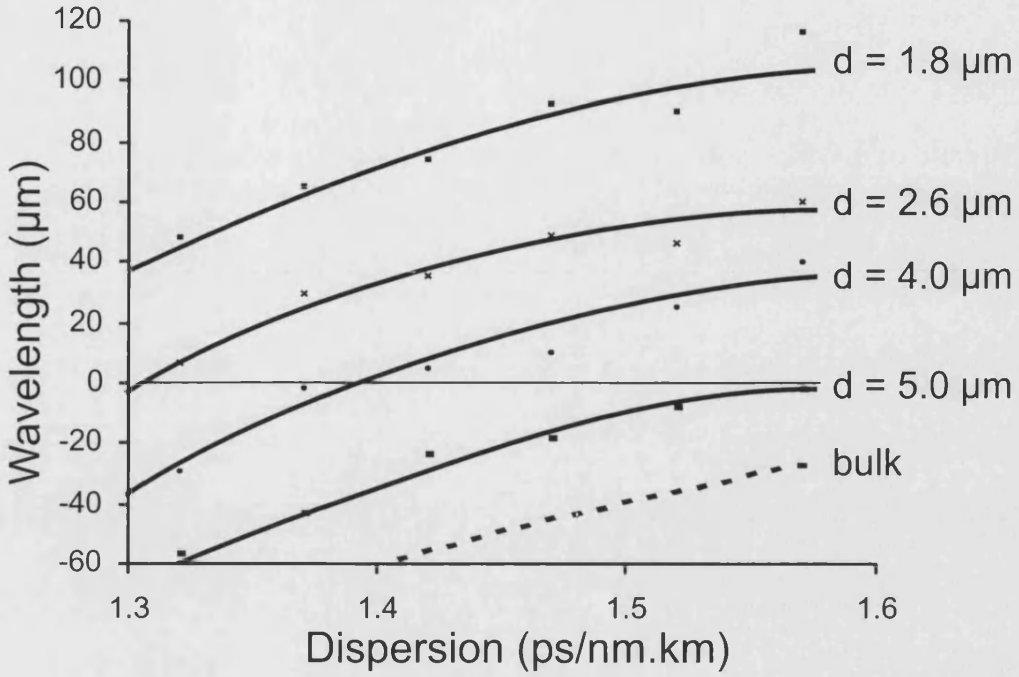

Figure 7.2: Measured group-velocity dispersion curves for bulk SF6 (broken curve) and for the fundamental mode in fibres with four different core sizes. Raw data is plotted as points together with spline fits.

modes had very similar dispersion profiles that were off set from each other by approximately 25 nm and only the polarisation mode with the highest ZDW is plotted here. Figure 7.3 shows the dispersion profiles for both polarisation states of the fundamental mode for the SF6 fibre with the 2.6 μm diameter core.

Figure 7.4[2] shows the result of a loss measurement made on the fibre shown in figure 7.1. SF6 is transparent over the spectral range 500 - 2000 nm, with a minimum bulk loss of about 1 dB/m[56]. The minimum observed loss in the fibre is 2 dB/m at a wavelength of 1200 nm. Loss at long wavelengths is dominated by confinement loss (which has a dramatic dependence on wavelength), while water absorption accounts for the large peak at around 1400 nm.

[2]Data provided by Dr. Kumar

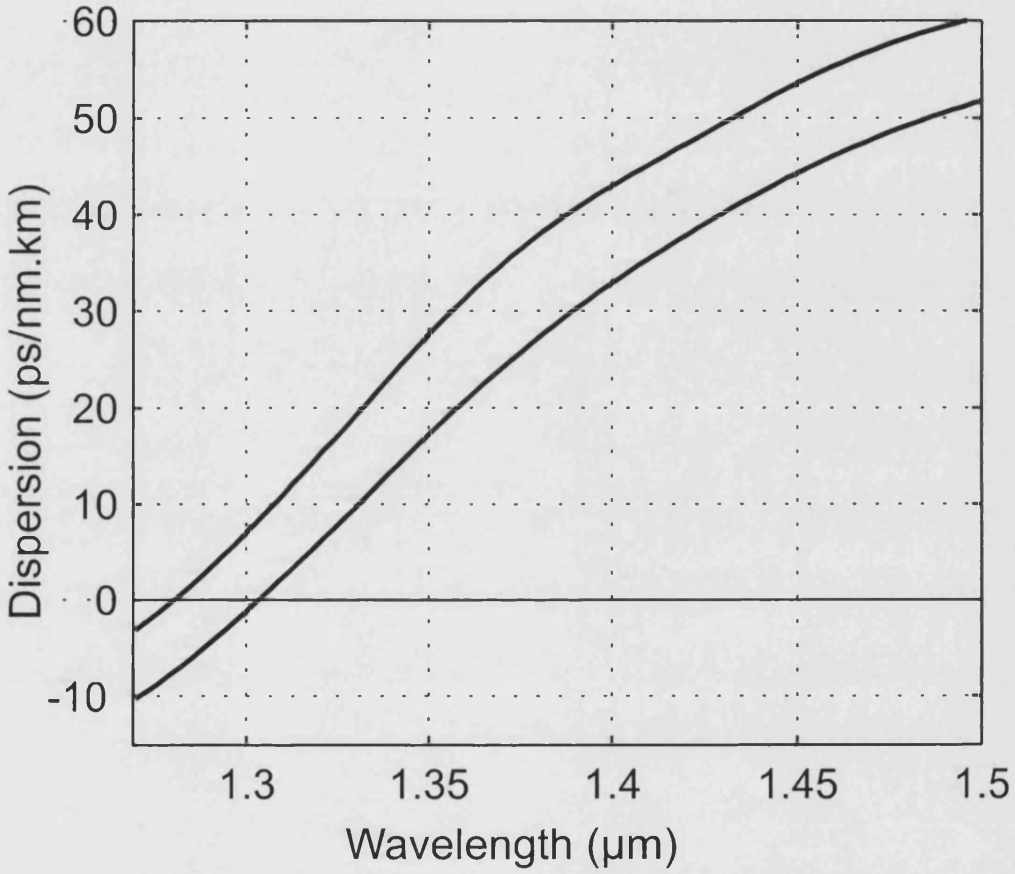

Figure 7.3: Measured group-velocity dispersion curves for the two polarisation states for the fundamental mode of the SF6 with an approximate core diameter of 2.6 μm.

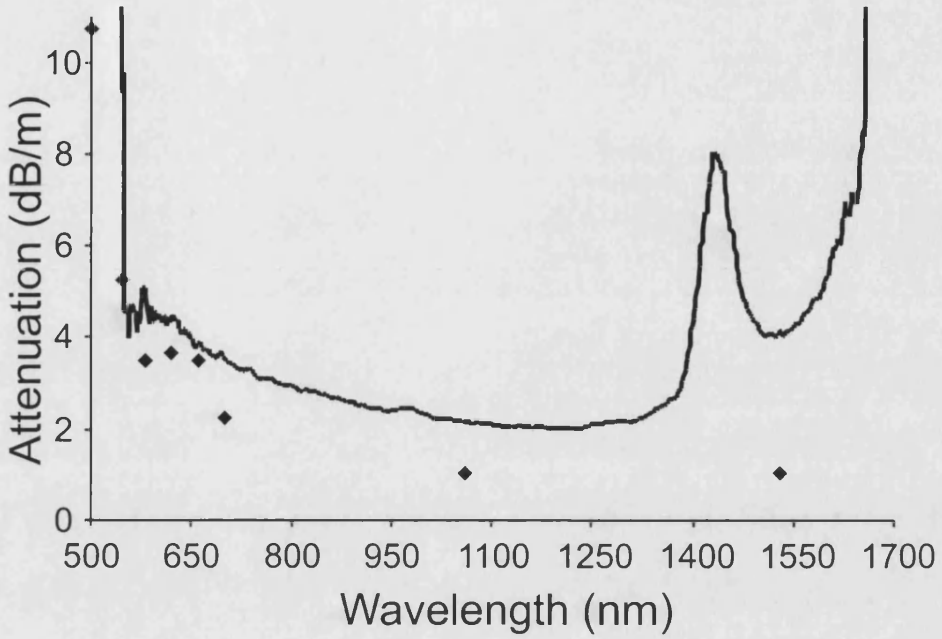

Figure 7.4: Measured loss in SF6 PCF with a 2.6 μm core, as shown in figure 7.1. The square points are for bulk SF6 glass.

7.2 Results

The equipment detailed in section 6.2 was used to study the effects of propagating ultra short pulses in this fibre.

Pulses were launched into $\approx$ 60 cm of the SF6 fibre with a 2.6 μm core diameter in a similar experiment to that described in section 6.3. Figure 7.5 shows the spectra recorded using the Jobin-Yvon spectrometer for various powers, both recorded at the fibre output (A log plot of the same data is also provided).

As can be seen, there are two spectral traces that deviate out to longer wavelengths. These correspond to the formation and subsequent frequency shift of the first and second order solitons in an almost identical manner to that observed in the UFD-PCF (see previous chapter).

Using equation 6.1 with a value of $n_2 = 2.2 \times 10^{-19} m^2/W$, a dispersion of 60 ps/nm.km and a estimated effective area of 6.8 μm^2, the powers required to create the fundamental and second-order soliton are 4.7 mW and 18.7 mW

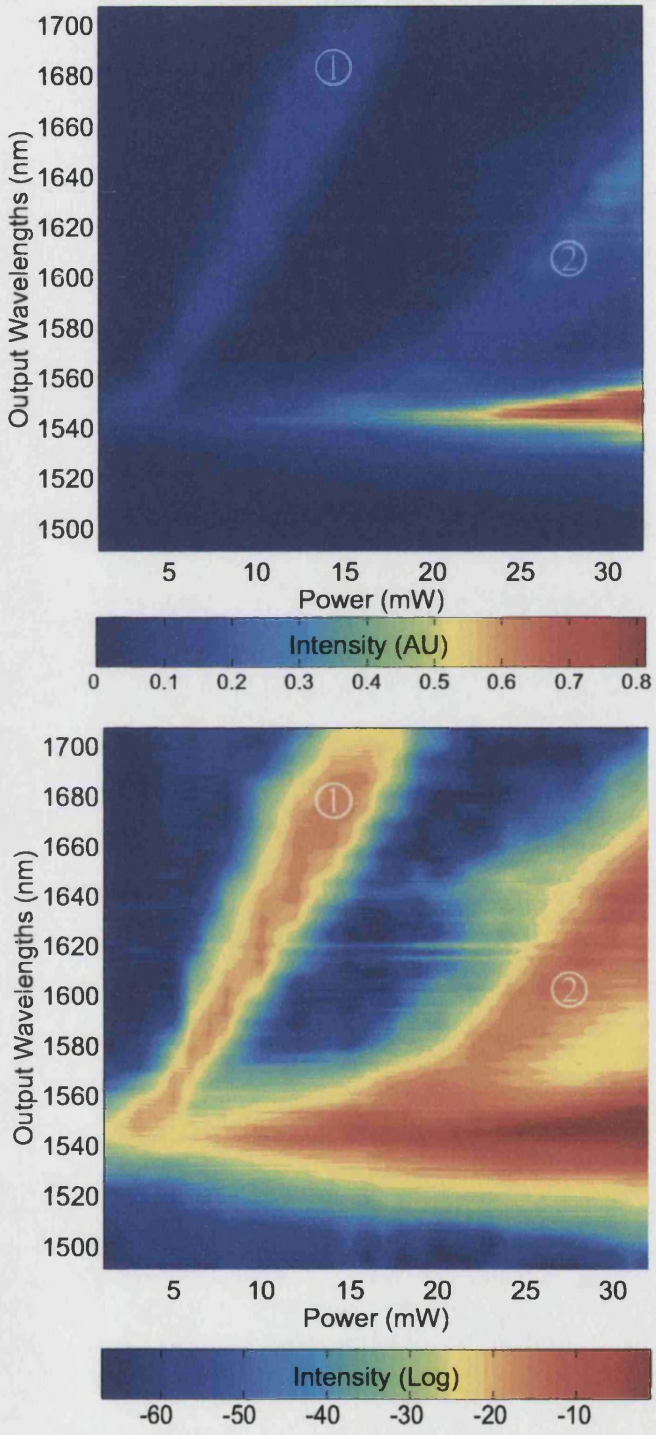

Figure 7.5: Generated spectrum with power from the microstructured SF6 fibre shown in figure 7.1 when pumped with 110 fs pulses at 1550 nm. The two plots are of the same data.

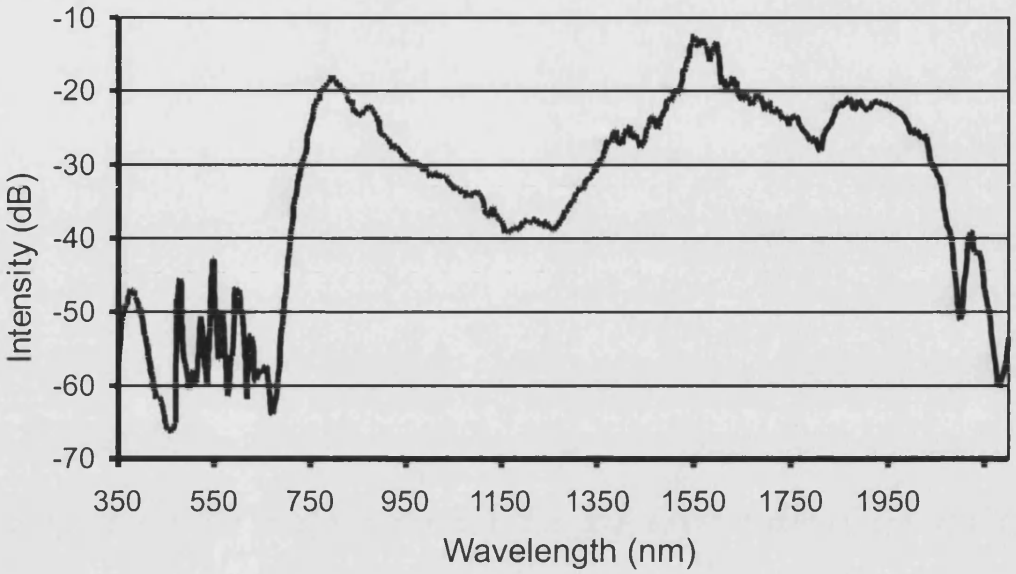

Figure 7.6: Optical spectrum of the continuum observed at the output of a 75 cm length of 2.6 μm core fibre.

respectively. As can be seen, this is in good agreement with experiment. Any energy left over from the formation of these solitons continues to propagate at the pump wavelength and broadens with higher powers.

The spectra was also measured using the Ando OSA and InGaAs photodiode based monochromator at the maximum power obtainable at the fibre output. Figure 7.6 shows the result of this measurement, a supercontinuum that extends from at least 350 nm to 2200 nm.

The supercontinuum was extremely sensitive to the input coupling. For the experiments detailed above optimal coupling was considered to be achieved when output power was at maximum. Figure 7.7 shows a selection of photographs taken with a digital camera where the input coupling of the fibre was varied by moving the fibre using a piezoelectric actuator.

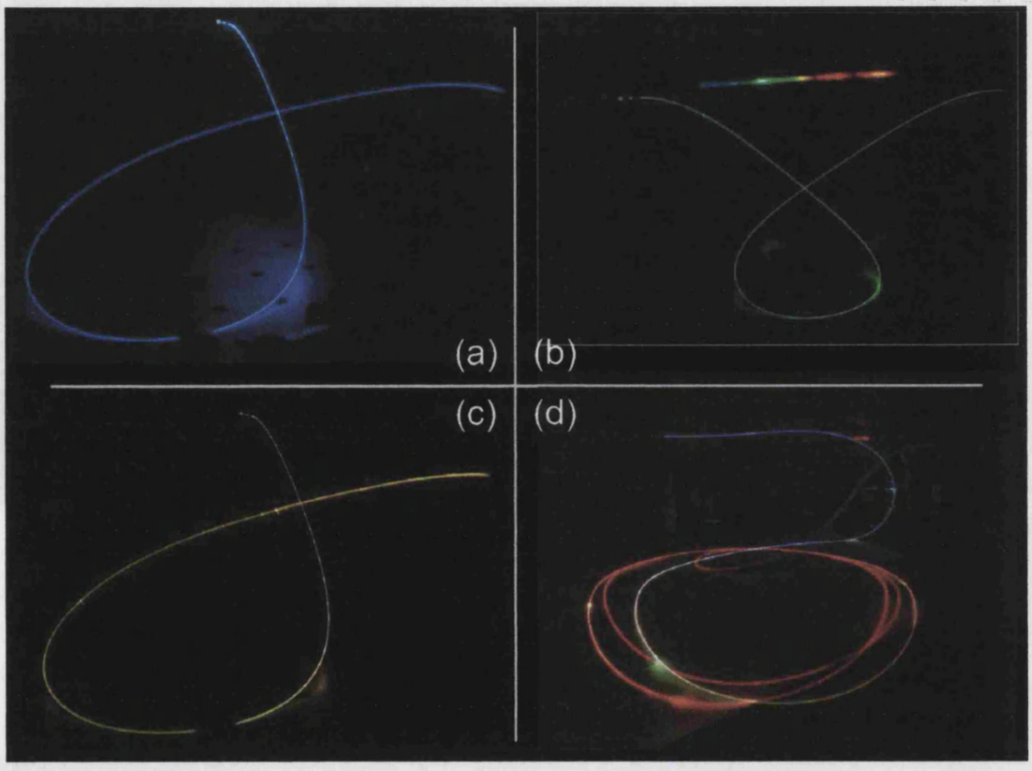

Figure 7.7: Photographs taken with a digital camera. (a)-(c) show a 75 cm length of the fibre shown in figure 7.1 with small variations in the input coupling. (b) shows visible part of the supercontinuum when the the coupling was optimised to give the largest output power. (d) shows several meters of the same fibre. The colour variation is due to the strong wavelength dependant loss in the visible.

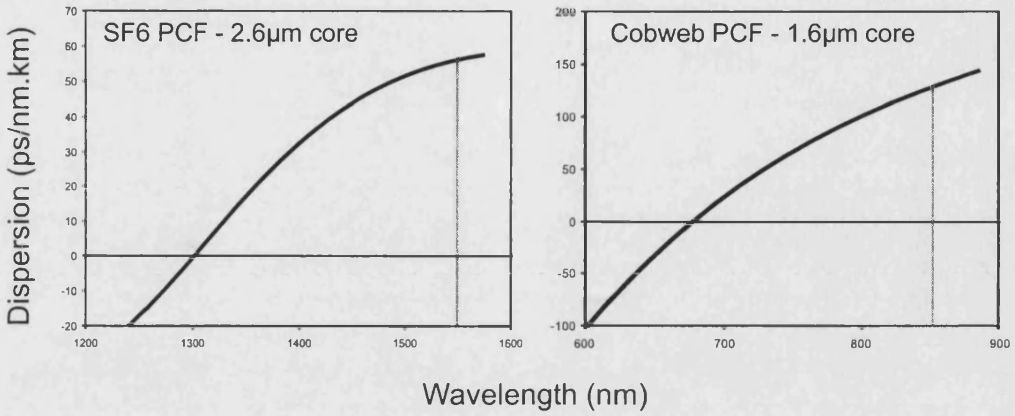

Figure 7.8: Dispersion profiles of SF6 PCF with 2.6 μm diameter core (left) and cobweb PCF with a 1.6 μm diameter core. The grey vertical lines represent the pump wavelengths used to generate the supercontinua shown in figure 7.9 and are 1550 nm and 850 nm respectively.

7.3 Discussion

The dispersion profiles of the SF6 fibres are very similar in shape to those of cobweb PCF[6] made from silica. Cobweb PCF were engineered to have ZDWs near the operating wavelengths of the mode-locked Ti:Sapphire laser. In a similar manner the SF6 fibres were designed to have ZDWs near to 1550 nm, easily obtainable using the Ti:Sapphire pumped OPO.

Figure 7.8 shows the dispersion curves and pump wavelengths for both the SF6 PCF (left), pump at 1550 nm, and cobweb PCF (right), pump at 850 nm. These plots look very similar and as dispersion is probably the most important property that governs how nonlinear effects generate new frequencies one might expect the supercontinua generated from these fibres to be similar.

Figure 7.9 shows the supercontinua for a cobweb PCF (lower axis) and the SF6 fibre with the 2.6 μm diameter core (upper axis)[3]. Both fibres were pumped with $\approx$ 100 fs pulse with average powers near 200 mW. As expected, the overall features of the supercontinua are very similar. The most obvious difference is the wavelength ranges of the supercontinua where the SF6 fibre spans an additional $\sim$ 400 nm. This is likely to be due to the higher nonlinearity of the SF6 glass.

[3]All cobweb PCF data courtesy of Dr. W.J. Wadsworth

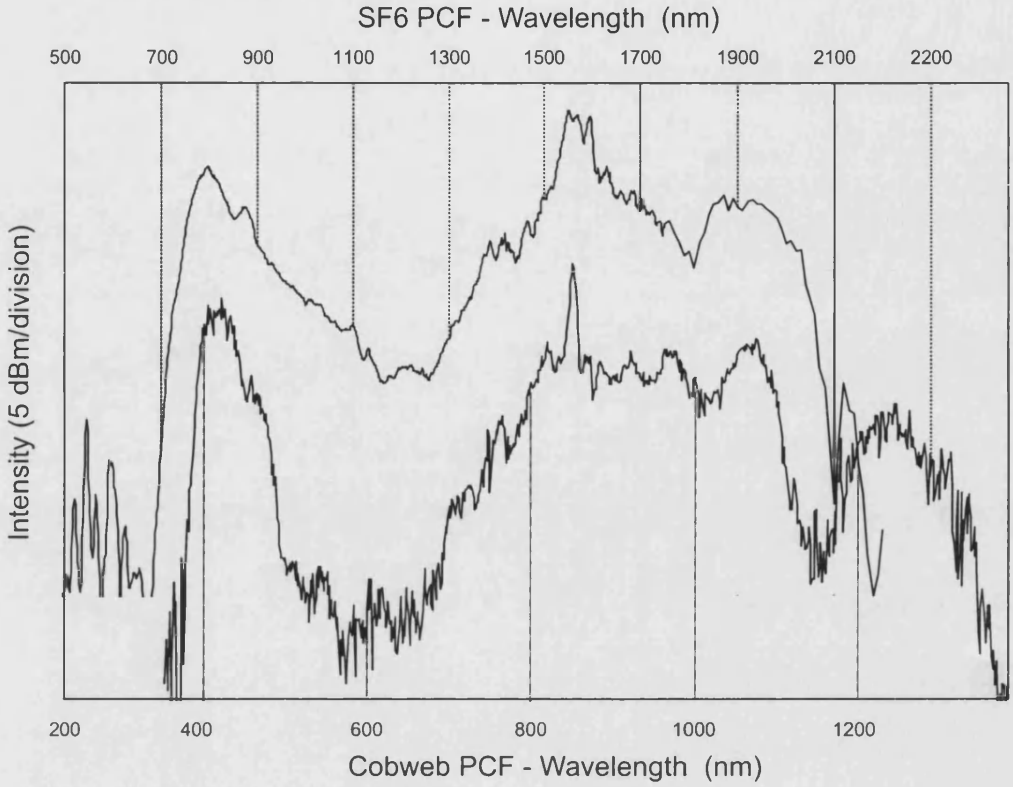

Figure 7.9: Comparison of supercontinuum generation using SF6 PCF with a 2.6 μm core and a cobweb PCF with a core diameter 1.6 μm. (a) shows the dispersion profiles of both fibres and (b) shows the generated supercontinua, (SF6 upper plot). Both fibres were pumped using 100 fs pulses at an average power of $\approx$ 200 mW. The SF6 fibre was pumped at 1550 nm and the cobweb fibre at 850 nm.

It is often desirable to obtain the broadest, flattest and brightest supercontinuum possible and it is likely that the supercontinuum measured here is far from optimum for microstructured fibres made from SF6. Problems with the current fibres potentially involve the quality of the available SF6 glass and fibre structure.

When compared to conventional optical fibre fabrication methods, the fabrication procedure for extruded SF6 fibre is still in its infancy. Fibres are drawn relatively slowly ($\approx$ 5 m/min) and have significant fluctuations in fibre diameter ($\approx$ 10%). Scattering points inside the fibre are apparent when propagating light down the fibre. Figure 7.7d clearly shows a number of these. Using an infra red viewer highlights this problem as a large amount of light is lost from these points. The physical causes of the scattering points are unknown but could include crystalli-

sation of the glass, the inclusion of air bubbles and contamination of the SF6 during processing.

Additionally, cleaving the fibre and coupling light efficiently is difficult. The power obtainable at the output of the fibre was consequently much lower than for the UFD-PCF. Usually only 30 mW of average power was available from the 240 mW input power.

As extruded fibre drawing technology progresses it should be possible to draw fibres with more uniform structures similar to those for cobweb PCF. Additionally other soft glasses with even higher value of nonlinearity may be used to further broaden and flatten the supercontinuum.

7.4 Conclusions

Spectacular broadband supercontinuum generation has been observed by pumping microstructured SF6 fibres with 100 fs pulses at 1550 nm. This continuum is very similar to that generated from cobweb PCF pumped with 100 fs at 850 nm.

The spectrum extends from at least 350 nm to 2200 nm which believed to be the broadest supercontinuum recorded from a single source to date. With further improvements to the fibre structure these fibres will enable the generation of octave spanning supercontinua using mode locked fibre laser sources at 1550 nm. Devices using fibres of this type will be compact and stable high brightness broadband light sources.

Chapter 8

Summary and future work

8.1 Summary

This thesis focuses on the fabrication and characterisation of a set of photonic crystal fibres with a ultra-flattened dispersion profiles. This characterisation involved the investigation of ultra-short pulse propagation in these fibres, together with measurements of their chromatic dispersion properties and physical structure.

Ultra-flattened dispersion PCF (UFD-PCF)

Ultra-flattened dispersion in photonic crystal fibre has been demonstrated for the first time. With improvements to the fabrication procedure, a set of fibres with ultra-flattened dispersion profiles were fabricated in lengths longer than 100 m. The values of dispersion for the flattened regions of the set of fibres varied from $\sim$ 12 to -7 ps/nm.km. The smallest value of dispersion for a flattened region was $\sim$ 0.5 ps/nm/km. The dispersion slope at 1550 nm, the centre of the flattened region, for the set of fibres was typically less than ± 0.005 ps/nm^2.km. A number of fibres (P7e and P7f) had measured slopes smaller than $\pm$ 0.007 ps/nm^2.km in a range of at least 260 nm from 1.44 to 1.7 μm. However, the measurements on fibres with of small dispersion and small dispersion slope are likely to be inaccurate

due to the experimental error (estimated to be approximately ±0.25 ps/nm.km). Fibre diameter fluctuations, estimated to be up to ±5 μm, seem to have little effect on the value of dispersion at 1550 nm.

Ultra-short pulse propagation and supercontinuum generation in UFD-PCF

By varying the injected laser power in a number of PCF with ultra-flattened dispersion profiles it has been shown how pump intensity and dispersion govern the nonlinear processes responsible for supercontinuum generation.

The Raman-assisted soliton-self-frequency-shifting in UFD-PCF (and SMF28) does not appear to be continuous with increasing power. This is corroborated by modelling and it is believed that this feature is previously unreported. The precise cause of these 'steps' is unknown but it is suggested that this could be a previously unreported feature of SSFS.

Even though solitons cannot form in fibres with exclusively normal dispersion, the spectra changes in a continuous manner in fibres with flattened dispersion regions during a transition from the anomalous to normal dispersion regimes. Specifically, the spectral features corresponding to higher-order soliton breakup appear to gradually merge with the SPM-broadened spectra. The exact cause for this was not found but is speculated to be partly due to fibre diameter fluctuations that shift the dispersion profile into the anomalous regime.

The ability to control the dispersion profile precisely over a broad wavelength range has important ramifications for the field of nonlinear fibre optics as nonlinear effects can then be enhanced and controlled by tayloring the dispersion profile and not merely by increasing the effective nonlinear coefficients of the material.

Ultra-short pulse propagation and supercontinuum generation in microstructured extruded SF6-glass fibres

Spectacular broadband supercontinuum generation has been observed spanning at least 350 nm to 2200 nm, which is believed to be the broadest supercontinuum

recorded to date.

This was achieved by pumping microstructured SF6-glass fibre with 100 fs pulses at 1550 nm. The generated supercontinuum is reminiscent of that generated from cobweb PCF pumped with 100 fs long pulses at 850 nm[6].

Fibres of this type will undoubtedly be used in future as components for compact and stable high-brightness broadband light sources.

8.2 Future work

The work presented in this thesis could be extended in many directions including:

It would be interesting to further characterise the nonlinear effects in the existing UFD-PCF and extruded SF6 glass fibre. For example, the OPO could be used to pump the fibres at different wavelengths, perhaps near their ZDW. It is likely that pumping near the ZDW would give rise to even broader supercontinuua.

More UFD-PCF could be drawn from existing preforms to investigate the effect of three ZDWs (in close proximity) on the nonlinear processes. This could easily be achieved by using the information in figure 5.2 to adjust the fibre pitch and hole diameter so that fibres have a relatively large negative dispersion slope at 1550nm.

In a paper published very recently[58] a new design of UFD-PCF is described. This 'graded index design' enables fibres with flattened dispersion and reduced confinement loss to be made with significantly fewer periods. The effective areas of fibres of this type are expected to be around five times smaller than the 44 μm^2 of the fibres presented in this thesis, resulting in a much higher attainable nonlinearity. This fibre could be fabricated in the near future.

UFD-PCF have the potential for use as broadband supercontinuum generators. For example, figure 8.1 shows the spectral profile resulting from pumping 100 m of the fibre P4a with 600 ps pulses from a microchip laser at 1065 nm. As can be seen, the supercontinuum generated is exceptionally flat with the exception

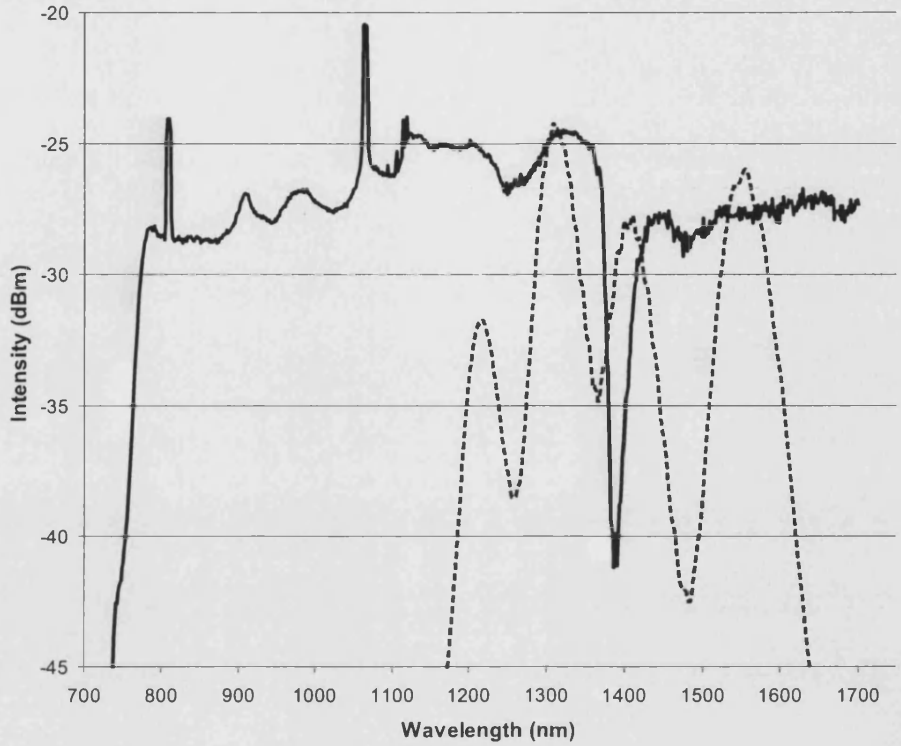

Figure 8.1: Ultra-broadband supercontinuum generation from 100 m of fibre P4a pumped using 600 ps pulses at 1065 nm. The large gap in the spectrum at 1380 nm is attenuation due to water. The dotted line shows the spectral profile of a commercial 'broadband' LED source.

of the attenuation due to water at 1380 nm. This is especially significant as microchip lasers typically cost around $6000 whereas Ti:Sapphire laser systems (normally used to generate supercontinuum from PCF) cost approximately an order of magnitude more.

Further improvements to the supercontinuum could be achieved by reducing the loss and further optimising the dispersion profile. This would be very useful in all applications requiring bright, broadband light sources.

Other future work utilising the nonlinear effects in fibre could involve incorporating UFD-PCF (made from silica and soft glasses) into devices and applications. Examples could include optical parametric amplifiers and oscillators and the building of a compact fibre laser broadband light source from highly nonlinear glass fibre.

Communications applications may be sought by matching the relevant fibre parameters (NA and effective area) to that of conventional fibre. Low-loss, low-nonlinearity fibre ultra-flattened dispersion fibre could have potential applications in (D)WDM.

Appendix A

Ultra-short pulse propagation in UFD-PCF - full data sets

Figures A.1 to A.13 show the various data sets recorded for fibres P4a-h, P7d-g and SMF28. Each page contains the fibres' dispersion curve, spectrum generated with output power (similar to that shown in figure 6.2b), a logarithmic version of the previous plot and a power summation plot similar to figure 6.3. In addition, a trace recorded by the 'Ando' OSA is shown for maximum output power of each fibre.

Figure A.14 shows a comparison of all the power/spectrum plots. Unlike the plots on the previous pages, these plots are set to same wavelength and power scales.

Although the OSA records the most of the generated spectra some light is lost along the length of the fibre. This loss appears to be very wavelength dependant as the photographs in figure A.15 show.

Dispersion

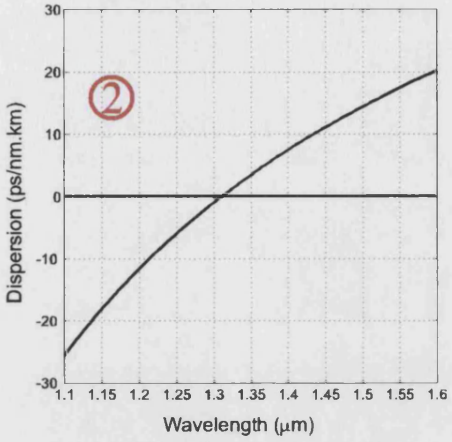

OSA and monochromator spectrum

①

Log power/spectrum

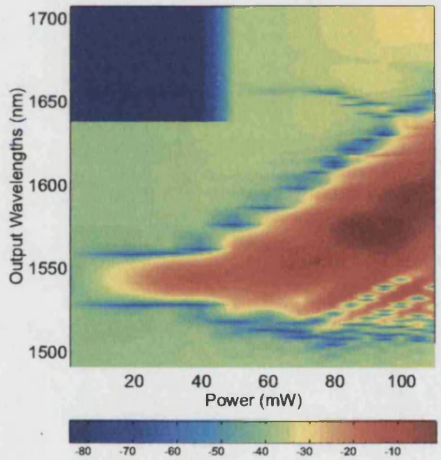

Power/spectrum

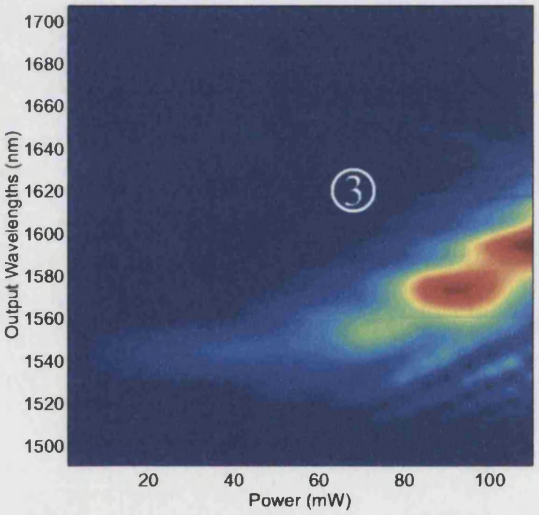

Power integral

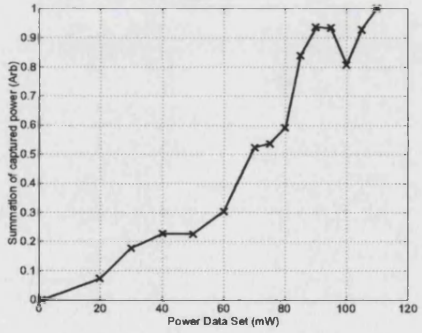

Notes:

1. Spectra not recorded with OSA for this fibre
2. Large scale used to show dispersion of this fibre
3. Step-like features visible in the soliton self frequency shift.

Figure A.1: Recorded spectra with power for the fibre P4a

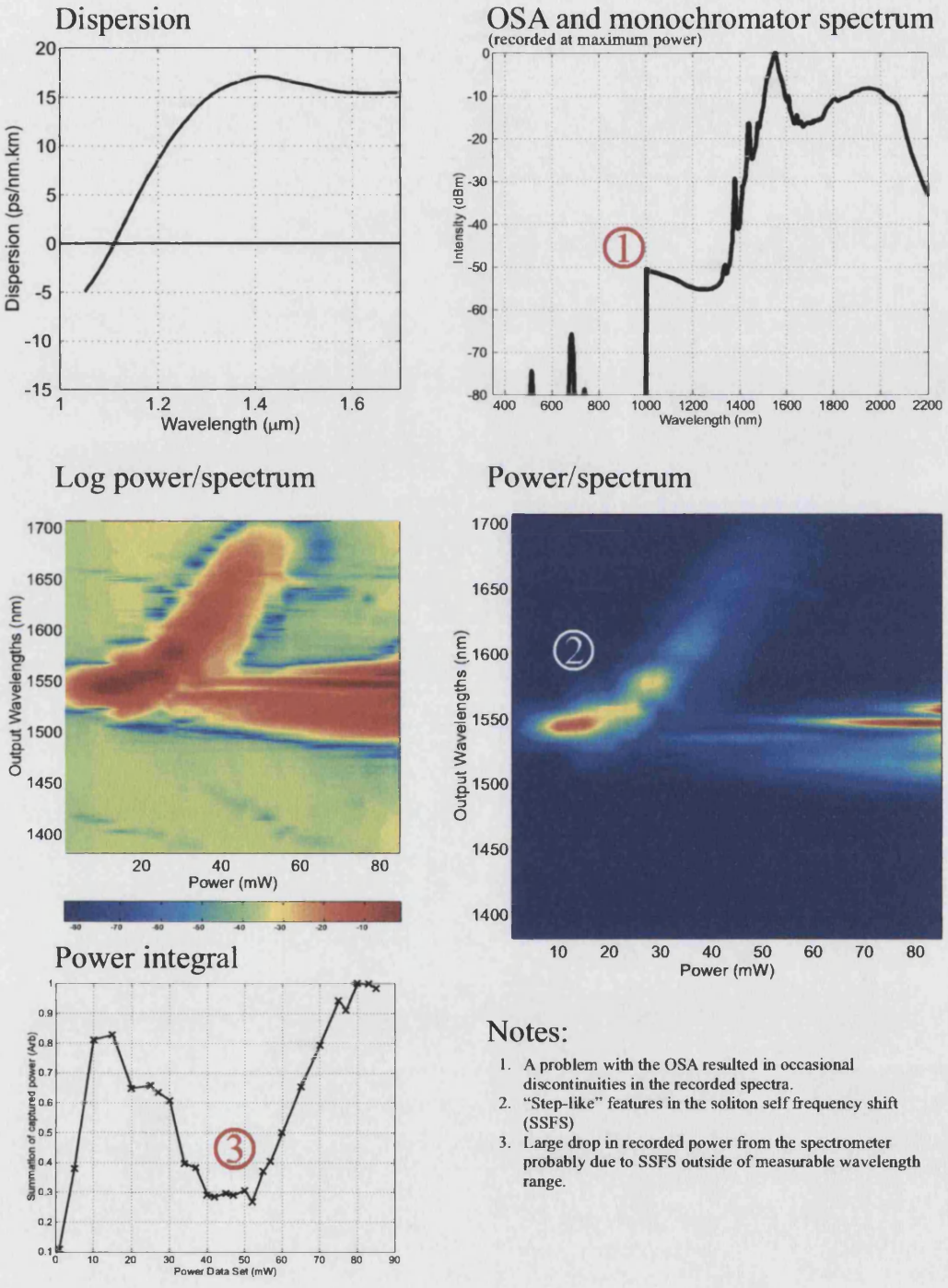

Figure A.2: Recorded spectra with power for the fibre P4a

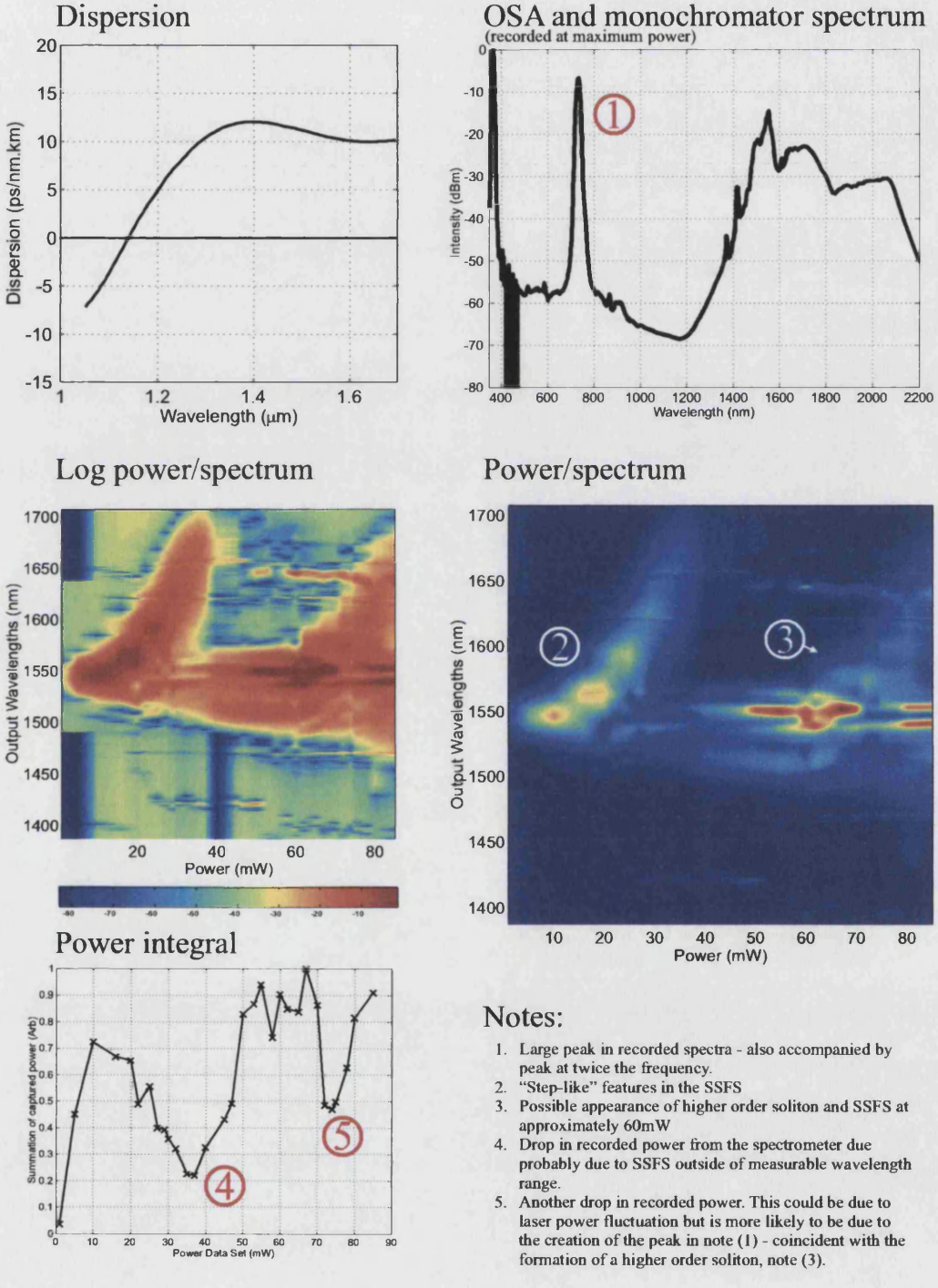

Notes:

1. Large peak in recorded spectra - also accompanied by peak at twice the frequency.
2. "Step-like" features in the SSFS
3. Possible appearance of higher order soliton and SSFS at approximately 60mW
4. Drop in recorded power from the spectrometer due probably due to SSFS outside of measurable wavelength range.
5. Another drop in recorded power. This could be due to laser power fluctuation but is more likely to be due to the creation of the peak in note (1) - coincident with the formation of a higher order soliton, note (3).

Figure A.3: Recorded spectra with power for the fibre P4b

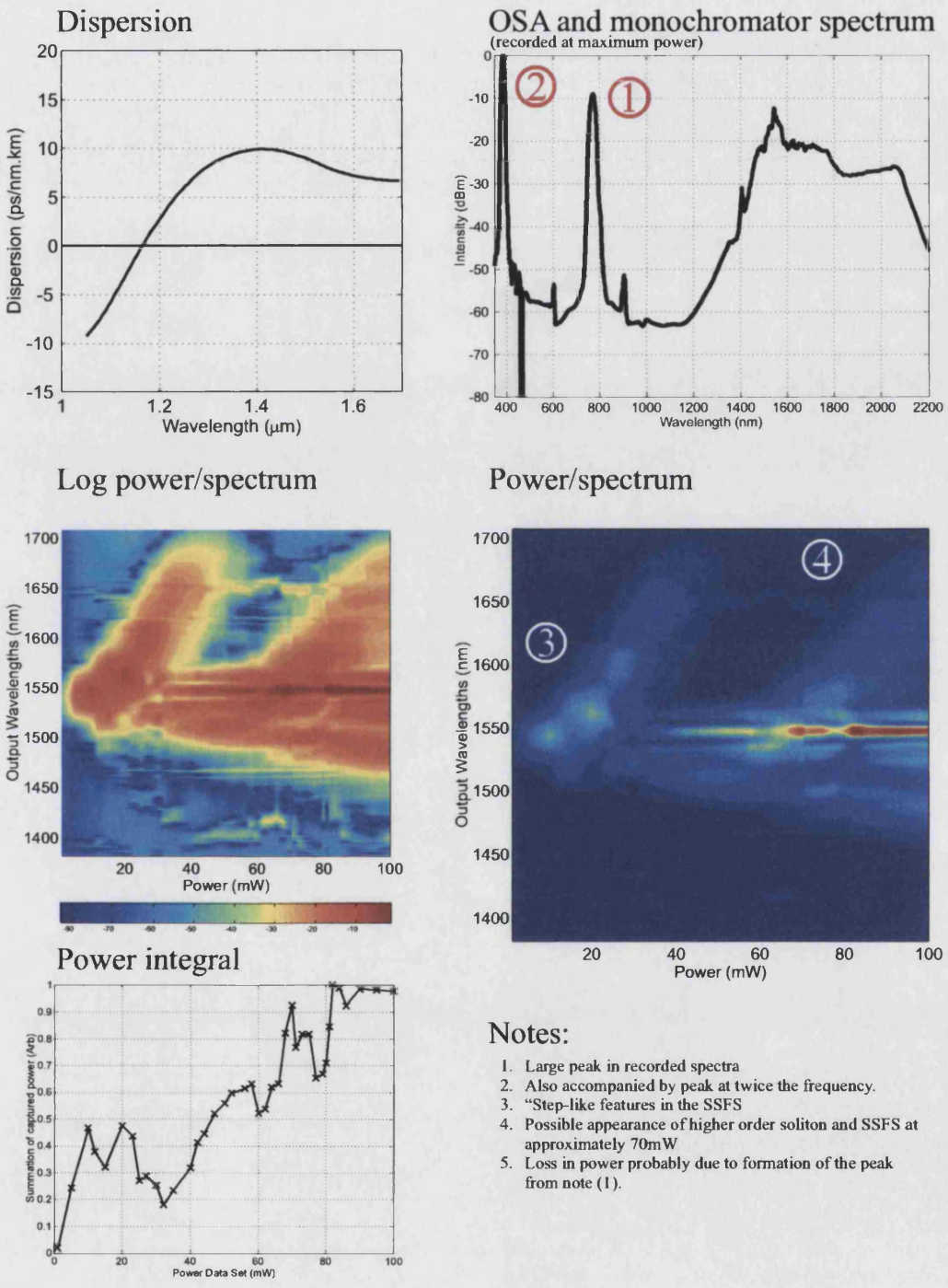

Notes:

1. Large peak in recorded spectra
2. Also accompanied by peak at twice the frequency.
3. "Step-like features in the SSFS
4. Possible appearance of higher order soliton and SSFS at approximately 70mW
5. Loss in power probably due to formation of the peak from note (1).

Figure A.4: Recorded spectra with power for the fibre P4c

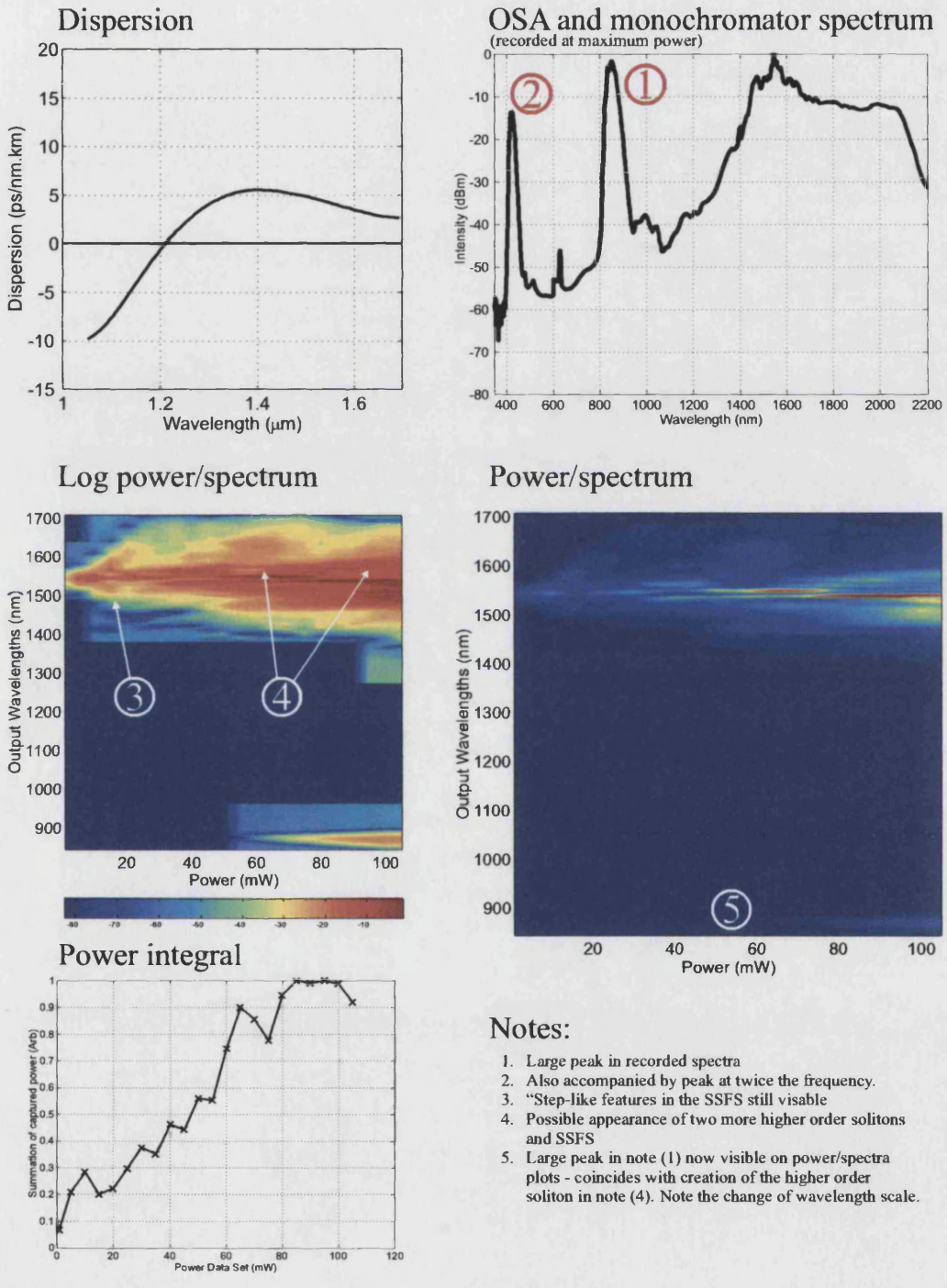

Notes:

1. Large peak in recorded spectra
2. Also accompanied by peak at twice the frequency.
3. "Step-like features in the SSFS still visable
4. Possible appearance of two more higher order solitons and SSFS
5. Large peak in note (1) now visible on power/spectra plots - coincides with creation of the higher order soliton in note (4). Note the change of wavelength scale.

Figure A.5: Recorded spectra with power for the fibre P4d

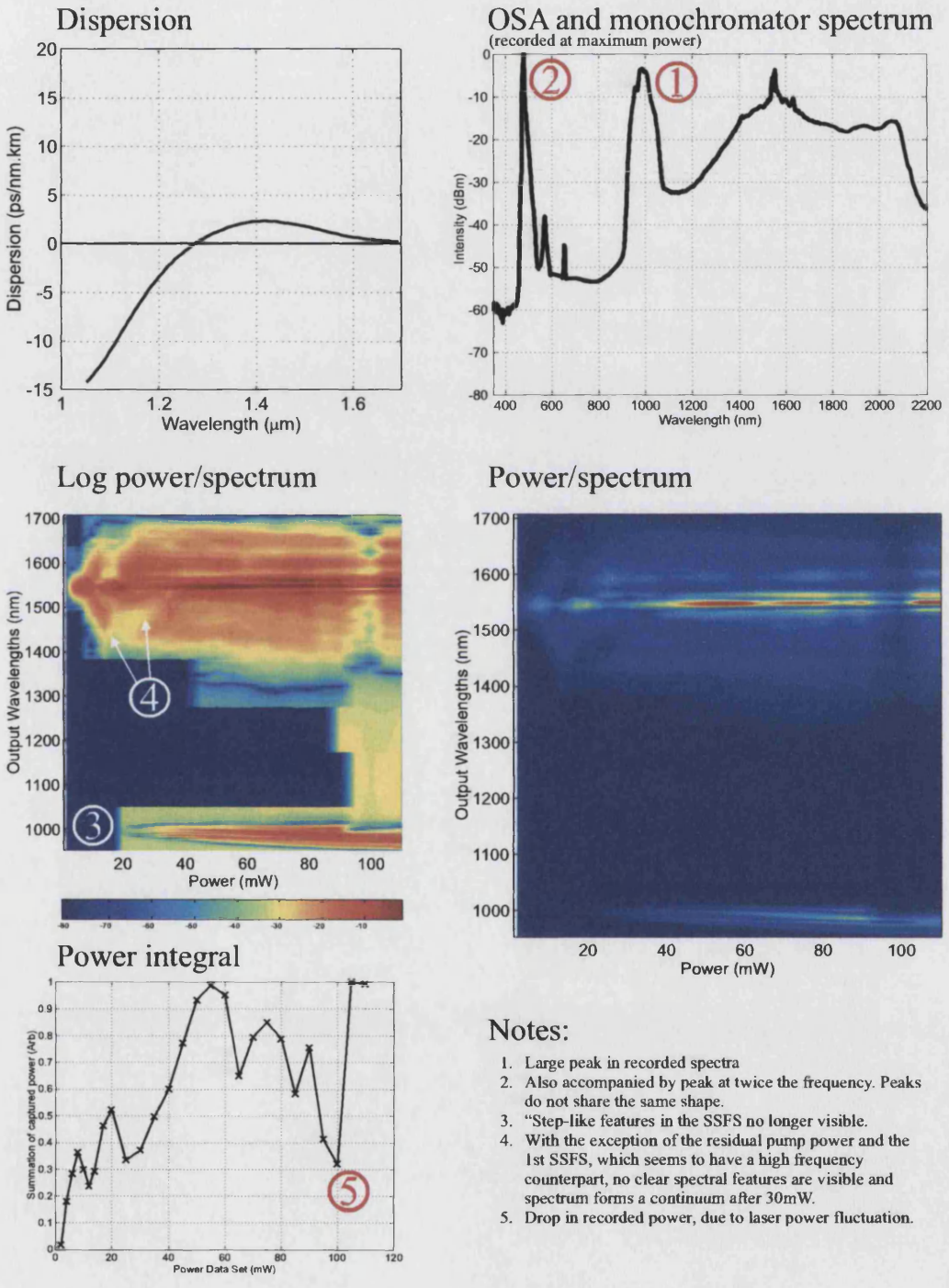

Notes:

1. Large peak in recorded spectra
2. Also accompanied by peak at twice the frequency. Peaks do not share the same shape.
3. "Step-like features in the SSFS no longer visible.
4. With the exception of the residual pump power and the 1st SSFS, which seems to have a high frequency counterpart, no clear spectral features are visible and spectrum forms a continuum after 30mW.
5. Drop in recorded power, due to laser power fluctuation.

Figure A.6: Recorded spectra with power for the fibre P4e

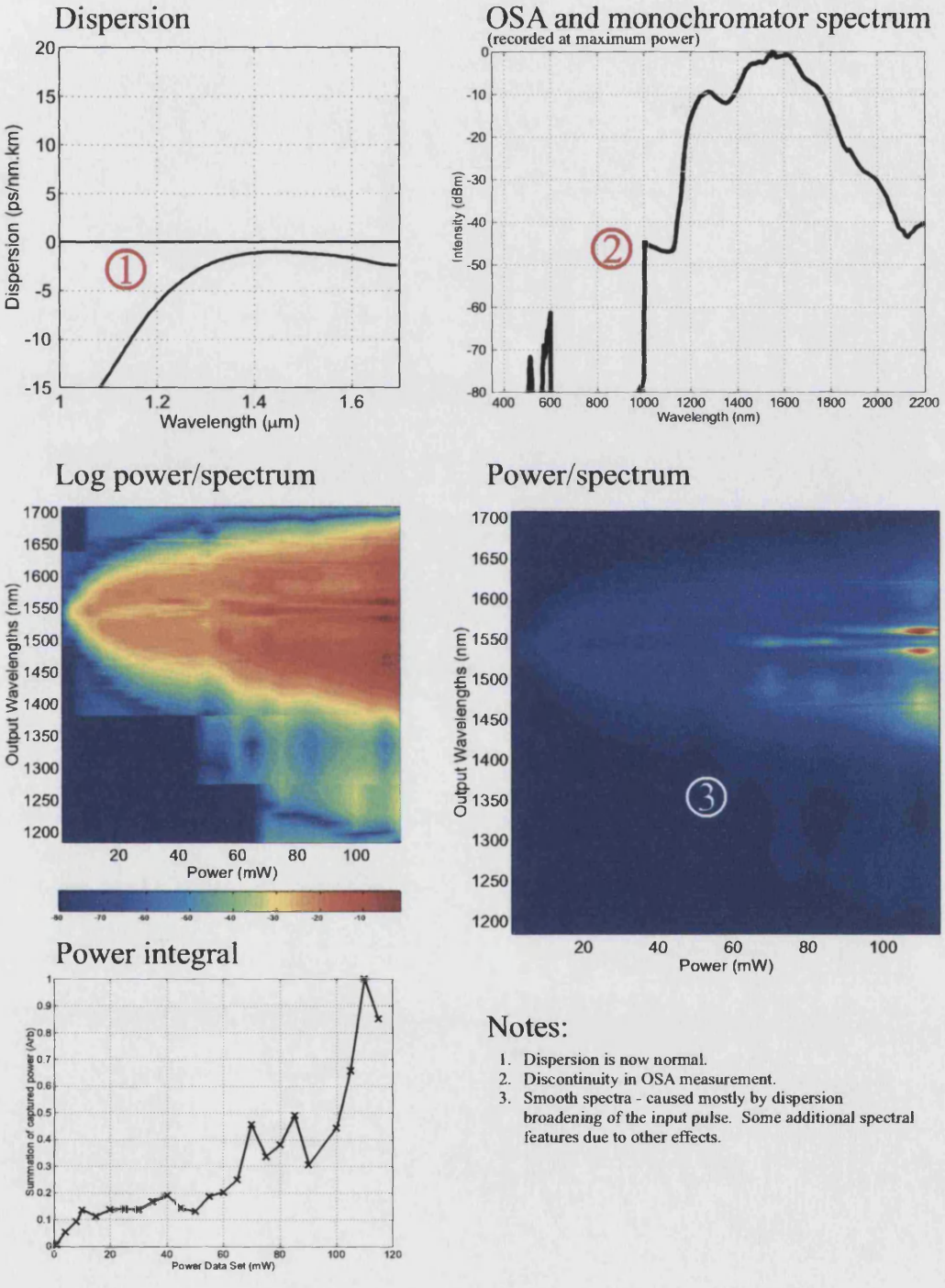

Notes:

1. Dispersion is now normal.
2. Discontinuity in OSA measurement.
3. Smooth spectra - caused mostly by dispersion broadening of the input pulse. Some additional spectral features due to other effects.

Figure A.7: Recorded spectra with power for the fibre P4f

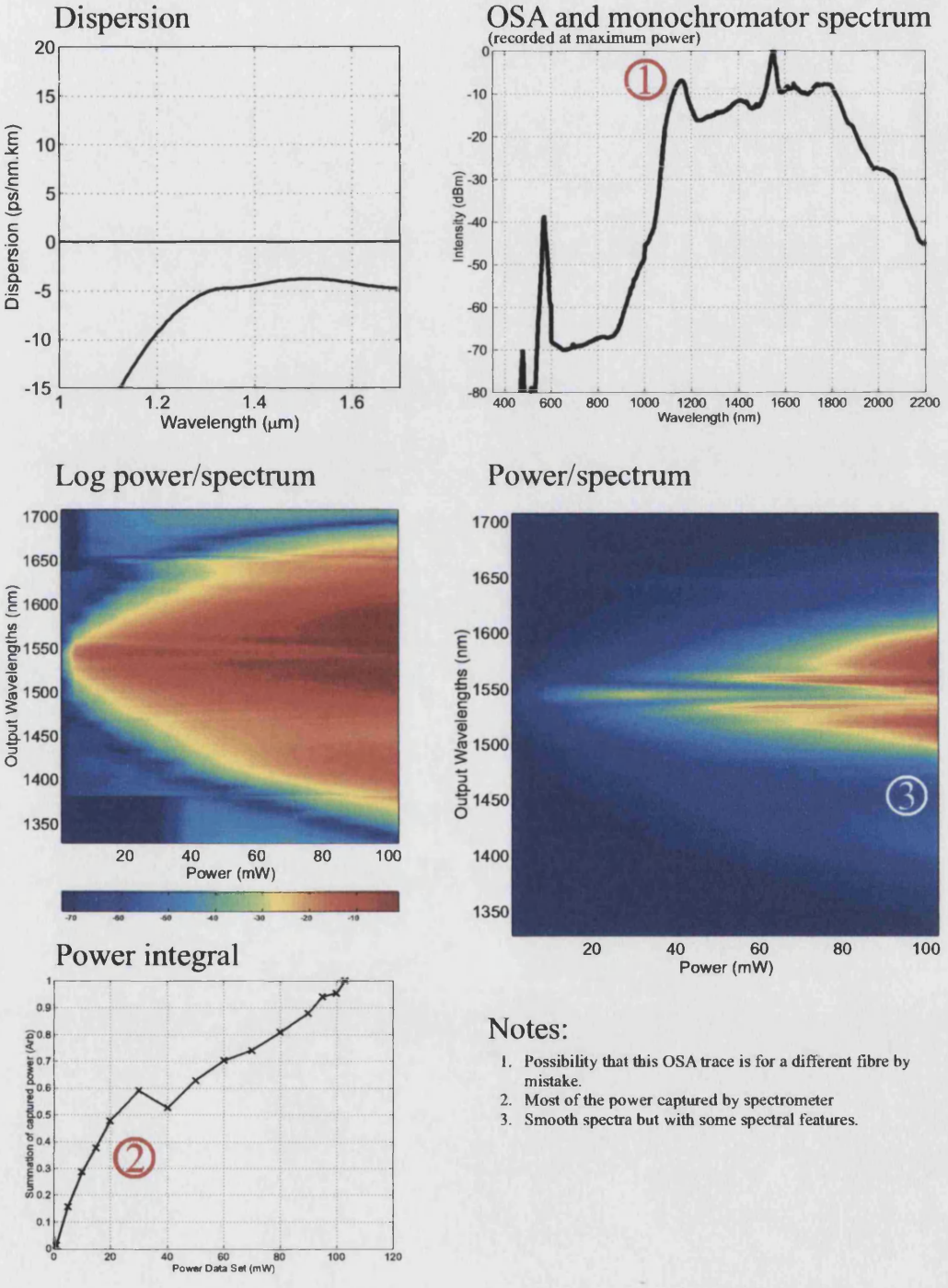

Notes:

1. Possibility that this OSA trace is for a different fibre by mistake.
2. Most of the power captured by spectrometer
3. Smooth spectra but with some spectral features.

Figure A.8: Recorded spectra with power for the fibre P4g

Dispersion

OSA and monochromator spectrum
(recorded at maximum power)

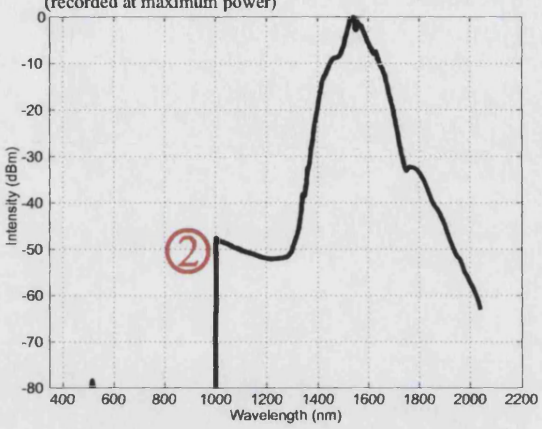

Log power/spectrum

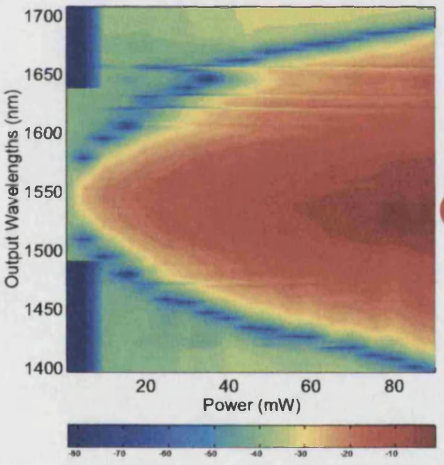

Power/spectrum

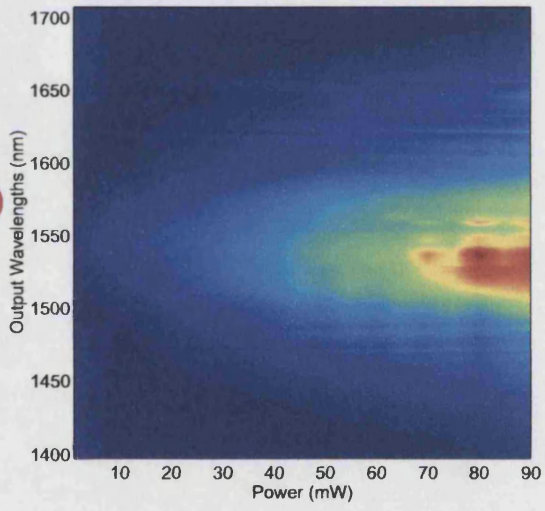

Power integral

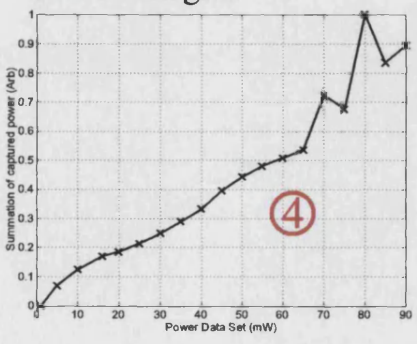

Notes:

1. Dispersion not measured for this fibre. Likely to have similar shape to P4g with a value of -7 ps/nm.km in the flattened region.
2. Problem with OSA measurement.
3. Smooth spectra.
4. Almost all power captured by spectrometer - straight line.

Figure A.9: Recorded spectra with power for the fibre P4h

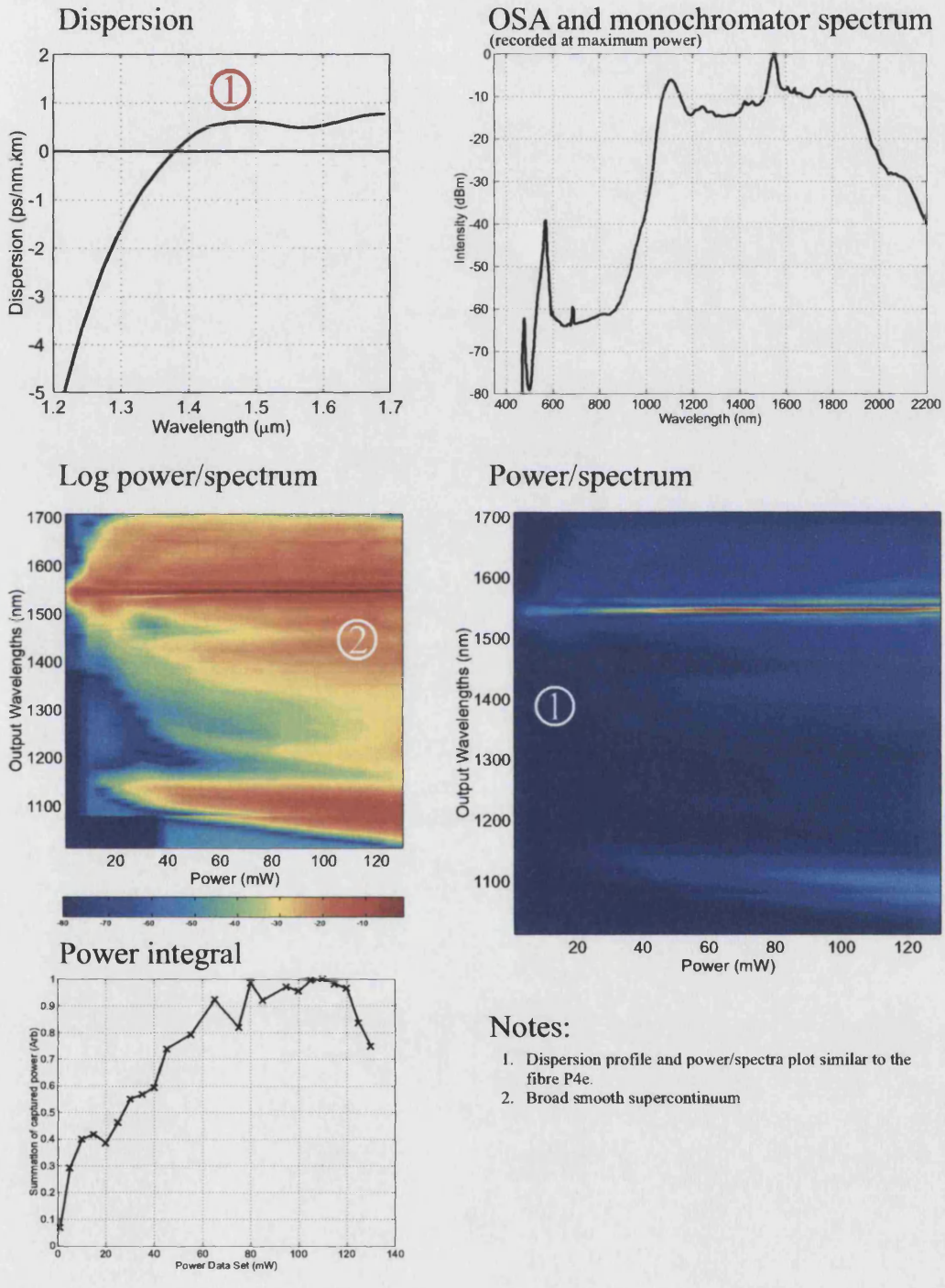

Notes:

1. Dispersion profile and power/spectra plot similar to the fibre P4e.
2. Broad smooth supercontinuum

Figure A.10: Recorded spectra with power for the fibre P7d

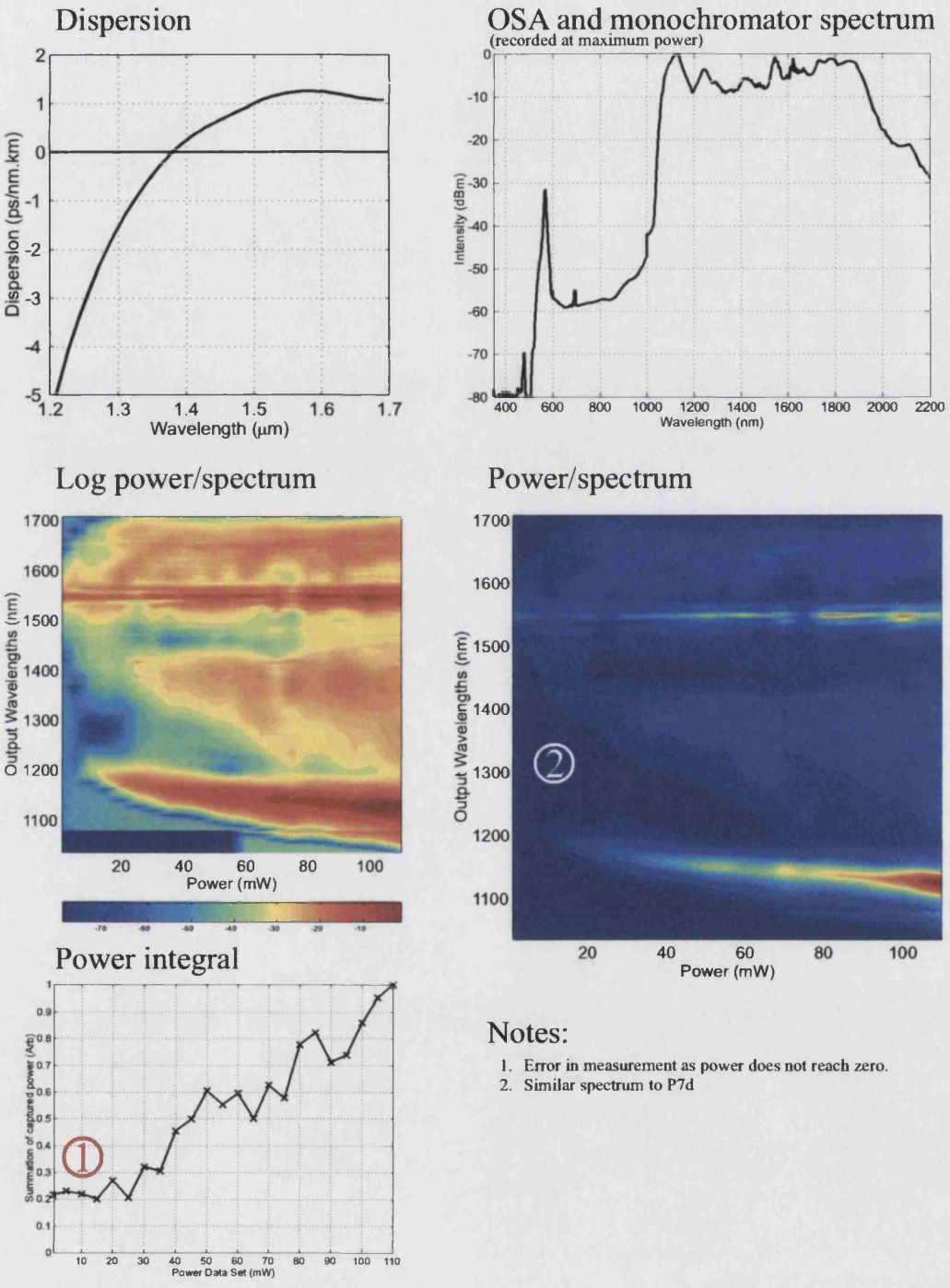

Figure A.11: Recorded spectra with power for the fibre P7e

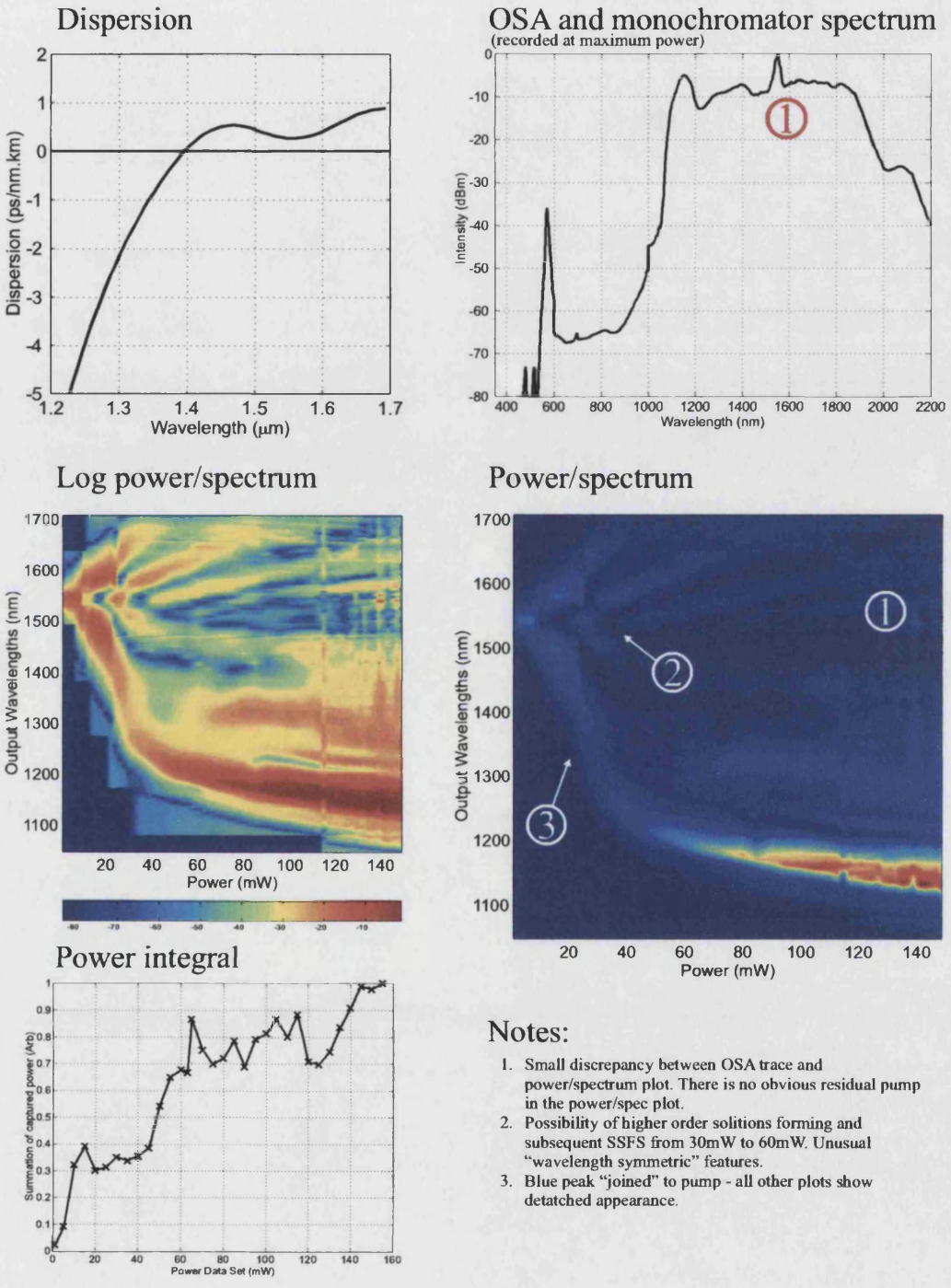

Figure A.12: Recorded spectra with power for the fibre P7f

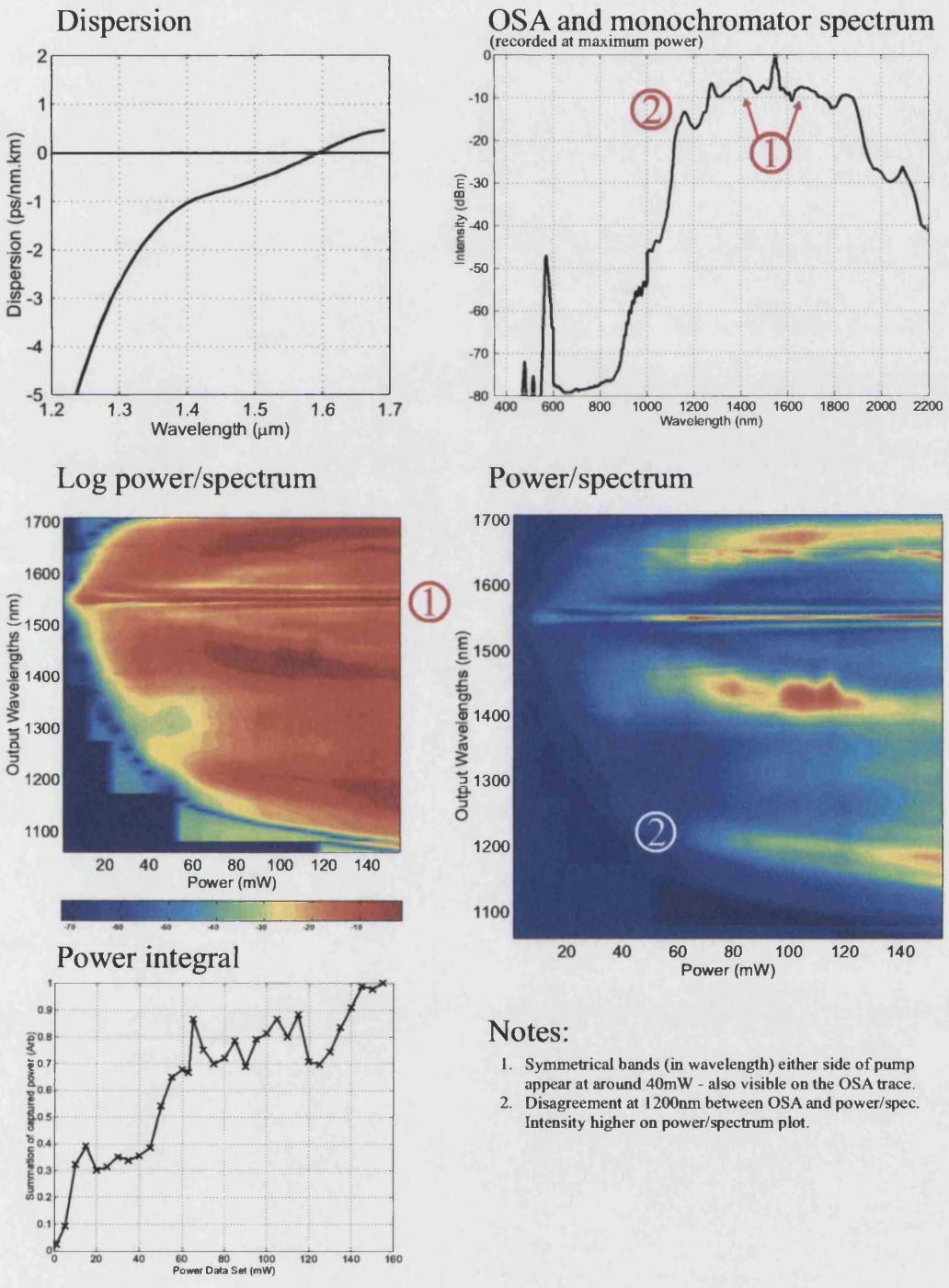

Figure A.13: Recorded spectra with power for the fibre P7g

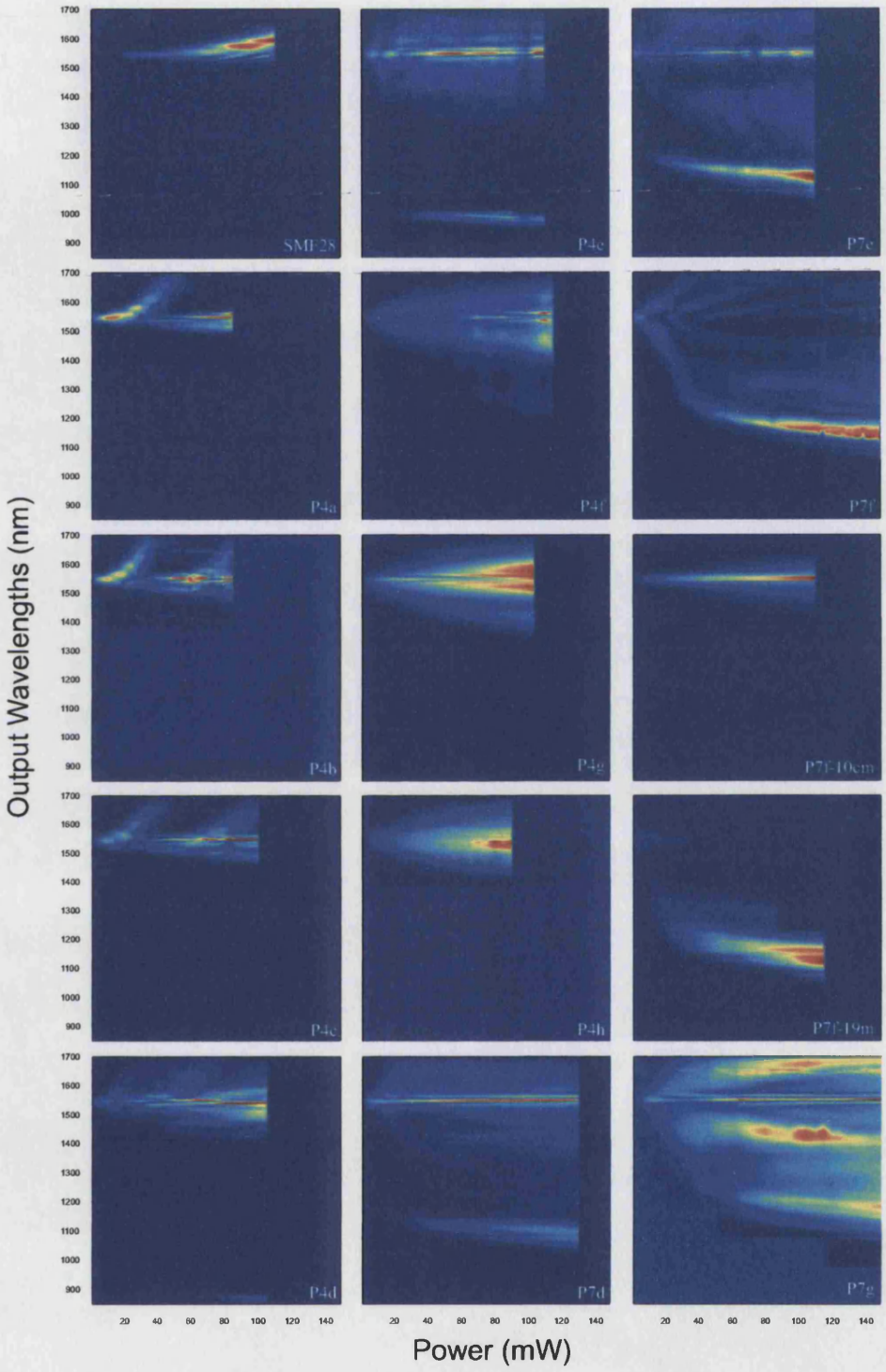

Figure A.14: Comparison of power/spectra measurements for SMF28 and all P4 and P7 fibres. All fibres are 1 m in length with the exception of measurements on 10 cm and 19 m of the fibre P7f.

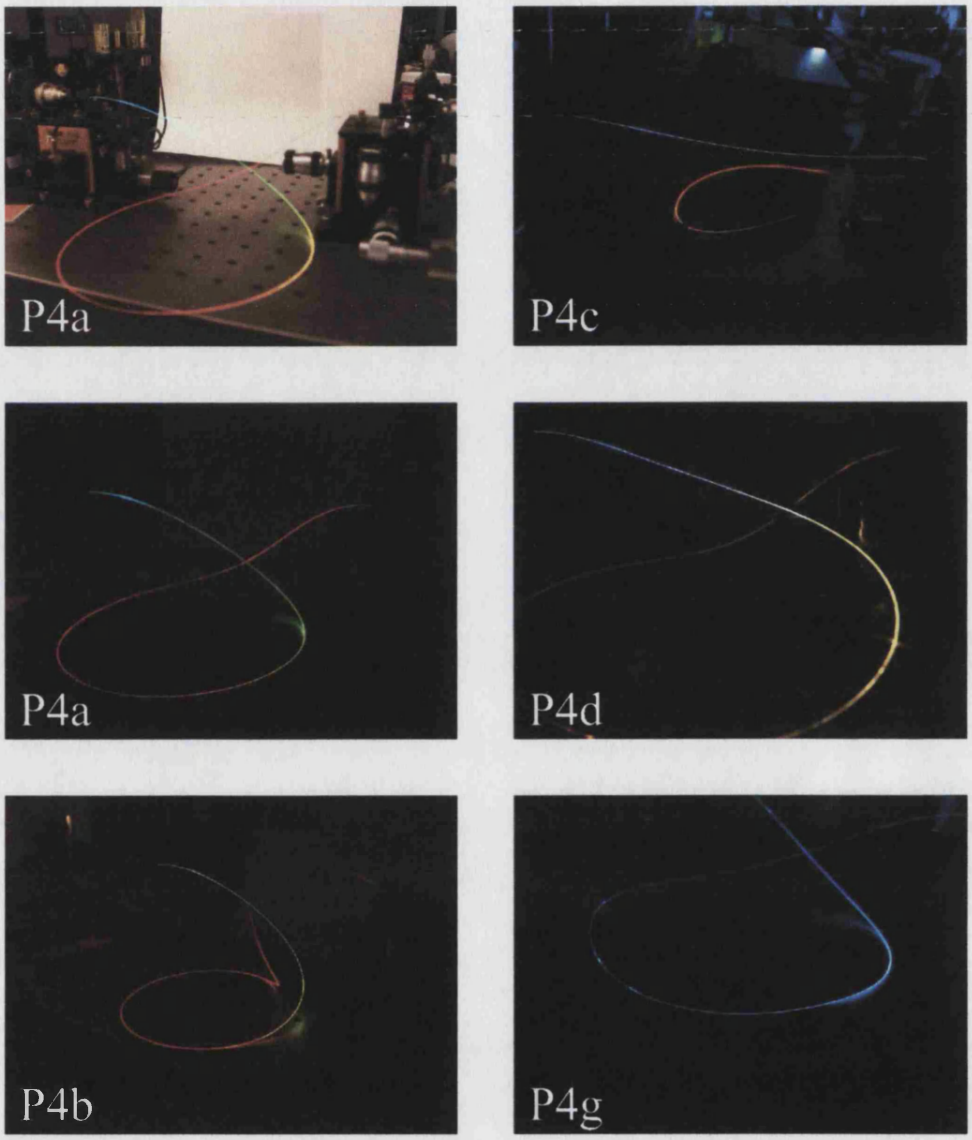

Figure A.15: Photographs of the visible continuum generated in the P4 fibres and lost during propagation.

Appendix B

Publications

B.1 Papers:

1. *Transformation and control of ultra-short pulses in dispersion-engineered photonic crystal fibres*
   W.H. Reeves, D.V. Skryabin, F. Biancalana, J.C. Knight, P.St.J. Russell, F. Ominetto, A. Efimov, and A.J. Taylor
   Nature 424:511-515, 31st July 2003

2. *Demonstration of ultra-flattened dispersion in photonic crystal fibers*
   W.H. Reeves, J.C. Knight, P.St.J. Russell, and P.J. Roberts, Opt. Express 10, 609-613 (2002)
   http://www.opticsexpress.org/abstract.cfm?URI=OPEX-10-14-609

3. *Yb3+ - Doped PCF Laser*
   W.J. Wadsworth, J.C. Knight, **W.H. Reeves**, P.St.J. Russell, J. Arriaga, Electronics letters, 2000, Vol. 36 No.13. pp.1452-1454.

4. *Excitation of cladding modes in photonic crystal fibers by flexural acoustic waves*
   A. Diez, T.A. Birks,**W.H. Reeves**, B.J. Mangan and P.St.J. Russell, Opt. Lett. 25 (1499-1501) 2000

5. *Extruded soft glass photonic crystal fiber for ultrabroad supercontinuum generation*
   V.V. Ravi Kanth Kumar, A.K. George, **W.H. Reeves**, J.C. Knight, P.St.J. Russell. Opt. Express 10, 1520-1525 (2002)
   http://www.opticsexpress.org/abstract.cfm?URI=OPEX-10-25-1520

B.2 Conferences:

1. *Group velocity dispersion in photonic crystal fibres*
   W.H. Reeves, W.J. Wadsworth, A. Ortigosa-Blanch, J.C. Knight, and P.St.J. Russell, PREP 2002, Nottingham (UK), April 2002.

2. *Properties and applications of photonic crystal fibres*
   W.J. Wadsworth, J.C. Knight, R.M. Percival, G. Bouwmans, A. Ortigosa-Blanch, **W.H. Reeves** and P.St.J. Russell, IQEC / LAT 2002, Moscow (Russia), June 2002 Paper QThH1 (Invited)

3. *Photonic crystal fibres for non linear applications*
   W.H. Reeves, W.J. Wadsworth, A. Ortigosa-Blanch, J.C. Knight, and P.St.J. Russell, In-fibre Bragg gratings and special fibres, Coventry (UK), October 2001.

4. *Tapered Photonic Crystal Fibre Beam Expander*
   W.H. Reeves, G Kakarantzas, J.C. Knight, T.A. Birks, B.J. Mangan, P.St.J. Russell, Proc. IOP Applied Optics and Opto-Electronics Conference, Loughbourgh (UK), 17-21 September 2000, IP.1.7

5. *Dispersion-Flattened Photonic Crystal Fibers at 1550nm*
   W.H. Reeves,J.C. Knight,P.St.J. Russell, and P.J. Roberts, OFC 2003 Atlanta GA (USA), March 2003 Paper FI3.

6. *Modified Group-Velocity Dispersion in Extruded Photonic Crystal Fiber*
   V.V Ravi Kanth Kumar, A.K George, **W.H. Reeves**, J.C. Knight and P.St.J. Russell, OFC 2003 Atlanta GA (USA), March 2003 Paper WA5.

7. *"Holey" Optical Fibers: Cages for Light*
   J.C. Knight, F. Benabid, **W.H. Reeves**,T.A. Birks and P.St.J. Russell, OFC 2003 Atlanta GA (USA), March 2003 Paper FI1 (Invited).

8. *Generation and wavelength conversion of laser light in photonic crystal fibres*
   P.St.J. Russell, J.C. Knight, F. Benabid, G. Bouwmans, G. Antonopoulos, **W.H. Reeves**,and W.J. Wadsworth Advanced Solid State Photonics, San Antonio, Texas 2003 (Invited).

9. *Ultrafast optics in dispersion-flattened photonic crystal fibre*
   W.H. Reeves, J.C. Knight, D.V. Skryabin, P.St.J. Russell, F.G. Ominetto, A. Efimov, and A.J. Taylor. CLEO 2003 Baltimore (USA), June 2003, Paper CThV2

10. *Broad supercontinuum generation from soft glass extruded fibre*
    W.H. Reeves, V.V Ravi Kanth Kumar, A.K George, J.C. Knight, P.St.J. Russel, F.G. Ominetto, A. Efimov, and A.J. Taylor. CLEO 2003 Baltimore (USA), June 2003, Paper CTuA3

References

[1] S. Maloney. Seeing the light through standards. *Plenary Session OFC*, March 2003.

[2] J. C. Knight, T. A. Birks, P. St. J. Russell, and D. M. Atkin. All-silica single-mode optical fiber with photonic crystal cladding. *Optics Letters*, 21:1547, 1996.

[3] J.C. Knight, T.A.Birks, P.St.J. Russell, and D.M. Atkin. All-silica single-mode optical fiber with photonic crystal cladding. errata. *Optics Letters*, 22:961, 1997.

[4] T.A. Birks, J.C. Knight, and P. St. J. Russell. Endlessly single-mode photonic crystal fiber. *Optics Letters*, 22(13):961–963, July 1997.

[5] J.C. Knight, T.A. Birks, R.F. Cregan, P. St. J. Russell, and J. P. de Sandro. Large mode area photonic crystal fibre. *Electronics Letters*, 34(13):1347–1348, June 1998.

[6] W.J. Wadsworth, A. Ortigosa-Blanch, J.C. Knight, T.A. Birks, T-P.M. Man, and P.St.J. Russell. Supercontinuum generation in photonic crystal fibers and optical fiber tapers - a novel light source. *J. Opt. Soc. Am. B*, 19(9):2148–2155, September 2002.

[7] W.J. Wadsworth, J.C. Knight, W.H. Reeves, P.St.J. Russell, and J. Arriaga. Yb3+ doped PCF laser. *Electronics letters*, 36(13):1452–1454, 2000.

[8] A. Ortigosa-Blanch, J.C. Knight, W.J. Wadsworth, B.J. Mangan, T.A. Birks, and P.St.J.Russell. Highly birefringent photonic crystal fibers. *Optics Letters*, 25:1325–1327, 2000.

[9] R.F. Cregan, B.J. Mangan, J.C. Knight, T.A. Birks, P.St.J. Russell, P.J. Roberts, and D.C. Allan. Single-mode photonic band gap guidance of light in air. *Science*, 285:1537–1539, 3rd September 1999.

[10] F. Futami, Y. Takushima, and K. Kikuchi. Generation of wideband flat supercontinuum over a 280-nm spectral range from a dispersion-flattened optical fiber with normal group-velocity disperison. *IEICE Trans. Electron.*, E82-C(8):1531–1538, August 1999.

[11] J. Hansryd, P.A. Andrekson, M. Westlund, J. Li, and P.-O. Hedekvist. Fiber-based optical parametric amplifiers and their applications. *IEEE Journal of Selected Topics in Quantum Electronics*, 8(3):506–520, May-June 2002.

[12] Amnon Yariv. *Optical Electronics in Modern Communications.* Oxford University Press, 5th edition, 1997.

[13] A W Snyder and J D Love. *Optical Waveguide Theory.* Chapman and Hall, New York, 1983.

[14] Govind P. Agrawal. *Nonlinear Fiber Optics.* Academic Press, 3rd edition, 2001.

[15] J. A. Buck. *Fundamentals of Optical Fibers.* John Wiley and Sons, Inc., 1995.

[16] D.B. Keck, R.D. Maurer, and P.C. Schultz. On the ultimate lower limit of attenuation in glass optical waveguides. *Applied Physics Letters*, 22(7):307–309, April 1973.

[17] G.A. Thomas, B. I. Shraiman, P. F. Glodis, and M.J. Stephen. Towards the clarity limit in optical fibre. *Nature*, 404:262–264, March 2000.

[18] J. M. Senior. *Optical Fibre Communications Principles and Practice.* Pretice Hall, second edition, 1992.

[19] V.V. Ravi Kanth Kumar, A.K. George, W.H. Reeves, J.C. Knight, P.St.J. Russell, F.G. Omenetto, and A.J. Taylor. An extruded soft glass photonic crystal fibre for ultrabroad supercontinuum generation. *Optics Express*, 10(25):1520–1525, 16th December 2002.

[20] H. Han, H. Park, M. Cho, and J. Kim. Terahertz pulse propagation in a plastic photonic crystal fiber. *Applied Physics Letters*, 80(15):2634–2636, April 2002.

[21] J.C. Knight, T.A. Birks, P.St.J. Russell, and J.P. de Sandro. Properties of photonics crystal fibre and the effective index model. *JOSA A*, 15:748, 1998.

[22] T. Hasegawa, E. Sasaoka, M. Onishi, M. Nishimura, Y. Tsuji, and M. Koshiba. Hole-assisted lightguide fibre for large anomalous dispersion and low optical loss. *Optics Express*, 9(13):681–686, December 2001.

[23] F. Benabid, J.C. Knight, G. Antonopoulos, and P.St.J Russell. Stimulated raman scattering in hydrogen-filled hollow-core photonic crystal fiber. *Science*, 298(5592):399–402, October 2002.

[24] F. Benabid, J.C. Knight, and P.St.J. Russell. Particle levitation and guidance in hollow-core photonic crystal fiber. *Optics express*, 10(21):1195–1203, October 2002.

[25] T. P. White, R. C. McPhedran, C. M. de Sterke, L. C. Botten, and M. J. Steel. Confinement losses in microstructured optical fibers. *Optics Letters*, 26(21):1660–1662, November 2001.

[26] D. Ferrarini, L. Vincetti, M. Zoboli, A. Cucinotta, and S. Selleri. Leakage properties of photonic crystal fibers. *Optics Express*, 10(23):1314–1319, November 2002.

[27] T. A. Birks, D. Mogilevtsev, J. C. Knight, P. St. J. Russell, J. Broeng, P. J. Roberts, J. A. West, D. C. Allan, and J. C. Fajardo. The analogy between photonic crystal fibres and step index fibres. *Optical Fibre Conference, Paper FG4-1*, pages 114–116, Friday, February 26 1999.

[28] W.J. Wadsworth, R.M. Percival, G. Bouwmans, J.C. Knight, and P.St.J. Russell. High power air-clad photonic crystal fibre laser. *Optics Express*, 11(1):48–53, January 2003.

[29] B.J. Mangan, J.C. Knight, T.A. Birks, P.St.J. Russell, and A.H. Greenaway. Experimental study of dual-core photonic crystal fibre. *Electronics Letters*, 36(16):1358–1359, August 2000.

[30] M. Tateda, N. Shibata, and S. Seikai. Interferometric method for chromatic dispersion measurement in a single-mode optical fiber. *IEEE Journal of Quantum Electronics*, QE-17(404), 1981.

[31] N. W. Ashcroft and N. D. Mermin. *Solid State Physics*. W. B. Saunders Company, international edition, 1976.

[32] F. M. Mitschke and L. F. Mollenauer. Discovery of the soliton self-frequency shift. *Optics Letters*, 11(10):659–661, October 1986.

[33] J. P. Gordon. Theory of the soliton self-frequency shift. *Optics Letters*, 11(10):662–664, October 1986.

[34] D. A. Jones, S. A. Diddams, J. K. Ranka, A. Stentz, R. S. Windeler, J. L. Hall, and S. T. Cundiff. Carrier-envelope phase control of femtosecond mode-locked lasers and direct optical frequency synthesis. *Science*, 288:635–639, 2000.

[35] I. Hartl, X. D. Li, C. Chudoba, R. Ghanta, T. Ko, J. G. Fujimoto, J. K. Ranka, R. S. Windeler, and A. J. Stentz. Ultrahigh-resolution optical coherence tomography using continuum generation in an air-silica micostructured optical fiber. *Optics Letters*, 26:608–610, 2001.

[36] R. Holzworth, J. Reichert, Th. Udem, T. W. Hansch, J. C. Knight, W. J. Wadsworth, and P. St. J. Russell. An optical frequency synthesiser for precision spectroscopy. *Physical Review Letters*, 85:2264–2267, 2000.

[37] R. Holzworth, M. Zimmermann, Th. Udem, T. W. Hansch, A. Nevsky, J. Von Zanthier, H. Walther, J. C. Knight, W. J. Wadsworth, P. St. J. Russell, M. N. Skortsov, and S. N. Bagayev. Absolute frequency measurement of iodine lines with a femtosecond optical synthesizer. *Applied Physics B*, 73:269–271, 2001.

[38] S. A. Diddams, D. J. Jones, J. Ye, T. Cundiff, J. L. Hall, J. K. Ranka, R. S. Windeler, R. Holzwarth, T. Udem, and T. W. Hansch. Direct link detween microwave and optical frequencies with a 300 THz femtosecond laser comb. *Physical Review Letters*, 84:5102–5105, 2000.

[39] J.K. Ranka, R.S. Windeler, and A.J. Stentz. Visible continuum generation in air-silica microstructure optical fibers with anomalous dispersion at 800nm. *Optics Letters*, 25(1):25–27, January 2000.

[40] J. Herrmann, U. Griebner, N. Zavoronkov, A. Husakou, D. Nikel, J. C. Knight, W. J. Wadsworth, P. St. J. Russell, and G. Korn. Experimental evidence for supercontinuum generation by fission of higher-order solitions in photonic fibers. *Physics Review Letters*, 88(17), April 2002.

[41] A. Ortigosa-Blanch, J. C. Knight, and P. St. J. Russell. Pulse breaking and supercontinuum generationwith 200-fs pump pulses in photonic crystal fibre. *J. Opt. Soc. Am. B*, 19(11):2567–2572, November 2002.

[42] J. M. Dudley, X. Gu, L. Xu, M. Kimmel, E. Zeek, P. O'Shea, R. Trebino, S. Coen, and R. S. Windeler. Cross-correlation frequency resolved optical gating analysis of broadband continuum generation in photonic crystal fiber: Simulations and experiments. *Optics Express*, 10(21):1215–1221, October 2002.

[43] B. R. Washburn, S. E. Ralph, and R. S. Windeler. Ultrashort pulse propagation in air-silica microstructure fiber. *Optics Express*, 10(13):575–580, July 2002.

[44] G. Genty, M. Lehtonen, H. Ludvigsen, J. Broeng, and M. Kaivola. Spectral broadening of femtosecond pulses into continuum radiation in microstructured fibers. *Optics Express*, 10(20):1083–1097, October 2002.

[45] J. Hansryd and P.A. Andrekson. Broad-band continuous-wave-pumped fiber optical parametric amplifier with 49-dB gain and wavelength-conversion efficiency. *IEEE Photon. Technol. Lett.*, 13:194, 2001.

[46] Y. Takushima and K Kikuchi. 10-GHz, over 20-channel multiwavelength pilse source by slicing super-continuum spectrum generated in normal-dispersion fiber. *IEEE Photon. Technol. Lett.*, 11:322, 1999.

[47] R. Lundin. Dispersion flattening in a w fiber. *Applied Optics*, 33(6):1011–1014, February 1994.

[48] Jaedeuk Lee, G. Hugh Song, Un-Chul Paek, and Yong Gon Seo. Design and fabrication of a nonzero-dispersion fiber with a maximally flat dispersion spectrum. *IEEE Photonics Technology Letters*, 13(4):317–319, April 2001.

[49] A. Ferrando, E. Silvestre, J.J Miret, and P. Andres. Nearly zero ultraflattened dispersion in photonic crystal fibers. *Optics Letters*, 25(11):790–792, June 2000.

[50] A. Ferrando, E. Silvestre, P. Andres, J.J. Miret, and M.V. Andres. Designing the properties of dispersion-flattened photonic crystal fibers. *Optics Express*, 9(13):687–697, December 2001. http://www.opticsexpress.org/abstract.cfm?URI=OPEX-9-13-687.

[51] R. F. Cregan, J. C. Knight, P. St. J. Russell, and P. J. Roberts. *J. Lightwave Tech.*, 17:2138–2141, 1999.

[52] W.H. Reeves, D.V. Skryabin, F. Biancalana, J.C. Knight, P.St.J. Russell, F. Omenetto, A. Efimov, and A.J. Taylor. Transformation and control of ultra-short pulses in dispersion-engineered photonic crystal fibres. *Nature*, 424:511–515, 31st July 2003.

[53] T.M. Monro, Y.D. West, D.W. Hewak, N.G.R. Broderick, and D.R. Richardson. Chalcogenide holey fibres. *Electronics letters*, 36(24), November 2000.

[54] M. A. Van Eijkelenborg, M. C. J. Large, A. Argyros, J. Zagari, S. Manos, I. Bassett N. A. Issa, S. Fleming, R. C. McPhedran, C. M. de Sterke, and N. A. P. Nicorovici. Microstructured polymer optical fiber. *Optics Express*, 9:319–327, 2001.

[55] T. M. Monro, K. M. Kiang, J. H. Lee, K. Frampton, Z. Yusoff, R. Moore, J. Tucknott, D. W. Hewak, H. N. Rutt, and D. J. Richardson. High nonlinearity extruded single-mode holey optical fibers. *Optical Fiber Communication Conference post deadline paper FA1, 1-3*, 2002.

[56] Schott Glass Company. *Data Sheet for N-SF6*, 2001.

[57] L.L. Chase, , and E.W. Van Stryland. *Nonlinear Optical Properties, in CRC Handbook of Laser Science and Technology Suppliment.* CRC Press, Boca Raton, 1995.

[58] K. Saitoh, M. Koshiba, T. Hasegawa, and E. Sasaoka. Chromatic dispersion control in photonic crystal fibres: Application to ultra-flattened dispersion. *Optics Express*, 11(8):843–852, April 2003.